

**ANALYSIS OF SPATTERING ACTIVITY
AT HALEMA‘UMA‘U IN 2015**

A THESIS SUBMITTED TO THE GRADUATE DIVISION OF THE
UNIVERSITY OF HAWAI‘I AT MĀNOA IN PARTIAL FULFILLMENT OF
THE REQUIREMENTS FOR THE DEGREE OF

MASTER OF SCIENCE
IN
GEOLOGY AND GEOPHYSICS

May 2017

By

Bianca G. Mintz

Thesis Committee:

Bruce F. Houghton, Chairperson

Tim Orr

Robert Wright

Keywords: spattering, lava lake, outgassing, Kīlauea, Hawaiian, Strombolian

Acknowledgments

First, I must thank the faculty and staff at the Department of Geology & Geophysics at the University of Hawai'i at Mānoa. From when I first entered the department as a freshman in August, 2012, to now as I complete up my masters' degree the entire department has provided overwhelming amounts of guidance, encouragement, and inspiration. I was truly touched to see so many of my professors attend my oral defense in February, 2017. The professors in this department have created an environment for students to learn the skills for becoming successful scientists. Their encouragement and guidance molded me into the geologist I am today and for that I am very grateful.

I would like to thank my advisor Bruce Houghton. When I first met Bruce I was interviewing for an undergraduate position in his lab (as a "lab rat"), and he told me that his goal was to have me love volcanoes. Bruce supported me both during my undergraduate degree and throughout my graduate degree as an advisor, mentor, leader, and role model. He continuously inspired me to push myself harder, to produce a higher level of quality results, and to accomplish my tasks efficiently. Bruce also saw in me an ability to accomplish things that I had never even considered to be possibilities. He opened my eyes to an absolutely incredible world and field of study, and yes he has given me an undying love for volcanoes.

A thank you also goes out to Alison Houghton for serving as a listening ear and great supporter as well. I want to thank Bruce's physical volcanology group (including those who have come and gone since I have been here) specifically: Sébastien Biasse, Wendy Cockshell, Kristine Curran, Samantha Isgett, Maria Janebo, Samuel Mitchell, and Nicolas Turner, for serving as colleagues, role models, and friends throughout the pursuit of both my bachelor's and my master's degree.

My committee members Tim Orr and Robert Wright provided valuable feedback and insight throughout the course of this study. In addition, the Hawaiian Volcano Observatory supplied essential data and information.

This work was funded by the National Disaster Preparedness Training Center (NDPTC). I would like to thank Karl Kim, the Director of NDPTC for providing me with the opportunity to peruse this study, to earn a master's degree, and to learn about natural disasters and community preparedness in the process.

Lastly I would like to thank my grandparents, my parents, and my siblings April, Jaden, and Evan. You are my first teachers, my strongest confidants, my greatest supporters, and my best friends. Without you none of this would have been possible. Everything I have accomplished here has been just as much for me as it is for you. Thank you.

Abstract

The classical explosive basaltic eruption spectrum is traditionally defined by the following end member eruption styles: Hawaiian and Strombolian. The field use of high-speed cameras has enabled volcanologists to make improved quantifications and more accurate descriptions of these classical eruptions styles and to quantify previously undecipherable activity (including activity on the basaltic eruption spectrum between the two defined end members).

Explosive activity in 2015 at the free surface of the Halema'uma'u lava lake at Kīlauea exhibited features of both sustained (Hawaiian) fountaining and transient (Strombolian) explosivity. Most of this activity is internally triggered by the internal rise of decoupled gas bubbles from below the lake's surface, but external triggering via rock falls, was also observed. Here I identify three styles of bubble bursting and spattering eruptive activity (isolated events, clusters of events, and prolonged episodes) at the lava lake, and distinguished them based on their temporal and spatial distributions. Isolated events are discrete single bubble bursts that persist for a few tenths of seconds to seconds and are separated by repose periods of similar or longer time scales. Cluster of events are closely spaced, repeated events grouped around a narrow point source, which persist for seconds to minutes. Prolonged episodes are groupings of numerous events closely linked in space and time that persist for tens of minutes to hours. Analysis of individual events from high-speed camera images indicates that they are made up of up to three phases: the bubble ascent phase, the bursting and pyroclast ejection phase, and the drain back (and rebound) phase. Based on the numerical parameters established in this study, the 2015 activity was relatively weak (i.e., of low intensity) but still falls in a region between those of continuous Hawaiian fountains and impulsive, short-lived Strombolian explosions, in terms of duration.

Table of Contents

Chapter 1: Introduction	1
1.1 Thesis Overview.....	1
1.2 Basaltic Eruption Styles	2
1.3 Volcanological Setting.....	6
1.4 Kīlauea Volcano.....	6
1.4.1 Eruptive Characteristics.....	6
1.4.2 Volcanic Structure	8
1.4.3 Kīlauea’s Summit	9
Chapter 2: Spattering Activity at Halema‘uma‘u in 2015 and the Implications for the Transition between Hawaiian and Strombolian Eruptions	14
2.1 Introduction	14
2.2 Methods.....	14
2.2.1 Data Collection	14
2.2.2 Data Processing	17
2.3 Results	20
2.3.1 Activity and Spattering Styles	20
2.3.2 Drain Back and Rebound.....	20
2.3.3 Relationship to the 24-hour Patterns of Lava Lake Behavior	23
2.3.4 Grain Size Analysis Calculations	24
2.3.5 Rock Fall-Triggered Activity	25
2.4 Interpretations.....	27
2.4.1 Descriptions of the Four High-Speed Videos.....	27
2.4.2 Pyroclast Dispersal Patterns	39
2.4.3 Analysis and Interpretation of Grain Size Data.....	39
2.4.4 Form and Scale of Activity and Decoupled Gas Bubble Size.....	45
2.4.5 Implications of the Rock Fall Event	49
2.5 Summary	49
Chapter 3: 24-Hour Trends in Spattering Activity at Halema‘uma‘u in 2015	51
3.1 Introduction	51
3.2 Methods.....	51

3.3 Activity Durations	52
3.3.1 Isolated Events.....	52
3.3.2 Cluster of Events	53
3.3.3 Prolonged Episodes	53
3.4 Activity Locations on the Lake	55
3.4.1 Isolated Events.....	55
3.4.2 Cluster of Events	63
3.4.3 Prolonged Episodes	63
3.4.4 Timings of Different Forms of Eruptive Behavior.....	70
3.4.5 Spatial Trends of Different Forms of Eruptive Behavior	72
3.4.6 Spatial Comparison of Prolonged Episodes	74
3.5 Rock Fall on April 24.....	74
3.6 Summary	76
Chapter 4: Discussion and Conclusions.....	78
4.1 Discussion	78
4.1.1 Characterizing the 24-hour Trends of Activity at the Lava Lake.....	78
4.1.2 Event Phases	80
4.1.3 Pyroclast Exit Velocities and Comparison to Strombolian and Hawaiian Eruptions...	81
4.1.4 Eruption Magnitude and Intensity	82
4.1.5 Effects and Implications of Externally Triggered Outgassing (Rock Falls)	82
4.2 Conclusions	83
4.2.1 Overall Research Conclusions.....	83
4.2.2 Current Research Limitations.....	86
4.2.3 High-Speed Cameras and Volcanology.....	89
4.2.4 Natural Hazard Implications.....	89
4.2.5 Future Work.....	90
References	92

List of Tables

Table 1.1 Eruptions at Kīlauea’s Summit	10
Table 2.1 Video Parameters	15
Table 2.2 Videos and Events	23
Table 3.1 Prolonged Episode Lengths for April 23 through April 24	66
Table 3.2 Prolonged Episode Lengths for December 10	67
Table 4.1 Average Initial Pyroclast Velocities	82

List of Figures

Figure 1.1 Plots of explosive eruption styles	3
Figure 1.2 Photographs of classical basaltic explosive eruption styles	5
Figure 1.3 Map of Hawaiian-Emperor Seamount chain, State of Hawai‘i, and Hawai‘i Island	7
Figure 1.4 Images of Kīlauea’s summit and lava lake.....	12
Figure 2.1 Image showing high-speed camera deployment locations.	16
Figure 2.2 High-speed video frame depicting bubble dimensions	18
Figure 2.3 High-speed video frames depicting isolated events and prolonged episodes.....	21
Figure 2.4 High-speed video frame depicting rebound	22
Figure 2.5 Still frames of December 10 rock fall event.....	26
Figure 2.6 High-speed video frames and plot of velocity versus time of a low intensity event...	30
Figure 2.7 High-speed video frames and plot of velocity versus time of a high intensity event..	31
Figure 2.8 RGB and binary high-speed video frame of pyroclast projection patterns	32
Figure 2.9 Plots of median diameter and total mass versus average mass eruption rate	40
Figure 2.10 Plots of mass percentage versus grain size of low and high intensity events.....	41
Figure 2.11 Grain size distributions for multiple eruptions.....	43
Figure 2.12 Plot of cumulative mass percent versus grain size for multiple eruptions	44
Figure 2.13 Plots of mean initial velocity and bubble area versus bursting velocity and plot of average mass eruption rate versus bubble area.	47
Figure 3.1 Plots of 24-hour activity at the lava lake on April 23 to April 24	60
Figure 3.2 Plot of the number of isolated events versus time from April 23 to April 24	62
Figure 3.3 Images of source locations for prolonged episodes from April 23 to April 24.....	64
Figure 3.4 Images of source locations for prolonged episodes from December 10	65
Figure 3.5 Plot of frequency of activity versus time from April 23 to April 24.....	71
Figure 3.6 Frame of activity location and frequency from April 23 to April 24.	73
Figure 3.7 Still frames of April 24 rock fall event.....	75
Figure 4.1 Plot of mass versus duration from select volcanoes including study results	85

Chapter 1: Introduction

1.1 Thesis Overview

The Halema'uma'u lava lake at the summit of Kīlauea volcano exhibits a range of outgassing and explosive eruptive behaviors. This thesis uses qualitative and quantitative observations of lava lake activity to properly place this activity, in terms of duration, on the basaltic eruption spectrum. Chapter 1 provides background information on the established basaltic eruption styles and about Kīlauea's volcanic setting and history, including its ongoing summit eruption (2008-present).

Chapter 2 categorizes activity at the lava lake in 2015, by analyzing patterns and trends in eruptive behavior over a 24-hour period related to lava lake outgassing. Such observations shed light on the diversity of this activity. I also discuss outgassing frequency and flow-direction trends. Three terms (isolated events, clusters of events, and prolonged episodes) are assigned to describe the pattern of activity, and various parameters associated with the activity are quantified.

Chapter 3 builds upon chapter 2, by focusing on events captured in four high-speed videos to analyze the components of this activity and to quantify various parameters associated with this activity. I compare and contrast this activity with the long-established end-member basaltic eruption styles, Strombolian explosions and Hawaiian fountains, and with globally more intense styles.

Chapter 4 links the particular styles of outgassing and eruption behaviors at the lava lake (analyzed in chapter 3) to the longer 24-hour observations (discussed in chapter 2) to justify the definitions I assign to the different outgassing styles. Additional discussion includes how this activity compares globally with more intense eruptions and where this activity fits along the

explosive basaltic eruption spectrum (in terms of duration and frequency). The chapter also discusses the importance of using high-speed cameras to study rapid outgassing processes at basaltic volcanoes, and future work. Overall this thesis has the goal of developing a formal classification scheme for the outgassing observed at the lava lake, particularly in 2015.

1.2 Basaltic Eruption Styles

The classical basaltic explosive eruption styles, i.e., Hawaiian and Strombolian, were first defined based on qualitative observations (e.g., Mercalli, 1881; Macdonald, 1972) at their respective type locales at Kīlauea and Mauna Loa volcanoes on the Island of Hawai‘i and at Stromboli Volcano in Italy. Later, George Walker (1973) established a quantitative classification scheme for explosive eruptions based on tephra dispersal area and its degree of fragmentation (Figure 1.1a).

Walker, however, did not base his classification on any deposits from either Stromboli or Kīlauea (Houghton et al., 2015) and erroneously stated that the products of Hawaiian fountaining eruptions were less widely dispersed than those of Strombolian explosions. In reality, the distinction is one of duration, with Strombolian explosions typically lasting seconds to tens of seconds and Hawaiian episodes characteristically lasting for hours to day (Houghton et al., 2015) (Figure 1.1b).

Strombolian explosions and Hawaiian fountains are considered to be the two end members of the weakly explosive basaltic eruption spectrum. Strombolian explosions are common at several volcanoes, including Stromboli (Italy), Etna (Italy), Erebus (Antarctica), and Yasur (Vanuatu). Hawaiian fountaining is common during the onset of eruptions at Mauna Loa and Kīlauea volcanoes in Hawai‘i, as well as at Etna in Italy, and Piton de la Fournaise in La Reunion.

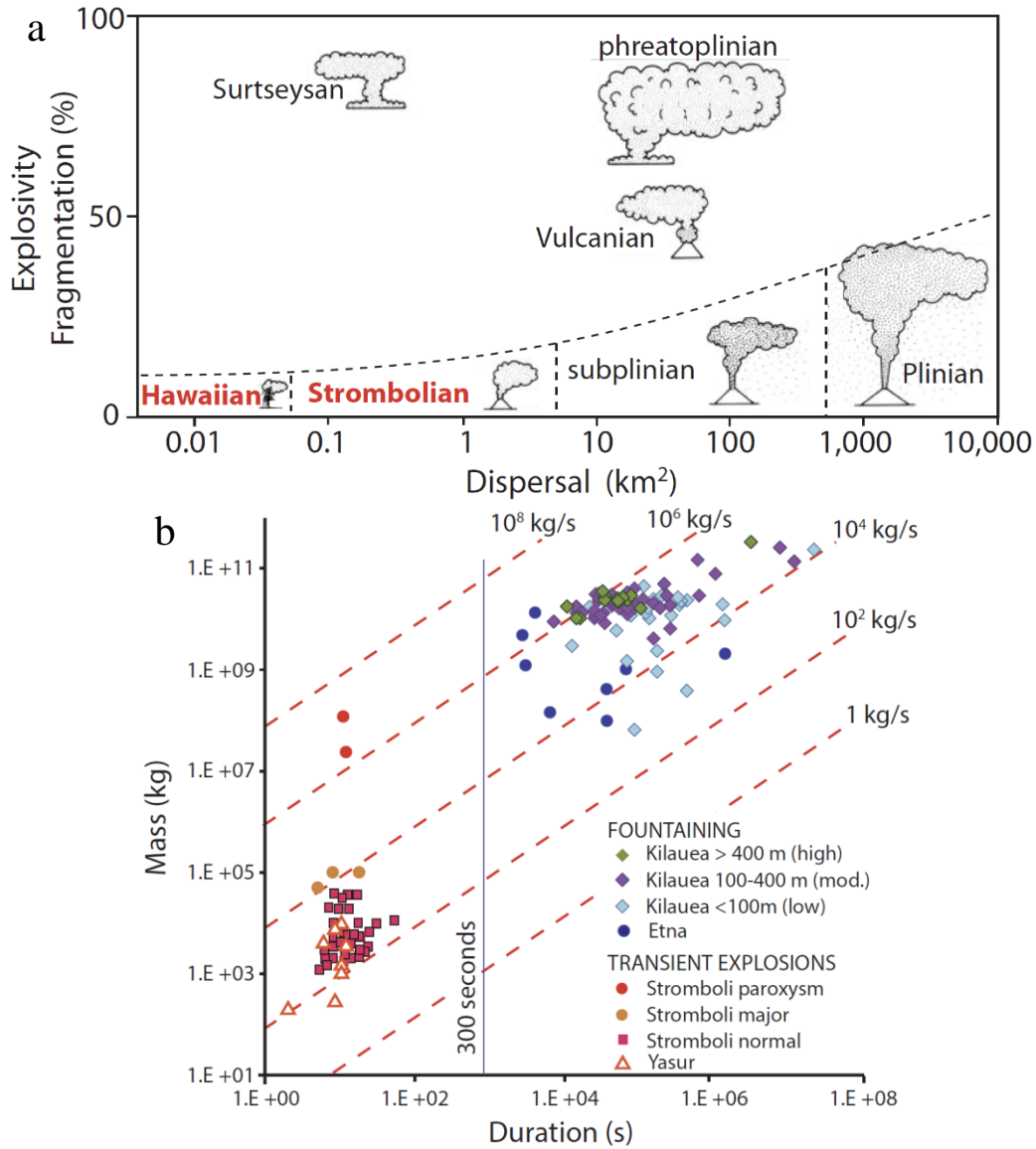


Figure 1.1 (a) Graph depicting explosive eruption styles based on quantifying the characteristics of deposits, adapted from Walker, 1983, and Cas and Wright, 1987. This thesis focuses on better defining the spectrum between the basaltic end members of the classical eruption styles: Hawaiian and Strombolian (in red). **(b)** Plot from Houghton et al., 2015, of duration and mass of basaltic activity at select volcanoes indicating that Strombolian and Hawaiian eruption styles are more aptly differentiated by duration as opposed to product dispersal and fragmentation. The red dashed lines represent equal mass discharge rate.

Strombolian eruptions are weak, discrete explosions that result from the release of gas from pressurized pockets. In some cases these explosions are ash-poor (Figure 1.2a) and in others they are ash-rich (Figure 1.2b) (Taddeucci et al., 2015). Hawaiian fountains, (Figure 1.2c) producing large pyroclasts and minor amounts of ash, can attain heights as high as 500 m, and are episodic with fountaining episodes and repose periods of variable durations (Taddeucci et al., 2015). During fissure eruptions, fountains eject material to less than 50 m above the vent (Figure 1.2d) (Taddeucci et al., 2015). Pyroclasts from these two styles are similar in size and ejection height. On average, ejecta sizes range from 10^{-2} to 10^{-1} m, but can range from 10^{-6} to 10 m (Taddeucci et al., 2015). Pyroclasts can reach up to a meter in diameter and can be ejected as high as a few hundreds of meters. Ejection velocities of products from Strombolian explosions, typically range from 50 to 100 m s^{-1} (Taddeucci et al., 2015), though velocities of up to 400 m s^{-1} have been documented (Taddeucci et al., 2015).

Strombolian and Hawaiian eruption styles differ in terms of mass produced (which may serve as an indicator of eruption magnitude) and in duration. At Stromboli volcano in Italy, individual explosions typically produce $10^3 - 10^4$ kg of erupted mass (Gaudin et al., 2014). These eruptions usually produce about $10^8 - 10^{11}$ kg of erupted mass per fountaining episode (Taddeucci et al., 2015). As stated earlier, Strombolian explosions are orders of magnitude shorter in duration than Hawaiian episodes.

With the advent of high-speed cameras and relatively easy access to the Halema'uma'u lava lake at Kīlauea caldera, I have identified and quantified an intermediary basaltic eruption style. Classifying basaltic eruption styles that fall between Strombolian explosions and Hawaiian fountains is imperative for improving understanding of the first-order constraints on basaltic volcanism.



Figure 1.2 (a) Long-exposure photograph of a typical ash-poor Strombolian explosion at Yasur volcano, Vanuatu (Taddeucci et al., 2015). (b) Photograph of an ash-rich Strombolian explosion at Yasur (Taddeucci et al., 2015). Based on the position of the scientists in photograph **b**, photograph **a** was captured farther from the vent. (c) Photograph of a 300-m-high Hawaiian lava fountain during episode 8 of the Kīlauea Iki eruption, Kīlauea volcano, Hawai‘i (U.S. Geological Survey photo, 07:00 HST December 11, 1959). (d) Photograph of a 10 to 20-m-high Hawaiian fountain from the Kamoamoia fissure eruption at Kīlauea volcano, Hawai‘i (U.S. Geological Survey photo, 09:17 HST March 6, 2011). Pyroclast are being ejected approximately 20 to 30 m into the air.

1.3 Volcanological Setting

The Hawaiian-Emperor seamount chain (Figure 1.3a), is a classic example of age-progressive volcanism (Clague and Dalrymple, 1987) fueled by a hot spot; age increases with distance from the hot spot. The chain extends from the Aleutian Trench – where the oldest volcanoes now seamounts formed about 81 Ma (Keller et al., 1995) – to the Lō‘ihi seamount, which is a site of active submarine volcanism. The chain has served as an inspiration for groundbreaking studies regarding intraplate hot spot (Wilson, 1963), mantle plume (Morgan, 1972) dynamics, the life-stages of Hawaiian shield volcanoes, plate-motion, etc.

The state of Hawai‘i comprises the eight main Hawaiian islands (Figure 1.3b), of which the Island of Hawai‘i (Figure 1.3c) is the youngest, forming the southernmost island of the Hawaiian-Emperor chain. The Island of Hawai‘i (Figure 1.3c) is composed of five subaerial volcanoes. These are, in order of decreasing age, Kohala, Hualālai, Mauna Kea, Mauna Loa, and Kīlauea (Moore and Clague, 1992). Kīlauea, the youngest subaerial volcano in the Hawaiian-Emperor chain, forms the southeast east tip and southeast flank of the island, and is adjacent to Mauna Loa to the southeast.

1.4 Kīlauea Volcano

1.4.1 Eruptive Characteristics

Currently Kīlauea is in the shield-building stage of a Hawaiian volcanoes’ life time and erupts mostly tholeiitic basalts (Macdonald et al., 1983). Over the last 25 ka, Kīlauea has undergone three effusive and two explosive eruptive periods (Swanson et al., 2014). The two explosive periods, constituting about 60% of the 25 ka, were from vents focused within the summit caldera and include phreatic and phreatomagmatic phases – indicating that the caldera frequently intersected the water table (Swanson et al., 2014). Currently, Kīlauea is in a

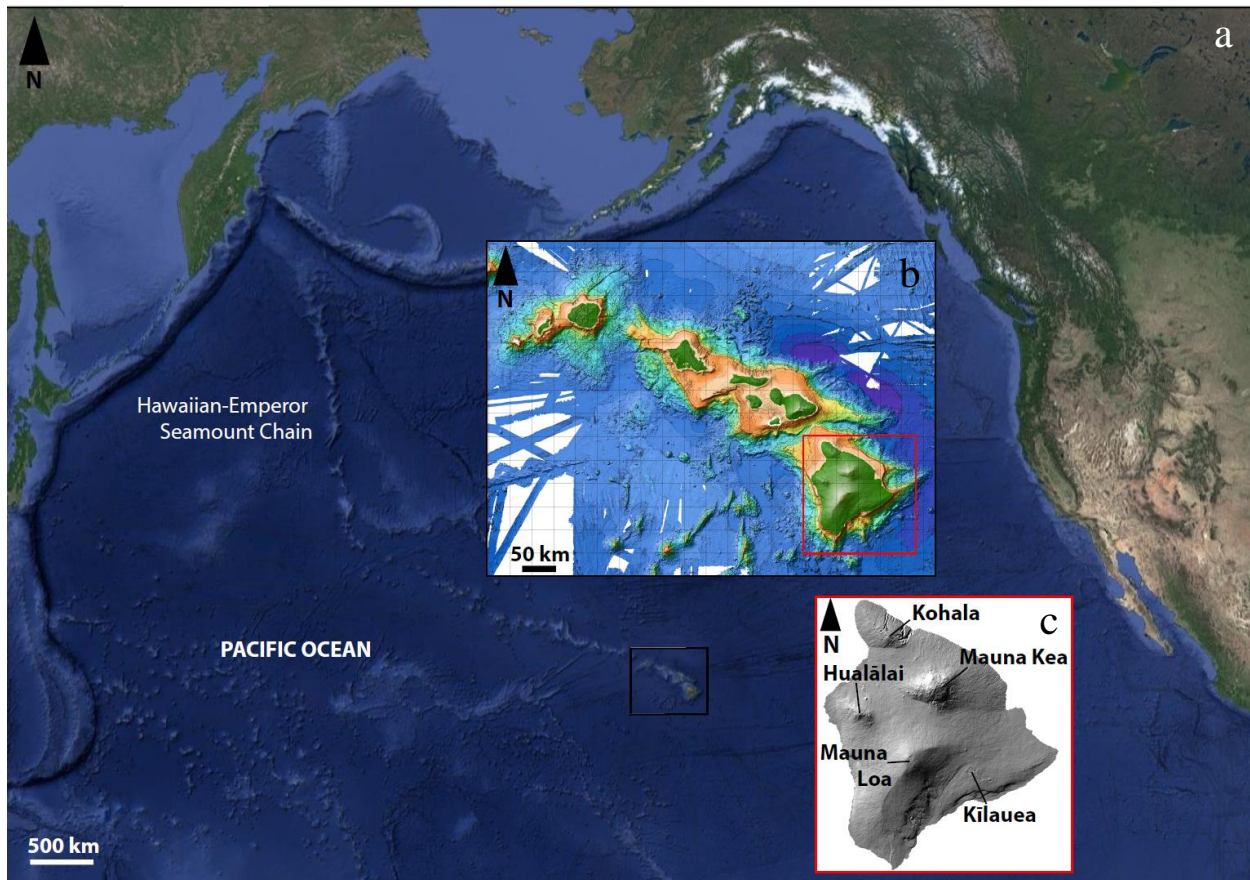


Figure 1.3 (a) Large scale map showing the Hawaiian-Emperor Seamount chain and its position in the Pacific Ocean (source: Google Earth). (b) Inset bathymetric map of the state of Hawai'i (source: Hawai'i Mapping Research Group, School of Ocean and Earth Science and Technology, University of Hawai'i at Mānoa). (c) Inset 10 m DEM of Hawai'i Island, indicating the five sub-aerial volcanoes comprising the island (source: USGS).

predominantly effusive state, with Hawaiian explosive eruptions occurring intermittently.

Kīlauea is arguably one of the most active volcanoes in the world, having repaved 90% of itself with new material in the last 1,000 years (Holcomb, 1987). The volcano has erupted almost annually since the 1950s and has been erupting almost continuously as part of a single eruptive sequence since 1983.

1.4.2 Volcanic Structure

Magma rises from the mantle, via the hot spot, and is stored in reservoirs beneath the surface of Kīlauea (Eaton and Murata, 1960; Tilling and Dvorak, 1993). In general, magma is supplied to Kīlauea at about $0.1 \text{ km}^3 \text{ yr}^{-1}$, but this rate varies on monthly and yearly time scales (Poland et al., 2014). Poland et al., 2014 proposed a model indicating that Kīlauea's summit has three reservoirs where magma is stored on a "long-term" basis: the south caldera reservoir, the Halema'uma'u reservoir, and the Keanakāko'i reservoir. Magma stored in summit reservoirs can erupt at the summit caldera. Kīlauea's two rift zones, the Southwest Rift Zone and the East Rift Zone, enable magma to leave the summit reservoirs and travel as intrusions. The East Rift Zone is deeper than the Southwest Rift Zone and supplies Kīlauea with a structural boundary (Poland et al., 2014). Both rift zones provide pathways for magma to travel away from the caldera (Poland et al., 2014). Although not all intrusions lead to eruptions, the current Pu'u 'Ō'ō eruption is supplied by magma having traveled away from the summit via the East Rift Zone.

1.4.2.1 Magma Pulses

Swanson et al., (2016) used multiple lines of evidence from the Halema'uma'u lava lake, to propose that small-scale magma pulses occur every few months underneath Kīlauea. Higher lava lake levels, along with higher tephra accumulation, occur cyclically over periods of a few months (Swanson et al., 2016). These indicators correlate positively with radial summit tilt,

gravity anomalies, glass MgO, and usually show positive correlation with vertical deformation rates derived from GPS measurements (Swanson et al., 2016). The cycles are attributed to pulses in deep magma supply (Swanson et al., 2016). Consequently, during magma pulses the lava lake is higher and increased amounts of tephra are ejected (Swanson et al., 2016).

1.4.3 Kīlauea's Summit

1.4.3.1 Eruptive History at Kīlauea's Summit

Kīlauea's is about 1,250 m above sea level (Poland et al., 2014) and contains a caldera within which is the Halema'uma'u crater. The Halema'uma'u crater sits in the southwest portion of Kīlauea caldera and has been in existence at least since Kīlauea was first visited by Westerners. A lava lake within the Kīlauea caldera (at Kīlauea's summit) was first described in 1823 (Ellis, 1825), within Halema'uma'u crater. This lava lake was present most of the time, until the lake drained abruptly in 1924 (Jagger and Finch, 1924). In 1911, Frank Perret (Perret 1913a, and 1913b) used Kīlauea's lava lake to conduct the first set of detailed and continuous measurements on any lava lake in the world. In 1924, the summit experienced episodic, short-term phreatic explosions (Jagger and Finch, 1924), which widened Halema'uma'u crater. After the lava lake drained, sporadic Hawaiian eruptions continued at the summit (Macdonald et al., 1983) over the ensuing decades (Table 1.1) (Macdonald, 1986). A lava lake existed for nine months from 1967 to 1968, within the Halema'uma'u crater (Kinoshita et al., 1969). After that lake drained, a few fountaining eruptions in Kīlauea caldera occurred until 1982 (Table 1.1) (Macdonald et al., 1983). No other eruptive activity was recorded at the summit between 1982 and 2008.

Table 1.1 Eruptions at Kīlauea’s Summit

Year	Location
1927	Halema‘uma‘u crater
1929*	Halema‘uma‘u crater
1930	Halema‘uma‘u crater
1931	Halema‘uma‘u crater
1934	Halema‘uma‘u crater
1952	Halema‘uma‘u crater
1954	Halema‘uma‘u crater & Kīlauea caldera
1961*	Halema‘uma‘u crater
1971	Kīlauea caldera
1974	Kīlauea caldera
1975	Kīlauea caldera
1982	Kīlauea caldera
* indicates multiple eruptions Macdonald et al., 1983 and Macdonald, 1986	

1.4.3.2 Present Summit Eruption

Seismic tremor at Kīlauea’s summit increased in November 2007 as did SO₂ gas emissions in December 2007, despite the fact that Kīlauea was deflating at the time (Patrick et al., 2013). Gas emissions and seismic tremor continued to increase to a few times greater than background levels by early March 2008 (Patrick et al., 2013). By mid-March, SO₂ levels were at least an order of magnitude greater than those recorded in late December (Wilson et al., 2008). These increases in tremor and gas emissions culminated in an explosion at 2:58 HST on March 19, 2008 forming a new 35-m-wide (Patrick et al., 2013) crater, near the base of the crater wall on the southeast side of Halema‘uma‘u (Figure 1.4a,b). A lava free surface was first observed in July 2008 and was measured at about 200 m below the rim in 2009 (Patrick et al., 2015). Prior to the 2008 explosions, Halema‘uma‘u crater had been open to the public for viewing; it was closed in April 2008 and remains closed today.

In January 2010, the lava lake sunk to 220 m below the crater rim (Patrick et al., 2013). By the end of 2013 the new crater had widened to 215 m (northwest-southeast) \times 160 m (northeast – southwest) via wall collapses (Patrick et al., 2013). At the time, the lava lake had reached a height of 22 m below the crater rim (Patrick et al., 2013), but mostly remained between 30 and 60 m below the rim (Patrick et al., 2013). In April 2015, the lava lake overflowed briefly onto the Halema‘uma‘u crater floor for the first time, and again in October 2016. The crater has continued to expand; based on an October 2016 Digital Globe image the lava lake maintains dimensions of \sim 255 m (northwest-southeast) \times \sim 195 m (northeast – southwest).

1.4.3.3 The Lava Lake

The summit lava lake undergoes a variety of dynamic behaviors, which have been described and studied since Westerners first visited Kīlauea. The surface of the lava lake is covered in dark crustal plates that are tens of meters wide, and 5 – 6 cm thick based on a formula from Hon et al., 1994 (Patrick et al., 2015). The plates align along sutures (of glowing more fluid lava) through which passive outgassing occurs (Patrick et al., 2015). The lava lake maintains a general flow direction (which has been observed based on plate motion) from north to south. Plate motion, flow direction, and outgassing patterns indicate that generally upwelling occurs along the northern margin of the lake and downwelling occurs along the southern margin of the lake. In addition, there is a more active area of downwelling typically characterized by spattering at the southeast corner of the lake, informally referred to as the “southeast sink.” The plates are advected by convective motion within the underlying lake. However partial and complete reversals of plate motion (linked to spattering activity throughout the lava lake) are not uncommon (Patrick et al, 2015; 2016).

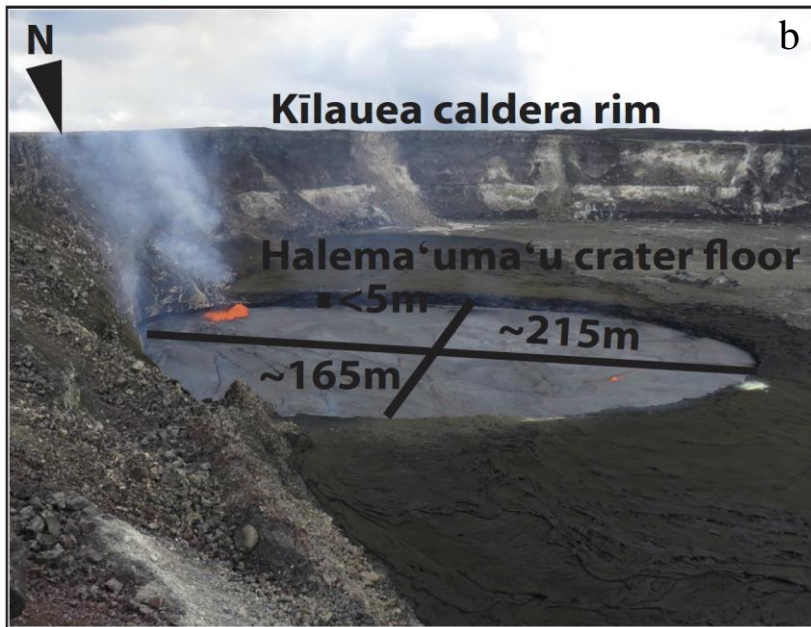
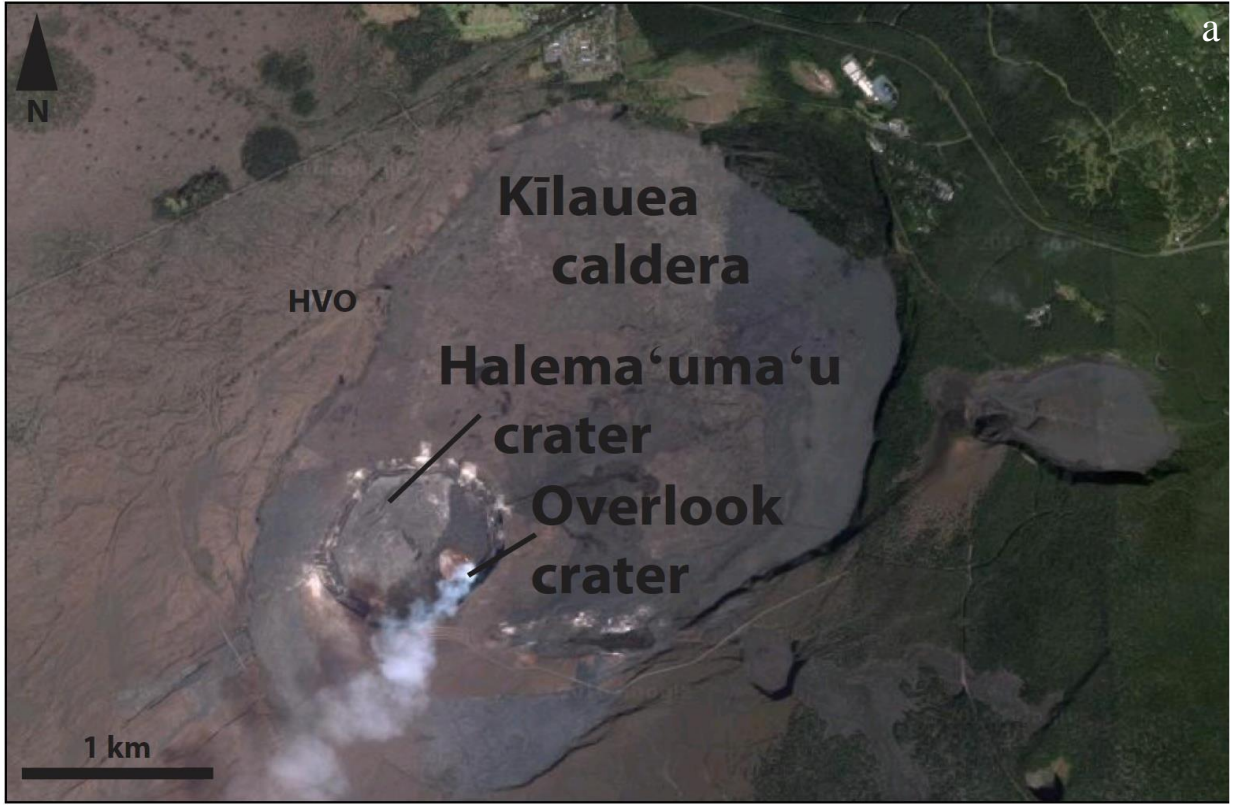


Figure 1.4 (a) Image showing the respective positions of Kilauea caldera, Halema'uma'u crater and Overlook crater (source: Google Earth). **(b)** Photograph of the lava lake within Overlook crater (U.S. Geological Survey photo, September 10, 2016). Note the outgassing activity along the southern margin of the lava lake.

1.4.3.4 Gas Pistoning at the Lava Lake

Gas pistoning events, at the lava lake, consist of the following sequence: a rise in lake levels (when the lake is not spattering) that are terminated by short-lived spattering (marked by high levels of outgassing and tremor) and rapid collapse of the lake surface (Patrick et al., 2015). Gas pistoning occurs when the lake undergoes only passive outgassing at plate boundaries and does not experience major outgassing (spattering) (Patrick et al., 2015). Likely, the lack of significant outgassing causes gas to accumulate below the surface of the lava lake in a shallow foam layer lifting the free surface (Patrick et al., 2015). On the other hand, episodes of spattering brought on by the coalescence of gas bubbles within the shallow foam layer, result in a marked but prolonged increase in outgassing, enabling the lake to gradually decrease in elevation (Patrick et al., 2015). These effects on the surface of the lava lake generally occur along hour-long time scales, although they have declined in intensity since 2013. Video observations combined with and geophysical (seismic and infrasound) measurements (Patrick et al., 2015) indicate that the lava lake shifts between “spattering” and “non-spattering” regimes.

Chapter 2: Spattering Activity at Halema‘uma‘u in 2015 and the Implications for the Transition between Hawaiian and Strombolian Eruptions

2.1 Introduction

Explosive activity in 2015 at the free surface of the Halema‘uma‘u lava lake at Kīlauea exhibited features of both sustained (Hawaiian) fountaining and transient (Strombolian) explosivity. The lava lake thus provides a window into the diversity of basaltic eruptions. Here, I analyze four high-speed videos of activity at the lava lake to quantify this behavior on time scales as short as 2×10^{-3} seconds.

Qualitative descriptions of the four high-speed videos, and one case study of rock fall-triggered activity, are provided and a variety of parameters are quantified and discussed, including bubble dimensions, bubble ascent velocities, initial pyroclast velocities, magma drain back and rebound, mass eruption rate, pyroclast shapes, etc. The amount of mass erupted is considered a measure of magnitude, and activity intensity is measured by the mass eruption rate. These parameters enable us to define this activity formally and to properly place this activity within the spectrum of explosive basaltic eruptions. I contrast my observations with those of Strombolian explosions and Hawaiian fountains in Chapter 4.

2.2 Methods

2.2.1 Data Collection

High-speed videos, filmed at 200 and 500 frames/second with a Phantom[®] MIRO[®] 120 camera, were collected during two field deployments in April and December 2015. The camera was set up along Kīlauea’s caldera rim (Figure 2.1, Table 2.1). The camera location in each case was recorded with a GPS unit, accurate to within 10 m, and a laser range finder was used to measure the distance and azimuth to the free surface. The videos were recorded at 1920×1200

Table 2.1 Video Parameters

Deployment	April 24, 2015	December 8, 2015	December 10, 2015
Camera Type	Phantom [®] MIRO [®] 120	Phantom [®] MIRO [®] 120	SONY [®]
Frames/Second	200	500	30
Seconds/Frame	0.005	0.002	0.03
Focal Length [mm]	70	300	35
Scale	1 pixel = 0.03786 m	1 pixel = 0.10167 m	1 pixel = 0.092 m
Pixels – horizontal	1920	1920	1052
Pixels – vertical	1200	1200	816
Field of View - horizontal [m]	72.7	19.5	96.7
Field of View - vertical [m]	45.4	12.2	75.1
Geographic Location of the Camera [m]	2146974.66 m E 2147159.60 m N	260374.68 m E 260617.47 m N	260673.08 m E 2147237.28 m N
Horizontal Distance between Camera and Lake Surface [m]	Video I: 225 Video II: 220	Video III: 315 Video IV: 315	202
Vertical Distance between Camera and Lake Surface [m]	88	125	115
Lake Surface Distance Below Crater Rim [m]	14	42	42
Azimuth of the Line of Sight [°]	Video I: 306 Video II: 291	Video III: 42 Video IV: 42	295

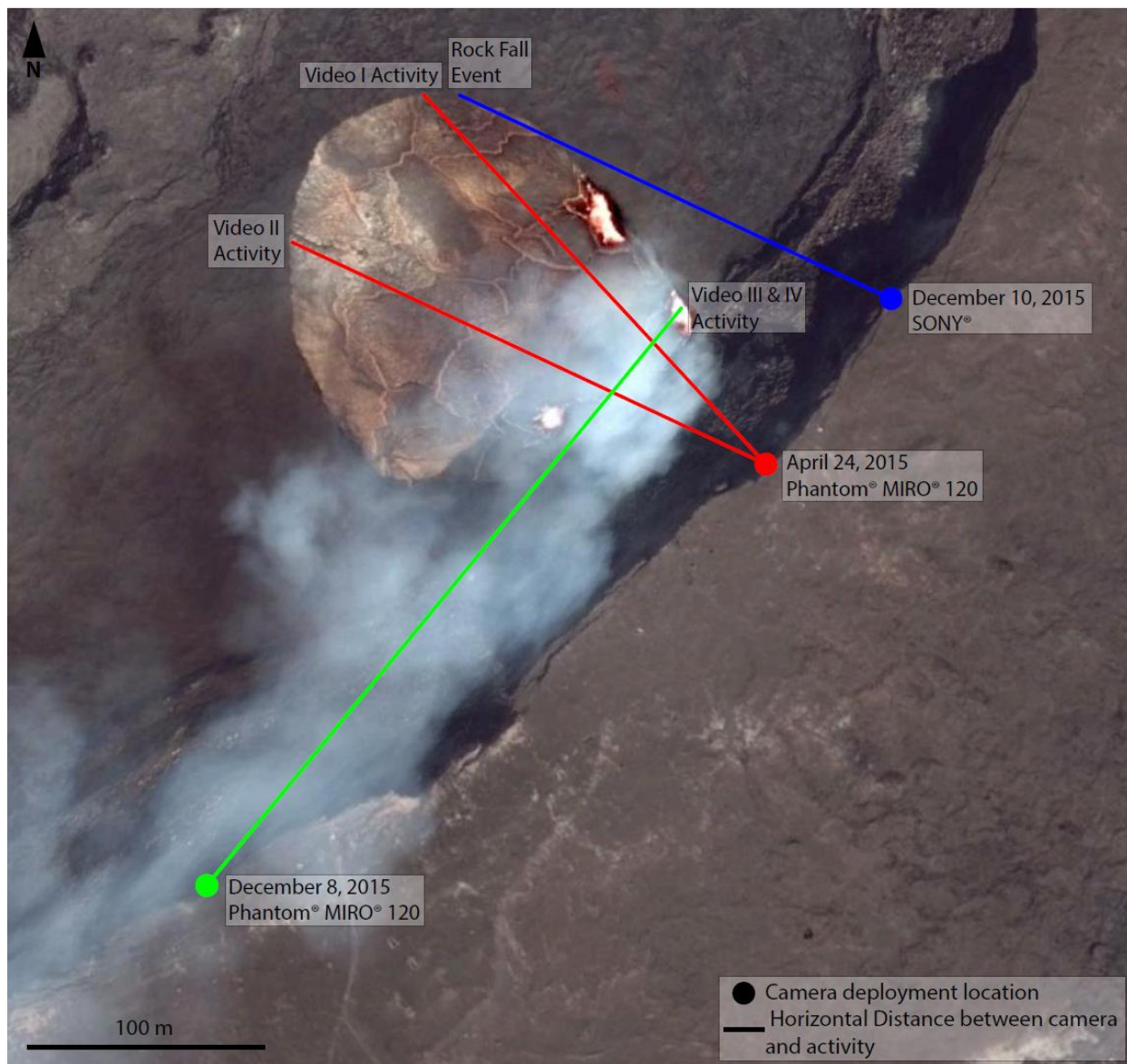


Figure 2.1 Image showing the camera deployment locations along the Kilauea caldera rim and the horizontal distances between the cameras and the activity for the four high-speed videos and the rock fall event video (source: Google Earth).

pixels. For the April deployment, this corresponds to a field of view of about 72.7×45.4 m; videos acquired in December had a field of view of about 19.5×12.2 m.

All of the high-speed videos focused on spattering activity at the lava lake. The high-speed videos, filmed on April 24, focused on the northern region of the lava lake. This is considered a region of almost continuous upwelling. The high-speed videos filmed during the December 8 deployment captured activity in the southeast sink, an area of the lava lake characterized by downwelling and spattering. The footage from December 10, of rock-fall triggered spattering was set up on the caldera rim at a line-of-sight distance of 202 m with a field of view of about 97×75 m. Table 2.1 lists various video parameters for each deployment.

2.2.2 Data Processing

To quantify activity in the high-speed videos, it was necessary to first extract each video frame as a bitmap image. This was done using the Phantom[®] Camera Control application. The images were then loaded into ImageJ, an open source image processing program for additional analyses. Bubbles are identified by a doming of the lava surface. Dimensions of the doming lava surface, inferred to be the bubble, were measured, until just prior to bursting (Figure 2.2). I measured the diameter of the domed surface parallel to the free surface (where the doming lava surface meets the free surface) just prior to the bursting of the bubble. The maximum dome height is measured just prior to bursting, at the center of the doming surface in the plane of the image inferred to be the center of the bubble. Area of a lava dome (again inferred to be the area of the bubble) is calculated using the area formula for an ellipse: $[\pi \times (\text{diameter}) \times \text{height}]$. I assume that most, if not all of the bubble is encased within the doming lava at its maximum height, based on the video footage.

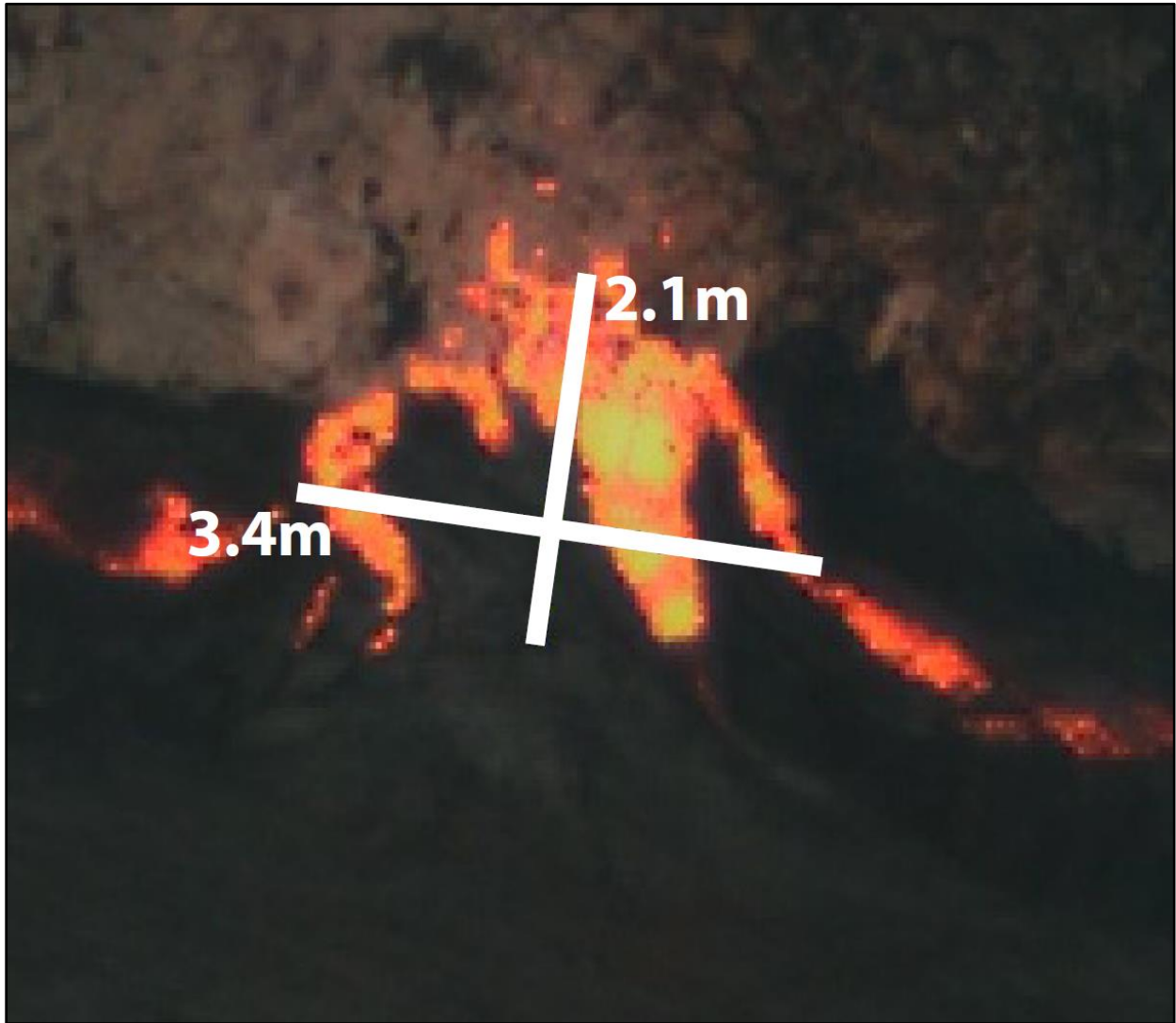


Figure 2.2 Frame from one of the high-speed movies showing how the bubble dimensions (bubble diameter and bubble height) are measured.

Bubble ascent velocities, inferred from the rate at which the doming surface rises upwards regardless of whether or not the surface is crust-capped, are measured when the bubble first observably comes into contact with the free surface (indicated by the first observable doming in the free surface). The rise velocity is the first velocity recorded when the surface first begins to dome. The bursting velocity is the velocity when the bubble bursts, which is visibly noticeable in the images. Bubble ascent velocities, initial pyroclast velocities, and drainage of adjacent melt into the resulting void with or without rebound of a secondary jet (lacking pyroclasts) were measured using MTrackJ, a plug-in for ImageJ. MTrackJ allows the user to track feature change/particle motion by manually selecting an equivalent pixel point in a sequence of images (such as the top point of an emerging bubble). MTrackJ determines the spatial difference between selected points and, using the time elapsed between frames, calculates velocity.

To calculate grain size, mass eruption rate, and to conduct a pyroclast shape analysis, all of the pyroclasts visible in a single image were manually colored in black, while the rest of the image was converted to white, using Adobe® Photoshop®. The binary image was then loaded into ImageJ to calculate the area of each black pyroclast, as well as other shape-related parameters, such as form factor and equivalent diameter of a circle with identical area (to the pyroclast). Because the images are in 2D, pyroclast volumes were estimated by multiplying the area of each by its minor axis. Mass eruption rate was determined using a density measurement of 290 kg m^{-3} (personal communication Houghton, 2016), the inferred total volume of the pyroclasts, and the time separation between images. The density used is the average obtained from 100 Halema'uma'u pyroclasts, collected from a suite of pyroclasts ejected onto the caldera rim, during an unusually vigorous explosion on January 8, 2016.

2.3 Results

2.3.1 Activity and Spattering Styles

I use three terms to classify the behavior I studied at the lava lake: isolated events, clusters of events and prolonged episodes (Figure 2.3). In using the phrase “event” I refer to all of the phenomena associated with a particular bubble rise including: the rise of a doming lava surface (inferred to encase the bubble), the bubble burst, the ejection of pyroclasts, and drain back and rebound (which are described in section 2.3.2). I define *isolated events* as discrete single bubble bursts through the free surface. These bursts throw fluidal bombs, with meter to decimeter diameters, to elevations of meters to a few tens of meters above the collapsing bubble remnant, and typically persist for a few tenths of seconds to seconds, with relatively long repose intervals. *Clusters of events* are closely spaced, repeated bubble bursts grouped around a narrow or point source, which also project fluidal bombs meters to a few meters into the air. *Episodes* (or prolonged episodes) are protracted groupings of numerous bubble bursts that are closely linked in space and time and are most intense, producing repeated, and often overlapping ejection of pyroclasts to meters to tens of meters in height. Prolonged episodes tend to extend along arcs parallel to the lake margin, but have also been observed in the center of the lava lake, and sometimes migrate with the prevailing lava lake circulation. They often persist for tens of minutes to hours.

2.3.2 Drain Back and Rebound

I also identified additional phenomena: drain back and rebound (Figure 2.4). *Drain back* is the flow or drainage of lava lake melt into the cavity that forms after a bubble bursts through the free surface. Upon bursting, the cavity experiences a sudden depressurization causing the bubble cavity to collapse and melt to fill the newly created void. This is associated with each

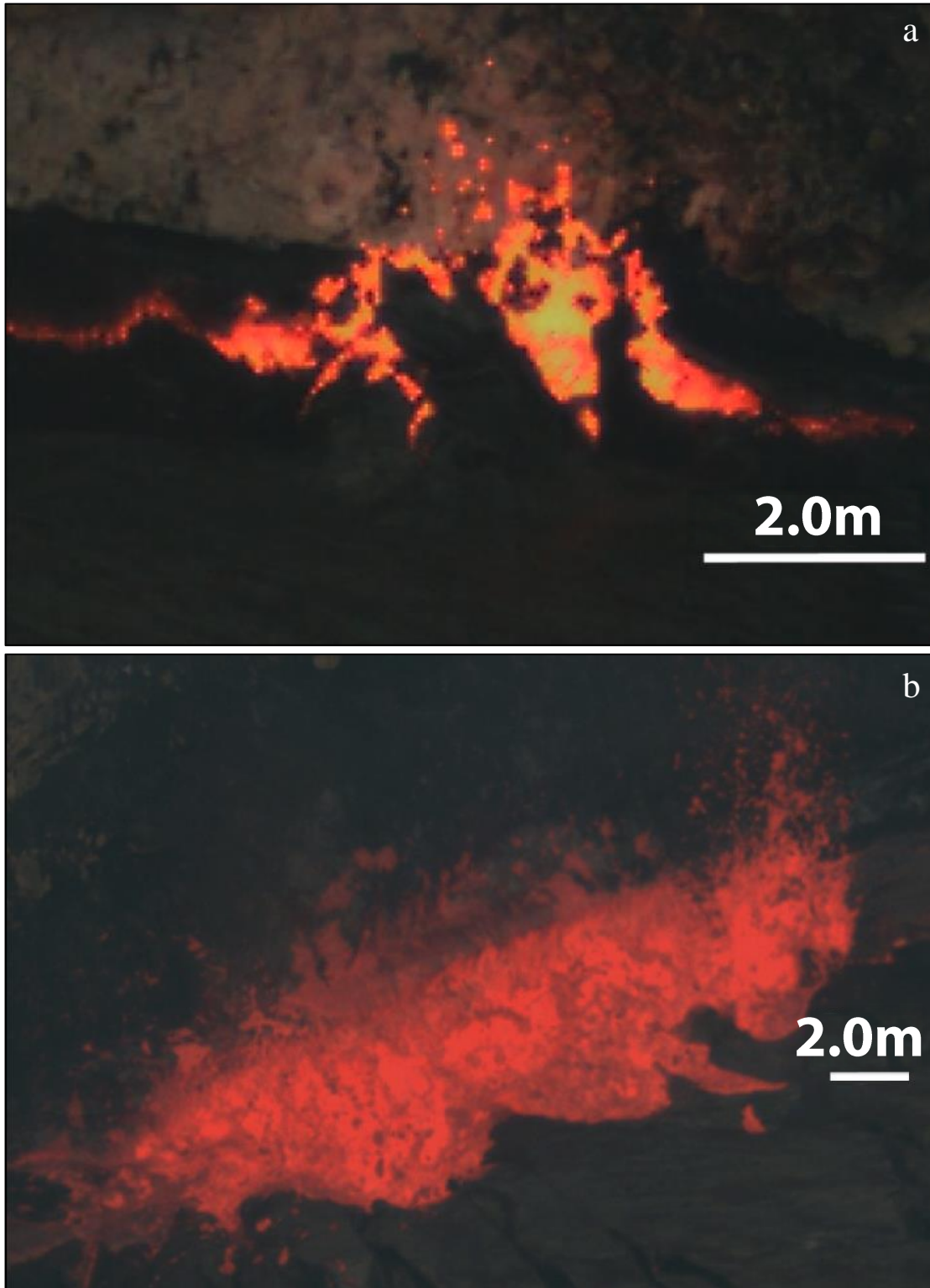


Figure 2.3 (a) Frame from one of the high-speed videos of a typical isolated event. (b) Frame from one of the high-speed videos of a typical prolonged episode.

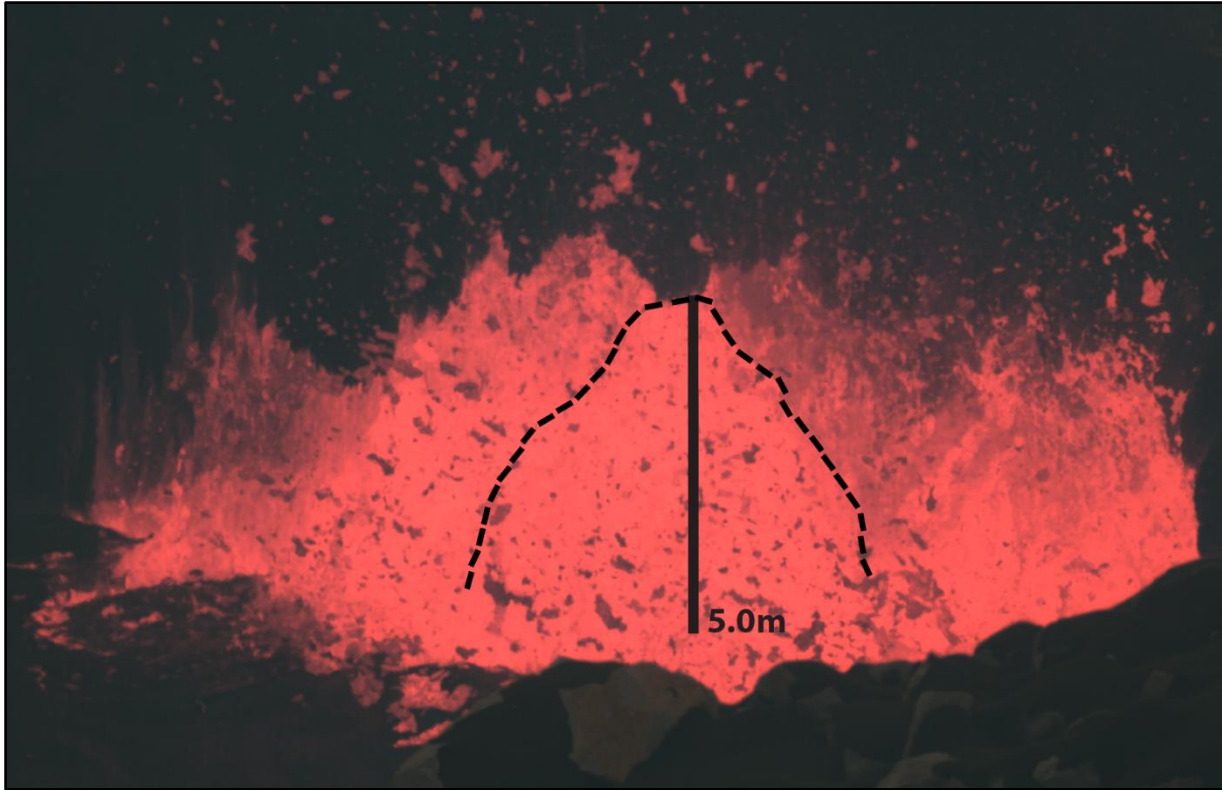


Figure 2.4 Frame from one of the high-speed videos showing how rebound height is measured. The dashed line is drawn along the boundary of the rebound. Pyroclasts ejected during the bursting of the bubble (which causes the depressurization in the cavity and results in the drain back and rebound processes) are descending in the air. The pyroclasts have also cooled significantly from their ejection temperatures based on their darker color, when compared to the surrounding melt.

event, regardless of whether that event is an isolated event, or one of a cluster of events, or one of a prolonged episode. As the cavity is collapsing, some of the melt may be projected vertically, (Orr, 2014), which we refer to as *rebound*. This projected melt rises as a jet, but does not fragment and instead simply descends after reaching its (the rebound's) peak height. No pyroclasts were associated with the rebounds from any of the events described here.

2.3.3 Relationship to the 24-hour Patterns of Lava Lake Behavior

I analyzed four high-speed videos, two of which were recorded on April 24, 2015 (referred to as Videos I and II), and two of which were recorded on December 8, 2015 (referred to as Videos III and IV). Videos I and II filmed regions in the northern portion of the lava lake and each lasted for 18.26 seconds. Video I includes a single isolated event, referred to as Event A. Video II records part of a prolonged episode. I selected four events composing the episode to investigate in greater detail; I refer to these events as Events B, C, D and E. Videos III and IV filmed isolated events occurring in the southeast sink and both recorded 7.30 seconds of footage. Video III contains Event F and Video IV contains Event G. These details are summarized in Table 2.2.

Table 2.2 Videos and Events

Video	Date and Time of Filming [HST]	Video Length [s]	Event	Event Type	Event Location
I	April 24, 2015 – 8:47	18.26	A	isolated events	northern region
II	April 24, 2015 – 9:22	18.26	B C D E	events composing a prolonged episode	started in the northern region then migrated along the rim to the western region
III	December 8, 2015 – 13:16	7.30	F	isolated events	southeast sink
IV	December 8, 2015 – 14:28	7.30	G	isolated events	southeast sink

The following is a brief description of how the seven events analyzed, using the high-

speed camera, relate to activity on a broader time scale. Chapter 3 goes into greater detail with regards to 24-hour patterns of activity. I can place Events A through E within a 24-hour time window, on April 24, 2015, over which the location and duration to a precision of 1 seconds of all events was analyzed (see Chapter 3).

Event A was one of 1,760 isolated events to occur within a 24-hour window at the lava lake. Event A occurred in the upwelling region near the northern edge of the lava lake, close to the crater wall, where many similar events took place. Event A lasted for 2.45 seconds, which is shorter than the average of 6 seconds for isolated events which occurred during this 24-hour period. The duration of Event A, however, still fell within one standard deviation of the average duration.

Events B, C, D, and E, belonged to a prolonged episode; the prolonged episode was one of 21 episodes to occur within the 24-hour period bracketing the filmed episode. This particular episode lasted for 2.29 hours, which was longer than the average of 1.74 hours, for prolonged episodes within this 24-hour period, but still within one standard deviation. The frame rate on HVO's 24-hour webcam did not have a high enough resolution to depict how many events made up the episode. The high-speed camera recorded 28 events within the episode during the 18.26 seconds the camera was filming.

Events F and G occurred in the southeast sink, which was out of the field of view for the web camera that recorded the 24-hour video. Therefore these events were not placed within a similar 24-hour context, as the ones on April 24 were.

2.3.4 Grain Size Analysis Calculations

I conducted a grain size analysis for transported pyroclasts for all of the events. I calculated an approximate volume of each pyroclast by assuming the two smaller axes are

identical, and thus multiplying the area by the minor axis, which were computed in ImageJ. The mass was calculated for the frame with the greatest number of ejected particles, and for frames both before and after the frame with the maximum number of ejected pyroclasts at intervals of 0.1 seconds.

The mass eruption rate was derived by dividing the change in mass by 0.1 seconds. An average mass eruption rate was also calculated for each event by averaging the mass of pyroclasts visible in the image from the peak of the explosion and dividing it by the lapsed time. This assumes no clasts had been lost from the jet by that time, which is a reasonable observation based on the images. Mass eruption rate serves as the principal measure of intensity in the analysis presented below.

2.3.5 Rock Fall-Triggered Activity

Rock falls from the crater wall have been observed both when the lava lake is rising, triggered by thermal expansion, and when the lava lake is falling, due to collapse of the juvenile lava veneer adhered to the crater walls. Large blocks of the fresh lava often break off and fall into the lake. Although most spattering activity results from decoupled gas bubbles rising from within the lava lake, rock falls act as an additional, random, external trigger for outgassing. As the event discussed below illustrates, rock falls can start spattering activity by disturbing the lava lake and initiating outgassing. Such an event is depicted in Figure 2.5 and described below.

2.3.5.1 Event Description

A rock fall-triggered prolonged episode was recorded by a SONY® camera filming at 30 frames/second, on December 10, 2015. Initially a rock mass, of area 11.1 m^2 fell, about 32 m from the crater wall to the lake's surface reaching a velocity of 51.2 m s^{-1} at impact. Upon impacting the lake, the rock created a void in the free surface. As the rock descended down into the lava lake the surrounding melt drained into the void space and fountained to a height of 19 m,

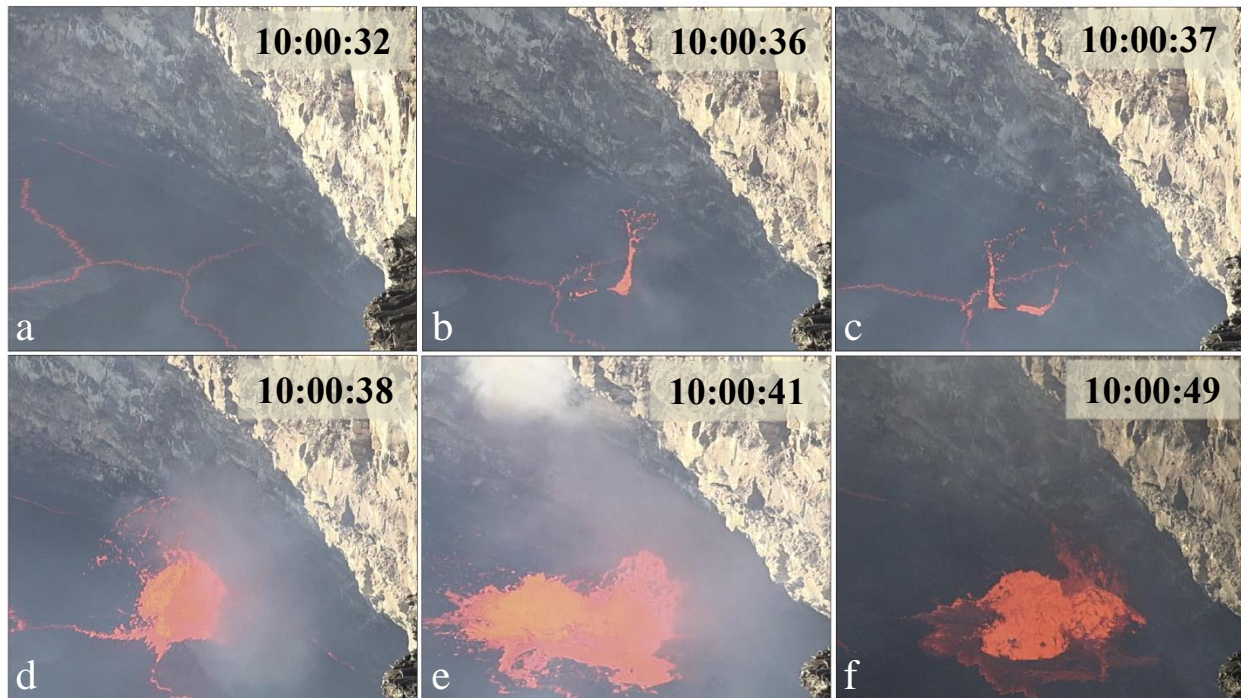


Figure 2.5 Still frames from the rock fall video showing (a) the undisturbed free surface of the lava lake; (b) spattering triggered by the first rock fall to the right (to the left the second rock fall is just impacting the free surface); (c) spattering triggered by the second rock fall, on the left, while to the right spatter from the first rock fall is falling back; (d) the initial spattering triggered by the third rock fall; (e) sustained ongoing spattering triggered by the third rock fall; (f) continued spattering triggered by the third rock fall, with bursting bubbles that have become more uniform/round in shape with compared to the events composing the spattering in image e.

at an initial rate of 35.8 m s^{-1} . The spatter area was approximately 37 m^2 .

About 0.73 seconds after the first rock began its descent, a second rock mass, about 12.2 m^2 in area, fell about 35 m from the crater wall to the free surface, reaching a velocity of about 48.2 m s^{-1} . The lake reacted similarly to the first rock fall, and melt flowed into the void in the lava lake and rebounded upward attaining a height of 16 m, at an initial velocity of 38.5 m s^{-1} , and generating a spatter area of about 22 m^2 .

A significantly larger volume of rock, with an area of approximately 234 m^2 , then fell about 1.8 seconds after the second rock fall (2.6 second from the first rock). The third rock fall descended about 24 m to the lake's surface, also reaching a velocity of about 36.1 m s^{-1} . In response, a prolonged episode was triggered, lasting longer than the length of the video (which recorded for about 18 more seconds). Based on the webcam, the prolonged episode lasted for a total of 28 seconds. The first bubble-bursting event resulting from the third rock fall generated an area of about 234 m^2 of spatter initially, which ascended at a speed of about 58.8 m s^{-1} . Following the initial event, eight additional events were identified (during the remainder of the video). Immediately following the rock fall, the bubbles were irregularly shaped and did not rise nor burst uniformly; near the end of the video, the bubbles became more rounded and burst uniformly.

2.4 Interpretations

2.4.1 Descriptions of the Four High-Speed Videos

As discussed in section 2.3.3, and outlined in Table 2.2, four high-speed videos were recorded that collectively contain seven events, which are interpreted in further detail below. Video I filmed for 18.26 seconds on April 24, 2015. Event A was the first and main event captured by the high speed camera, and occurred at 08:47 HST. Immediately afterwards, the free

surface (having been disturbed by the event) began to reestablish stability and at least four relatively small isolated events, all ejecting pyroclasts, occurred along the edges of the original area of activity.

Video II, recorded on April 24, 2015, filmed 18.26 seconds of a prolonged episode where multiple bubble bursts occurred and overlapped with each other both spatially and temporally. Below I describe four of these bubble bursting events (Events B, C, D, and E) which occur at 09:22 HST, within the 2.29-hour-long episode. The episode began at 09:01:18 HST, and was originally focused on a single point source along the northern margin of the lake. About 24 seconds after onset, the spattering had elongated along the lake margin and increased in height. The spattering continued to extend, until splitting into two separate spattering sources at 09:04:52 HST. One of these sources moved towards the center of the upwelling area and then died, while the other migrated along the margin of the lava lake with the prevailing flow direction towards the south, continuing to elongate and increase in vigor. The four discrete bubble bursting events quantified below occurred during this part of the source's life-span, when the source was 23 m long. At 10:19:33 HST, the source again split into two, but recombined at 10:26:11 HST. Afterwards, the source continued to migrate along the lake margin towards the south, but died at about 11:18:47 HST, (after 34 seconds of waning) before reaching the southeast sink. Approximately 28 discrete bubble bursting events were recorded during Video II, including Events B, C, D, and E. Assuming that the rate at which events occur is relatively consistent over the duration of a prolonged episode's life, over 12,000 events may have made up the episode over the 2.29 hours that it lasted. Note that many events making up a prolonged episode overlap with each other in space and time.

Video III was recorded at 13:16 HST on December 8, and focused on the southeast sink for 7.30 seconds. One isolated event recorded during this time, Event F, is quantified below. Event F occurred in the center of the sink and was the first event to take place in the recording. In addition to Event F, there were at least four other observed events, two of which occurred on the western side of the southeast sink and that were partially obscured by the overhang. A third occurred on the eastern edge of the sink. The fourth occurred in the center but was smaller than Event F and projected pyroclasts lower than those associated with Event F.

The final video, Video IV was recorded at 14:28 HST on December 8 for 7.30 seconds. Event G was recorded during this video and is positioned in the center of the southeast sink. Other events occurred and overlapped with each other, immediately following Event G.

Figures 2.6, 2.7, and 2.8 visually and graphically depict some of these events. The events and their associated parameters are described in detail below. Some of the measurement methods were outlined in section 2.2.2. Pyroclasts used in the initial velocity ejecta calculations were chosen based on image resolution and the clearness of their trajectories, which was generally less than the number of pyroclasts observed in the event. The number of observed pyroclasts was used for the mass calculations and related shape and size calculations of the particles.

2.4.1.1 Event A

Event A, a short-lived isolated event, was at the low end of the intensity spectrum observed in the April and December 2015 high-speed videos. The event occurred at 08:47 HST on April 24, 2015, near the upwelling portion of the lava lake, close to the crater wall. At first, the lake's free surface rose with the Event A bubble, but as the bubble continued to rise and stretch the crust, it tore open and collapsed. The bubble first emerged through the free surface at a rise velocity of 2.3 m s^{-1} , measured as the rate at which the surface domed up, including when

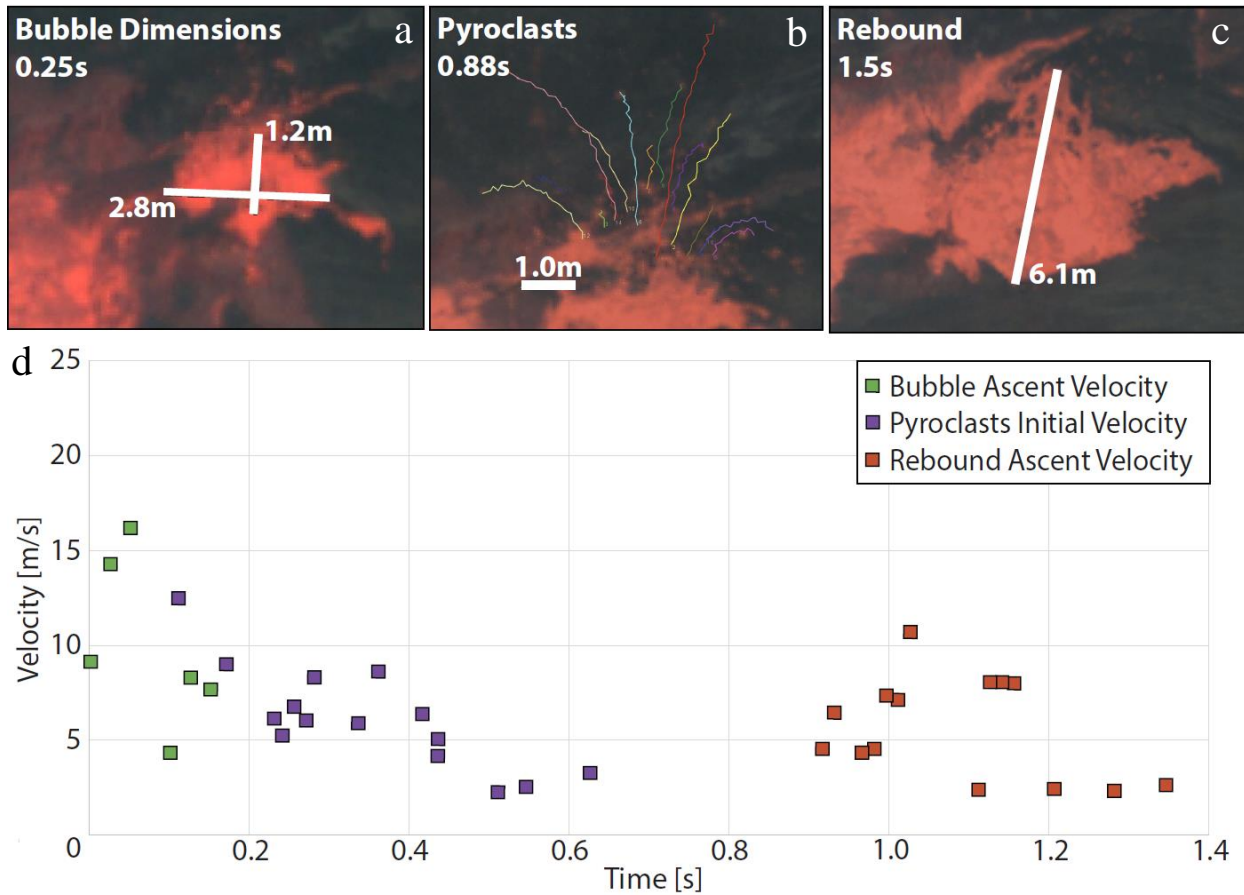


Figure 2.6 (a) Frame showing bubble dimensions of Event B. (b) Frame from ImageJ showing the trajectories of pyroclasts from Event B. (c) Frame showing the rebound height of Event B, based on the direction over which the rebound rose. (d) Time-series plot showing the velocity measurements of key features in Event B including: bubble ascent rate, initial pyroclast velocities, and rebound ascent rate. Event B was one of the weaker events.

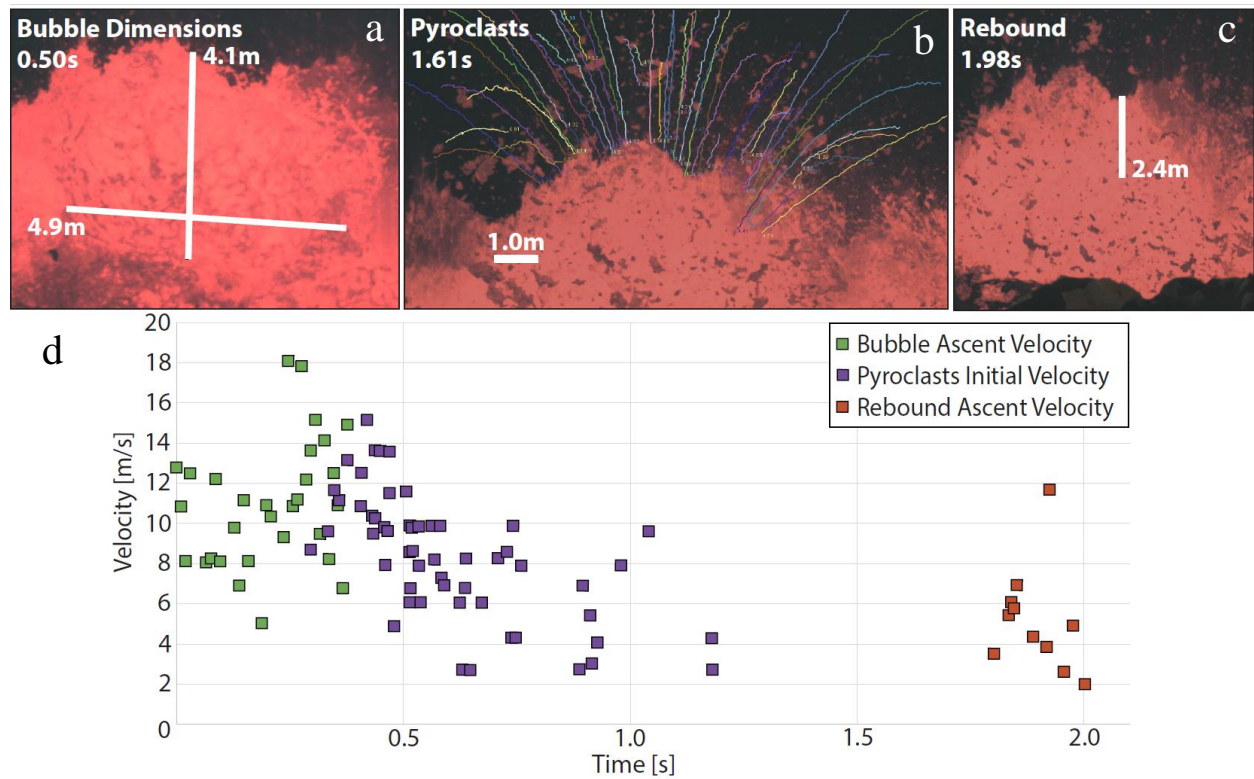


Figure 2.7 (a) Frame showing bubble dimensions of Event F. (b) Frame from ImageJ showing the trajectories of pyroclasts from Event F. (c) Frame showing the rebound height of Event F. (d) Time-series plot showing bubble ascent rate, initial pyroclast velocities, and rebound ascent rate for Event F, which was one of the higher intensity events.

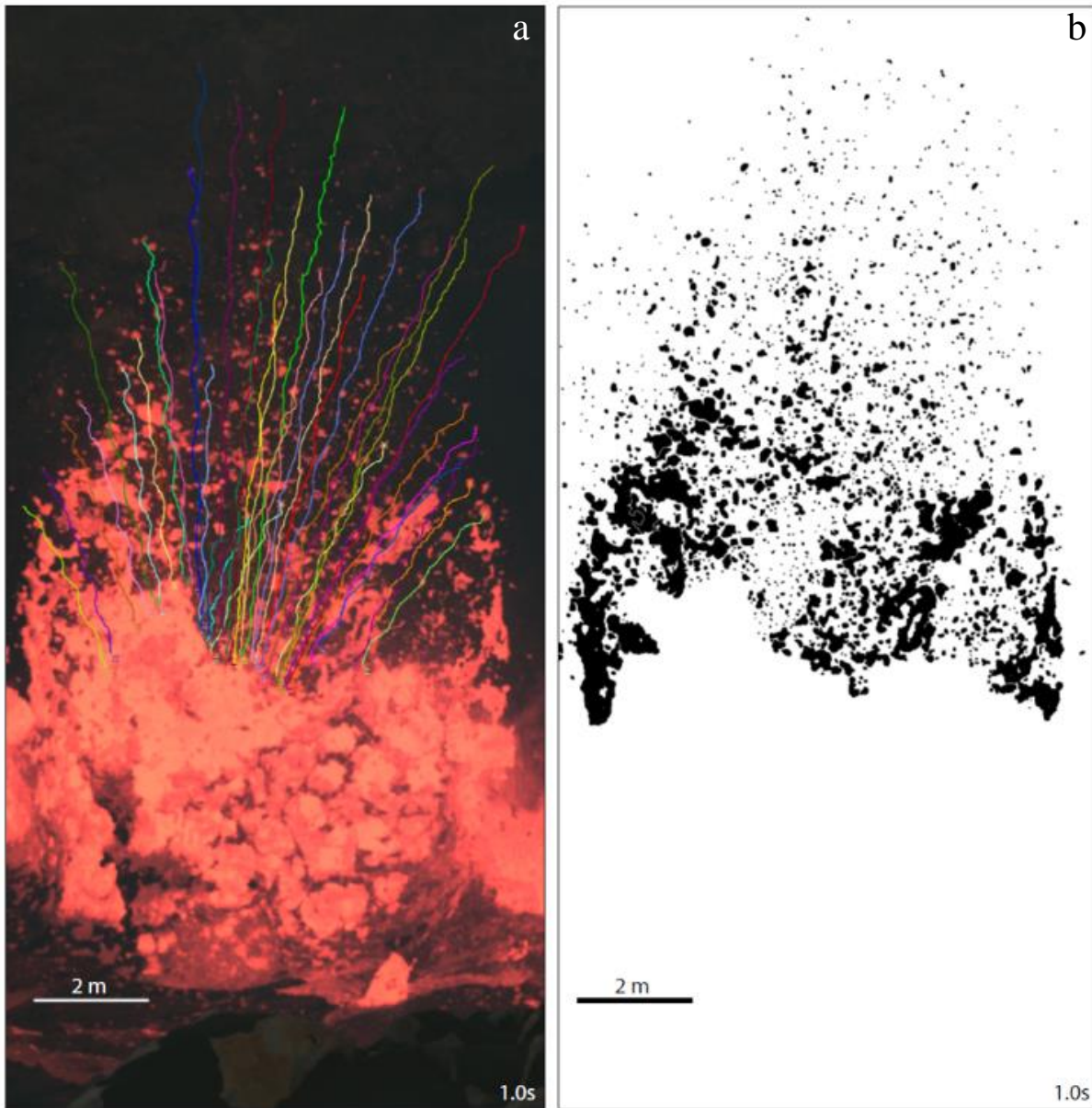


Figure 2.8 One frame from Event G (a high intensity event) focusing on ejected pyroclasts, 1.0 seconds from the start of the event. Image (a) depicts the pyroclast projection patterns and the paths along which they travel. Image (b) has been processed in Photoshop to show all of the ejected pyroclasts in black; the rest of the image turned white. Viewing the event in this way enables better visualization of the pyroclasts. This binary image (along with others) was also used in a variety of calculations including: MER, grain size, and shape analyses.

the surface was initially crust-capped and through to after the crust had collapsed away. Its velocity increased steadily until peaking at 6.1 m s^{-1} (representing the bursting velocity) 0.2 seconds into the event, after which the velocity abruptly dropped. The doming of the lava surface reached a maximum height above the surrounding surface of the lava lake of 2.1 m and a diameter at the time of bursting of 3.4 m. The domed surface rose and burst over a duration of 0.40 seconds.

The first pyroclasts were ejected about 2.16 seconds after the first sign of doming. 24 pyroclasts were chosen to calculate the mean initial velocity of the measured pyroclasts, which was 7.8 m s^{-1} . The total ejected mass was 105 kg. The average mass eruption rate was approximately 300 kg s^{-1} . Pyroclasts were mostly ejected from the peak of the domed lava surface, as the bubble burst through the top of the dome. Pyroclasts, ranging in diameter from $4.3 \times 10^{-2} \text{ m}$ (4.3 cm) to 1.2 m, were ejected during the event.

A subsequent rebound of melt from below the free surface became visible 0.70 seconds after the start of the event. The rebound attained a maximum height of 1.8 m. The rebound velocity peaked at 5.6 m s^{-1} at a time 0.76 seconds into the event, and then steadily decreased thereafter.

2.4.1.2 Event B

This event was of relatively low intensity; a meter-sized bubble rose along the north edge of the spattering source (through a crust-capped part of the lava lake surface), subsequently extending the length of the source. The bubble initially emerged with a rise velocity of 9.1 m s^{-1} . The velocity increased gradually, peaking at 16.2 m s^{-1} (representing the bursting velocity), 0.23 seconds into the event, after which the velocity decreased. The doming of the lava surface

attained a maximum height of 1.2 m and a diameter at the time of bursting of 2.9 m, and rose and burst over 0.18 seconds.

The first pyroclasts were ejected about 0.11 seconds into the event. The mean initial velocity of 16 measured pyroclasts was 7.2 m s^{-1} . At least 55 pyroclasts were ejected, which ranged in diameter from $1.2 \times 10^{-1} \text{ m}$ (12 cm) to $7.9 \times 10^{-1} \text{ m}$ (79 cm). A total of 200 kg of mass was ejected, and the average mass eruption rate was approximately 4320 kg s^{-1} . Ejecta were mostly focused at the peak of the domed lava surface, inferred to be the center of the bubble.

A subsequent rebound, made up of melt draining from below the free surface into the cavity, rose into view 0.70 seconds after the event began. The rebound reached 4.6 m in height. The rebound velocity reached a maximum rate of 10.7 m s^{-1} , 1.05 seconds after the doming first began, after which the velocity decreased with time. The average rebound velocity was 5.5 m s^{-1} .

2.4.1.3 Event C

Event C was a moderate intensity event involving a bubble rising from the crust-free portion of the spattering source. As the bubble associated with Event C was rising, other bubbles (part of the 28 which made up the spattering source over the 18.26 seconds of filming) were also rising and bursting in the vicinity. Due to these conditions, I was unable to measure the pre-bursting rise velocity of the doming lava surface. The event is first distinguishable just as the bubble bursts. Consequently, I do not have a time for when the lava dome first appeared (i.e., the start of the event), so the times and durations listed below are relative to the time of bursting (when the event was first identifiable). The bubble had a bursting velocity of 20.3 m s^{-1} , and the domed lava surface rose to a maximum height of 1.6 m and had a diameter of 3.3 m, at the time of bursting. After bursting, pieces of the lava dome walls continued to rise for an additional 0.15 seconds, although the velocity decreased with time.

The first pyroclasts were ejected at 0.14 seconds after the bubble burst. The mean initial velocity of 18 measured pyroclasts was 7.4 m s^{-1} . At least 78 pyroclasts, ranging in diameter from $9.0 \times 10^{-2} \text{ m}$ (9 cm) to $6.8 \times 10^{-1} \text{ m}$ (68 cm), were ejected. A total mass of 155 kg was measured. The average mass eruption rate was approximately 8900 kg s^{-1} . Although pyroclasts were mainly ejected from the peak of the domed lava surface, pyroclasts from this event were relatively more widely dispersed.

Melt from underneath the free surface drained back and rebounded 0.90 seconds after the bubble burst. The rebound attained a maximum height of 2.2 m. The rebound velocity increased relatively steadily to 7.7 m s^{-1} , at 1.01 seconds into the event; afterwards, the rebound velocity decreased. The average rebound velocity was 3.9 m s^{-1} .

2.4.1.4 Event D

This event was of relatively higher intensity compared to the other events; a bubble rose along the north edge of the spattering source through a crust-capped surface. The bubble initially reached the surface at a rise velocity of 6.1 m s^{-1} . Its velocity increased and the bubble burst at 9.8 m s^{-1} , 0.36 seconds into the event; after which the velocity declined. Compared to other events, the Event D bubble rose for a longer amount of time, prior to bursting. Consequently, the lava dome itself was vertically elongated in shape. This may imply that the rising decoupled gas bubble had an overall elongated shape. The bubble's maximum height was 1.8 m and the bubble's diameter at the time of bursting was 2.9 m. The doming of the lava surface rose over for 0.44 seconds.

The first pyroclasts were ejected about 0.22 seconds after the start of the event. The mean initial velocity of the 17 measured ejecta was 11.6 m s^{-1} . At least 125 pyroclasts were ejected and ranged in diameter from $8.0 \times 10^{-2} \text{ m}$ (8 cm) to 1.5 m. The total ejected mass was about 860 kg.

The average mass eruption rate was approximately $17,030 \text{ kg s}^{-1}$. Ejecta were focused tightly at the peak of the domed lava, more so than in any of the other events I quantified.

A rebound, composed of melt flowing from below the free surface, was first observed 0.83 seconds after the onset of the event. The rebound attained a maximum height of 2.2 m. The rebound velocity increased quickly to a maximum rate of 16.4 m s^{-1} , at 1.04 seconds into the event. The rebound had an average velocity of 6.4 m s^{-1} .

2.4.1.5 Event E

This event was of low intensity, and was unique in that the bubble associated with the event did not rise nor burst symmetrically. The northwest-margin rose quicker than, and burst before, the southeast-margin of the bubble. As a result, all observed pyroclasts were ejected from the northwest side of the bubble.

The Event E bubble rose through a crust-free surface in a relatively calm region of the spattering source, which enabled me to view the lava dome rise upwards through the free surface. When the lava dome first appeared, the rise velocity of the northwest-side of the dome, at 13.3 m s^{-1} , was not only significantly higher than the southeast-margin of the dome (5.0 m s^{-1}), but also was higher than the initial rise velocities of the other events. Only 0.08 seconds after the lava dome became visible, the northwest-margin attained a bursting velocity of 14.2 m s^{-1} . Similar to other events, the ascent rate on the southeast-margin of the event gradually increased until the event reached a bursting velocity of 13.6 m s^{-1} , 0.38 seconds into the event. The rise velocities of the dome (for both sides) was measured based on the rate at which the surface rose. The lava dome reached a height of 6.1 m above the surface of the lake, and a diameter at the time of bursting of 5.2 m. The northwest-margin of the dome rose for 0.15 seconds and the southeast-margin of the dome for 0.45 seconds.

The first pyroclasts were ejected about 0.21 seconds after the surface first began to dome upwards. The mean initial velocity of 12 measured clasts was 7.4 m s^{-1} . All measured and observed pyroclasts, 34, were ejected along the northwest-margin of the lava dome, with a total mass of 740 kg. These pyroclasts had diameters between $9.0 \times 10^{-2} \text{ m}$ (9 cm) and 1.3 m. The average mass eruption rate was approximately $2,740 \text{ kg s}^{-1}$.

A subsequent drain back and rebound related to the bubble burst became visible 0.57 seconds after the start of the event. The rebound attained a maximum height of 4.2 m. The rebound velocity increased swiftly to a maximum rate of 16.0 m s^{-1} , 0.83 seconds into the event. The average rebound velocity was 7.3 m s^{-1} .

2.4.1.6 Event F

Event F, an isolated event and one of the highest intensity events in this study, formed in the southeast sink and generated a wide dispersal of pyroclasts. The Event F bubble burst through a crust-free surface. The initial rise velocity was 12.9 m s^{-1} , measured as the rate at which the lava dome ascended. The dome's velocity increased progressively and peaked at 18.1 m s^{-1} , 0.26 seconds from when the dome first became visible, after which the velocity decreased. The domed surface rose to a maximum height of 4.1 m and attained a diameter at the time of bursting of 4.9 m. The doming of the lava surface lasted for over 0.39 seconds.

The first pyroclasts were ejected about 0.23 seconds after the dome first became visible. The mean initial velocity of 56 measured ejecta was 8.6 m s^{-1} . At least 1,195 pyroclasts, ranging in diameter from $1.1 \times 10^{-2} \text{ m}$ (1.1 cm) to 2.3 m, were ejected during the event, generating a total mass of 2,400 kg. The average mass eruption rate was approximately $87,000 \text{ kg s}^{-1}$. Pyroclasts were mostly ejected from the peak of the domed lava surface; however, unlike the other events,

the pyroclasts spread out in a much wider pattern, farther from the center than was observed in any of the other studied events.

Drain back and rebound of melt from below the free surface appeared after 0.41 seconds, reaching a maximum height of 2.4 m. The rebound velocity peaked at 11.7 m s^{-1} , at 0.69 seconds into the event. The average rebound velocity was 5.2 m s^{-1} .

2.4.1.7 Event G

Event G, another one of the higher intensity events in this study, formed as an isolated event in the southeast sink, and generated a relatively narrow dispersal of products. The initial rise velocity of the lava dome was 10.7 m s^{-1} . The velocity of the rising lava dome increased relatively steadily and peaked at, 36.2 m s^{-1} , 0.23 seconds into the event, when the bubble burst. The ascent rate decreased abruptly thereafter. The domed surface attained a maximum height of 3.4 m and a diameter at the time of bursting of 5.9 m. The dome rose for 0.29 seconds.

The first pyroclasts were ejected about 0.28 seconds after the start of the event. The mean initial velocity of the 42 measured pyroclasts was 12.7 m s^{-1} , based on their resolution and the clearness of their trajectory paths. As many as 1,803 pyroclasts, ranging in diameter from $1.1 \times 10^{-2} \text{ m}$ (1.1 cm) to 2.6 m, were ejected during the event. Pyroclast dispersal for this event was relatively narrow, compared the other events. The total ejected mass was 2,890 kg. The average mass eruption rate was approximately $52,540 \text{ kg s}^{-1}$. Ejecta was mostly expelled from the peak of the domed lava surface.

Rebound was not recorded because, after the Event G burst, other events immediately followed, obscuring the field of view.

2.4.2 Pyroclast Dispersal Patterns

All of the events, except for Event E, expelled pyroclasts from the peak of the domed lava surface, as the bubble burst through the top of the dome. Pyroclasts were ejected asymmetrically from the northwest-margin of the lava dome associated with Event E. This is likely because the northwest-margin of the dome rose faster and burst before the southeast-margin. In doing so, all of the observed pyroclasts were ejected from the northwest-margin and were directed in an angle away from the bubble.

For some of the events pyroclasts were more focused centrally at the top of the lava dome and were propelled upwards in a collimated and elongate fashion, characterized by a horizontally-narrow pyroclast dispersal range. For instance, during the ascent of pyroclasts associated with Event D, the width of pyroclast dispersal was only about 6 m. On the other end of the spectrum, pyroclasts tended to fan out in a much wider dispersal pattern. During their ascent, pyroclast dispersal was about 17 m in width for pyroclasts from Event F. The other events fell between these two extremes in terms of the width of dispersal amongst the pyroclasts upon ejection.

2.4.3 Analysis and Interpretation of Grain Size Data

A plot of median diameter versus average mass eruption rate is presented in Figure 2.9a, for the video frame for each studied event during which the maximum amount of erupted mass was present. The median diameter is measured as the grain size value at the 50th percentile on a cumulative grain size plot. While there is some scatter at lower mass eruption rates, the plot displays a broad contrast between low and high intensity events. This supports the notion that fragmentation is greater for higher intensity events. Figure 2.9b plots total mass versus average mass eruption rate. The total mass is measured as the sum of the mass of all the pyroclasts present in the frame when the maximum amount of erupted mass was present. There is a

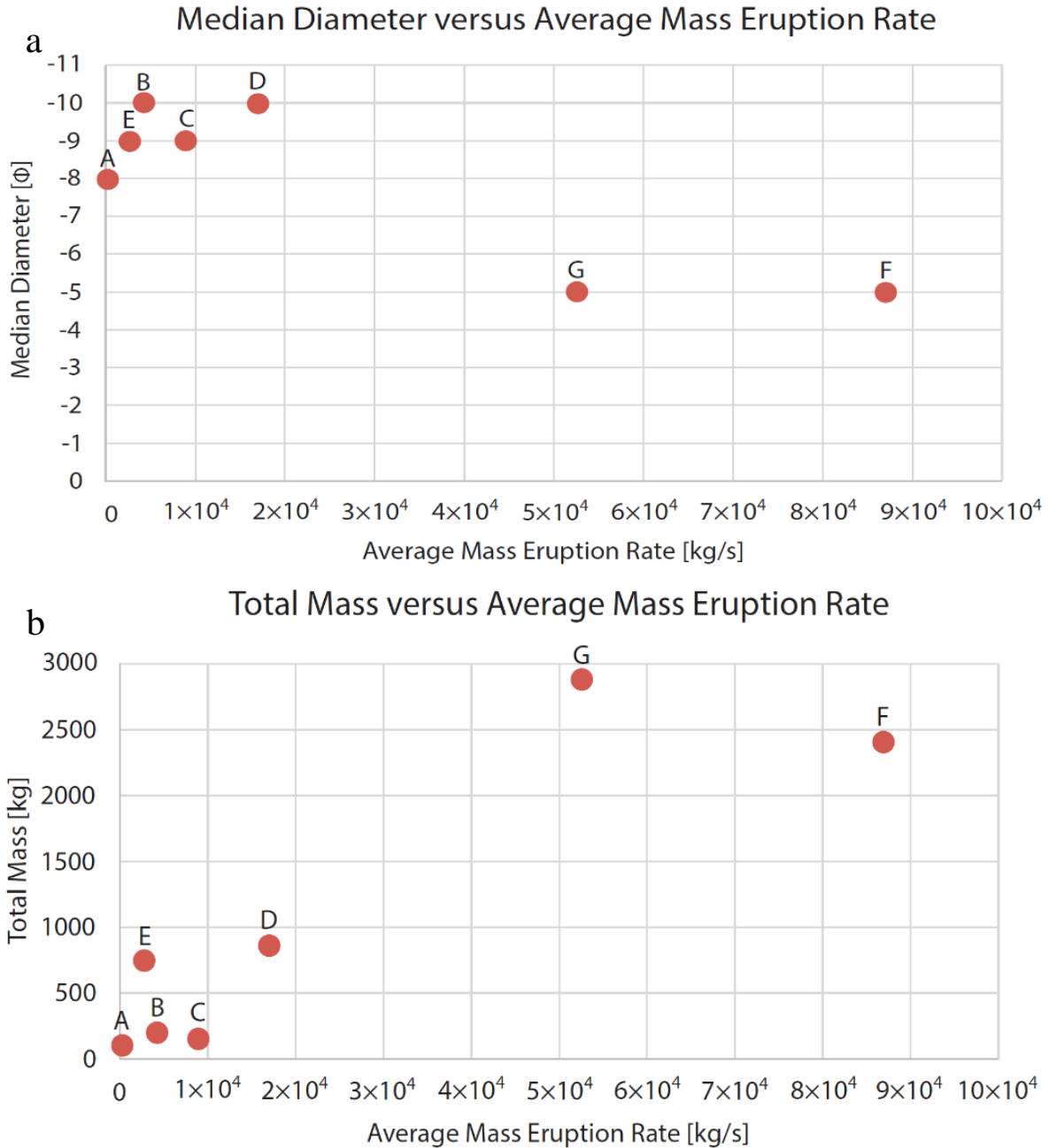


Figure 2.9 (a) Plot of the median diameter versus average mass eruption rate for each event, showing that high intensity events resulted in increased fragmentation. Median diameter is calculated as the grain size value at the 50th percentile on a cumulative grain size plot (Figure 2.11) (b) Plot of total mass versus average mass eruption rate for each event, showing that higher intensity events erupt more mass.

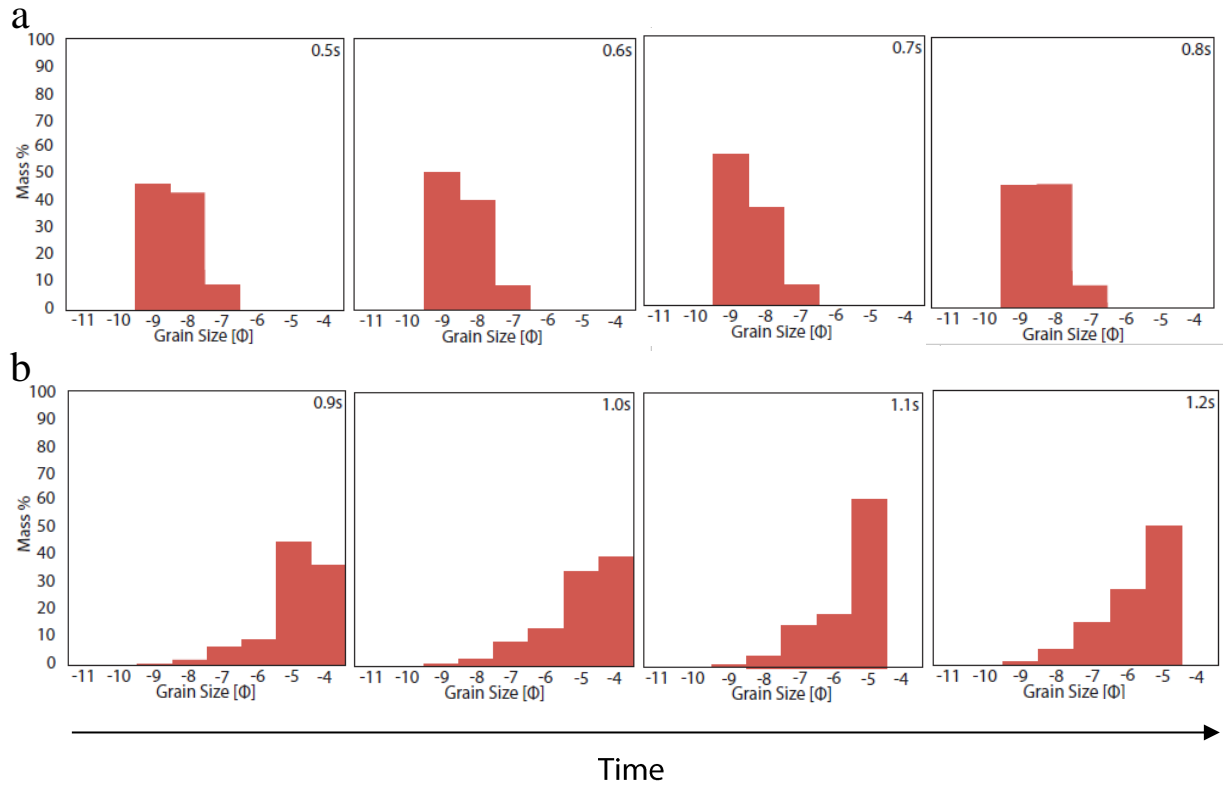


Figure 2.10 The elapsed time in the upper right corner of each plot is measured from the start of the event, so time increases towards the right of the page. **(a)** Mass percentage versus grain size plots for Event C, a low intensity event. The maximum amount of ejected mass was airborne at 0.7 seconds from the start of the event. **(b)** Mass percentage versus grain size plots for Event F, a high intensity event. The maximum amount of ejected mass was airborne 1.0 seconds from the start of the event. Note that these are not complete “total” grain size histograms due to limitations in discerning particles smaller than -4ϕ (16 mm).

predictable contrast between high and low intensity events. This reaffirms that higher intensity events erupt a greater amount of mass, i.e., that magnitude and intensity scale.

I also binned the clast data into phi groupings from -11ϕ (2048 mm) to -4ϕ (16 mm) based on the size of the minor axes. I plotted a histogram, for each image, of mass percent versus grain size. Figures 2.10a and 2.10b depict the grainsize histograms of a weak and a high intensity event, respectively. When the histograms are compared with each other over time (during each individual event), they represent a mostly stable grainsize distribution, suggesting that fragmentation efficiency is relatively constant with time. Note that each plot represents a point in time during a single isolated event and is in essence a “total” grain size distribution, except where the smallest ejecta may be below the resolution limit for the camera. For instance, the high intensity histogram in Figure 2.10b is incomplete as I cannot resolve particles smaller than -4ϕ (16 mm) in diameter. I also plot an example of my grainsize distributions alongside grainsize data for two much more powerful eruptions: the 21-24 July 2001 basaltic subplinian eruption of Etna (Scollo et al., 2007) and the May 2008 silicic Plinian eruption of Chaitén volcano (Alfano et al., 2016) (Figure 2.11). This histogram shows that, on a global scale, the trend of decreasing grain size (efficiency of fragmentation) with increasing eruption intensity is maintained over many orders of magnitude of mass discharge rate.

Figure 2.12 plots cumulative mass percent versus grain size, which was the plot used to determine the median diameter in Figure 2.9a. The Halema‘uma‘u events are better sorted (which can also be seen in Figures 2.10a and 2.10b) and contain negligible amounts of fine ash. This is a general feature of magmatic or ‘dry’ fall deposits (Houghton and Carey, 2015). Again I compare these results with the Etna and Chaitén eruptions, as examples of much larger and more intense explosive eruptions. The degree of sorting decreases within the subplinian (Etna) and

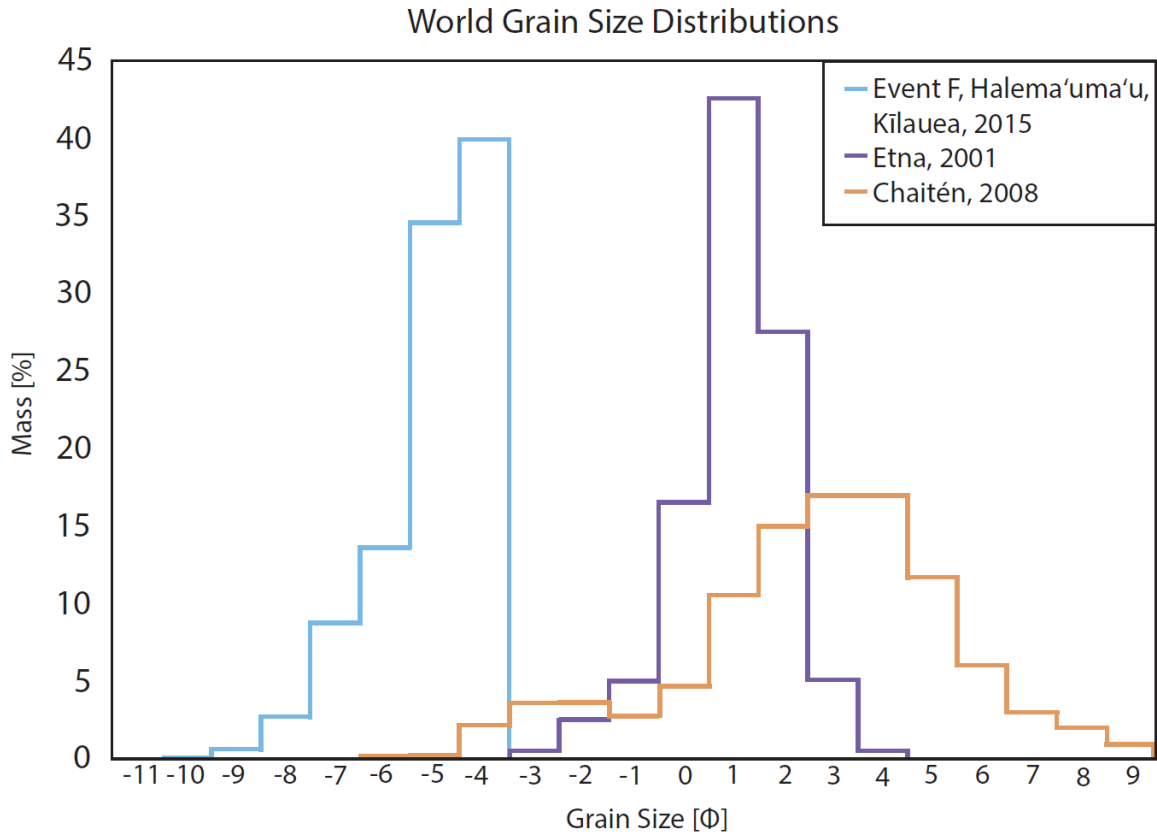


Figure 2.11 Grain size distribution comparing a high intensity Halema'uma'u event (Event F) to a basaltic subplinian eruption of Etna (2001) and a silicic Plinian eruption of Chaitén volcano (2008), both with increasing eruption intensity and subsequently increasing fragmentation efficiency. Note that Event F is an incomplete histogram due to my inability to resolve particles with diameters smaller than -4ϕ .

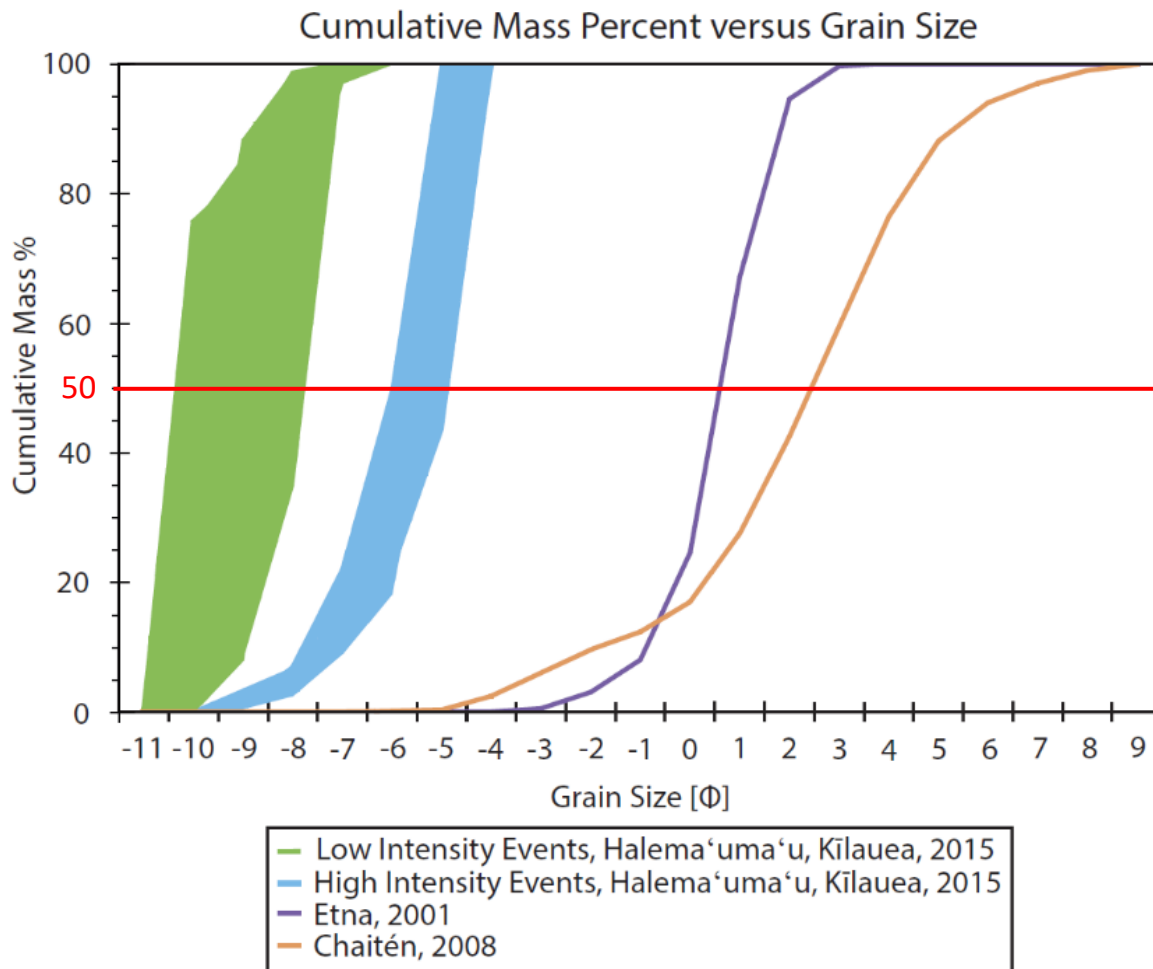


Figure 2.12 Plot of cumulative mass percent versus grain size. The green and blue areas on the plot, representing the low and high intensity events at Halema'uma'u respectively, depict the bounds of the individual events analyzed in this study. For all of the eruptions depicted here, as intensity increases, particles are more poorly sorted (the particles span a wider range of grain size values) and decrease in grain size, highlighting the relationship between intensity and fragmentation. This trend is even evident when comparing the difference between the low intensity events and the high intensity events at Halema'uma'u. The 50th percentile used to calculate the median diameter in Figure 2.9a is indicated here by the red line.

Plinian (Chaitén) eruptions. Material from Halema'uma'u eruptive activity are less fragmented, having higher grainsize modes. This again supports the notion that higher intensity eruptions result in greater degrees of fragmentation and are not as well sorted as low intensity eruptions.

2.4.4 Form and Scale of Activity and Decoupled Gas Bubble Size

2.4.4.1 *Pyroclast Size and Shape Analysis*

I calculated the following shape factors for each measured pyroclast associated with each event: area, perimeter, major and minor axes, form factor, and equivalent diameter of a circle of area equivalent to the pyroclast. For each event, three to four images were selected, at 0.1 second intervals, when large numbers of pyroclasts were visible. The average area of all of the pyroclasts, for all of the studied events, was $4.7 \times 10^{-2} \text{ m}^2$. The pyroclast with the greatest area, from Event F, measured 2.3 m^2 . The smallest measured pyroclast area, $1.0 \times 10^{-3} \text{ m}^2$, was observed in many events and lies at the resolution limits of this study. Event G boasted the pyroclast with the largest perimeter at 24.1 m, while the average perimeter was 0.7 m and the minimum perimeter was 0.03 m, again measured in multiple events and indicating the limitations of shape calculations in images.

Form factor was calculated using the following formula:

$$\text{Form Factor} = (4 \times \pi \times \text{area}) / (\text{perimeter})^2$$

Form factor is a measure of how spherical a particle is, with a value of 1 equaling a perfect sphere; lower values indicate that the particle is more irregular. For all pyroclasts from the events, the pyroclast with the highest form factor, indicating that it was the most regular, was calculated at 9.8×10^{-1} , observed in Events A, F, and G. The average form factor was 5.7×10^{-1} , and the minimum was 2.0×10^{-2} , measured in Event G. My data suggest overall the particles are

not very spherical, and that there was no significant difference between the sphericity of particles from low or high intensity events.

The diameter of a circle with equivalent area (to the pyroclast) was calculated with the formula:

$$\text{Equivalent diameter of a circle} = \sqrt{(\text{area} / \pi)}$$

The average equivalent diameter of the pyroclasts was 8.9×10^{-2} m (89 mm). The greatest equivalent diameter of a circle was 8.7×10^{-1} m (87 cm) and the smallest was 6.0×10^{-3} m (6 mm).

I did not find any correlation between these factors and the vigor of the events. There was not a significant enough disparity in eruption rate between the low intensity events and the high intensity events to generate noticeable differences in shape, probably reflecting that the range of viscosity of the ejected magma was very narrow over this period and conditions of fragmentation were little changed. The position on a bubble from which a pyroclast was ejected, i.e., center or edge, and time at which pyroclasts were ejected, showed no relation with any of the shape parameters. For instance, I could not say that more equant pyroclasts were ejected from the peak of the domed lava surface, or that larger pyroclasts were ejected at the beginning of bubble bursting, and vice versa. Based on this study, pyroclasts, regardless of size and shape, are ejected randomly during a bursting event.

2.4.4.2 Mean Pyroclast Initial Velocity versus Bursting Velocity

Mean initial velocities of ejecta broadly correlate with the velocities at which the rising bubbles burst (i.e., the bursting velocity) (Figure 2.13a). Pyroclasts attained higher ejection velocities when a bubble bursts with a greater vigor (i.e., with a higher velocity). For event E, I plot the northwest bursting velocity since all of the observed pyroclasts were ejected from the

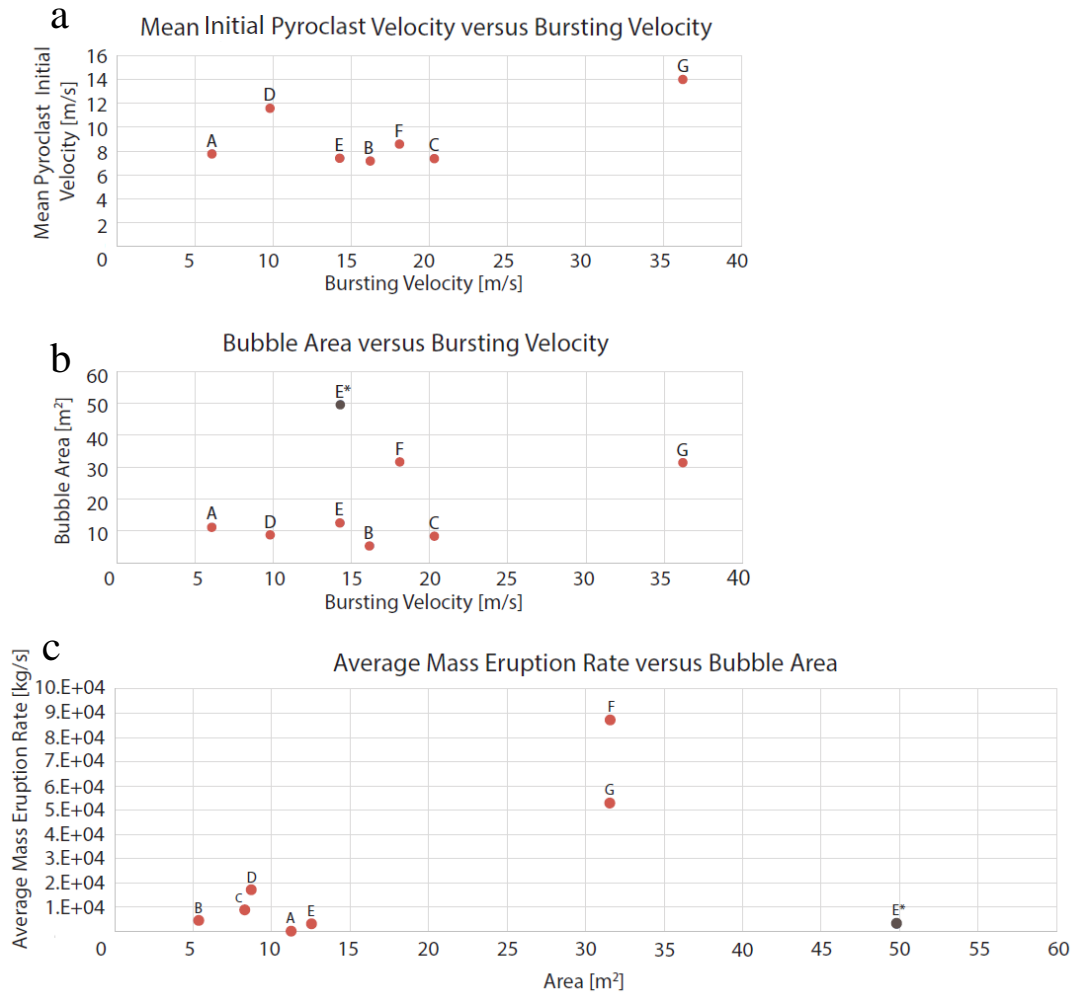


Figure 2.13 (a) Plot of mean initial pyroclast velocity versus bursting velocity, showing that pyroclasts attain higher ejection velocities when a bubble bursts with greater vigor. (b) Plot of bubble area versus bursting velocity, indicating that larger bubbles burst at higher velocities (c) Plot of average mass eruption rate versus bubble area, demonstrating that higher intensity events are associated with larger bubbles.

In plot **a**, Event E is plotted using the bursting velocity of the northwestern-half of the bubble (i.e., the half that burst and ejected pyroclasts). For plots **b** and **c** the Event E bubble area is calculated as half the total area of the bubble, because only half of the Event E bubble rose, burst, and ejected pyroclasts. E* represents the area of the entire bubble.

northwest-margin of the bubble. Events D and G displayed a slightly higher mean initial pyroclast velocity, when compared to the bursting velocity associated with the event. This could potentially be related to the events' collimated pyroclast dispersal pattern. Pyroclasts ejected during Events D and G were focused mostly at the peak of the domed lava surface during ejection. Based on the camera angle, this likely enables the pyroclasts' velocity measurements to be closer to "truer" velocities.

2.4.4.3 Bubble Area versus Bursting Velocity

Larger bubbles tend to burst at a higher velocity and/or with a greater intensity (Figure 2.13b). Event E was unique in that it did not rise or burst symmetrically. The northwest-margin rose quicker than, and burst before, the southeast-margin of the bubble. As a result, pyroclasts were ejected from the northwest-margin, and so I plot the northwest bursting velocity versus half of the area of bubble E (the northwest half).

Events F and G had the largest bubble areas (of all the events), and were the only two events to occur in the southeast sink. Additional events need to be studied both in the southeast sink and throughout the rest of the lava lake to determine if the largest bubbles form in the southeast sink.

2.4.4.4 MER versus Bursting Area

I have discussed how larger bubbles tend to have higher bursting velocities and greater initial velocities of ejecta (Figure 2.13c). This is predictable as buoyant ascent rates of bubbles through a fluid increase with bubble diameter. In the simplest case, where Stokes' Law can be applied, the velocity of rising bubbles scales with the square of diameter. Thus, larger bubbles tend to burst with greater vigor and have a greater mass eruption rate. Note that using only the area of the northwest-margin for Event E (given that pyroclasts were ejected from the northwest-

margin of the bubble associated with Event E) is more compatible with other events, when compared to plotting the average mass eruption rate against the entire bubble area for Event E (E*).

Additional events need to be analyzed before I can say that the events in the southeast sink have higher average mass eruption rates than events occurring throughout the lava lake.

2.4.5 Implications of the Rock Fall Event

The collapse of lithic material from the crater wall into the lava lake, beginning at 10:00 HST on December 10, provides key insights into the interplay of the crater margins and the behavior of the lava lake and outgassing activity. The rock fall perturbed the shallow foam layer of the lava lake. The fact that rock falls can trigger prolonged episodes of bubble bursting and spattering, that last long after the rock fall is over, implies that one cause of prolonged episodes is any external trigger that perturbs, and sets up a state of instability, within the shallow foam layer. The rock fall tears the crustal surface of the lake and probably initiates a prolonged period of coalescence of bubbles in the underlying foam layer. These decoupled gas bubbles rise through the free surface. However, more commonly without the presence of an identifiable external trigger such as the rock fall, internal instabilities within the foam layer and buoyant rise of large bubbles alone disrupt the stability for extended intervals and sustain a prolonged episode. The rock-fall driven events also show that prolonged episodes can be initiated close to the free surface and need not be driven by processes deep within the lake or within the conduit.

2.5 Summary

High-speed camera video analysis has enabled the identification of a variety of bubble bursting and spattering eruptive activity at the Halema'uma'u lava lake in 2015, defined as isolated events, clusters of events, and prolonged episodes. Most of the activity is internally

triggered, but external triggering, via rock falls, was also observed. In addition to distinguishing these events by spatial and temporal patterns I also quantify additional parameters associated with this activity including: bubble ascent velocities, initial pyroclast velocities, drain back and rebound, mass eruption rate, pyroclast dispersal patterns and the form and scale of the activity. These data suggest that the 2015 activity was relatively weak (i.e., of low intensity) but still falls in a region between those of continuous Hawaiian fountains and impulsive, short-lived Strombolian explosions, in terms of duration. The significance of this is explored in Chapter 4.

Chapter 3: 24-Hour Trends in Spattering Activity at Halema‘uma‘u in 2015

3.1 Introduction

I have identified, in Chapter 2, three styles of eruptive behavior at the Halema‘uma‘u lava lake at the summit of Kīlauea: isolated events from a point source, short-lived clusters of events from a point source, and prolonged episodes, from laterally extensive sources. Here I describe the lava lake’s behavior as a whole over a 24-hour period, followed by a more detailed analysis of the characteristics of eruptive behavior. For each behavior, I will discuss associated frequencies, durations, and positions on the lava lake. For prolonged episodes in particular, I look at how an episode can travel with or against the general north-to-south flow direction of the lava lake, and how large prolonged episodes can impact lava lake flow patterns. I also quantify the spatial lengths of prolonged episodes. Investigating the lava lake over a 24-hour period provides great insight into the diversity of eruptive behavior at Halema‘uma‘u and subsequently provides additional information regarding its place within the classical basaltic eruption spectrum.

3.2 Methods

A webcam operating in a near-IR “night” mode (Stardot® Netcam SC webcam) is maintained as part of the Hawaiian Volcano Observatory’s (HVO) general monitoring of Kīlauea’s summit lava lake. The camera is positioned on the southeast rim of Halema‘uma‘u with a field of view that includes most of the lava lake. Only a small fraction of the southern part of the lava lake, including the southeast sink, is blocked from view by the wall of Halema‘uma‘u crater in the foreground. In this study, I analyzed webcam images from a 24-hour-long period from 22:55 on April 23, 2015, to 22:55 on April 24, 2015. Events A through E (analyzed in

Chapter 2) occurred during this 24-hour period. At that time, the camera was collecting images at 1 frame per second with a pixel resolution of 1296×960 .

I also utilized images spanning the 24-hour period of December 10, 2015, collected by a thermal-IR camera (HTcam) that is also part of HVO's monitoring program. The December 10 images have a pixel resolution of 1320×900 and were archived at 1 frame per minute. The IR camera is positioned on the rim of Halema'uma'u about 60 m southeast of the webcam.

3.3 Activity Durations

3.3.1 Isolated Events

All isolated events were measured during the 24-hour analysis spanning April 23 through April 24, totaling 1,760 events. The duration of an event was measured as the time from when the free surface first visibly started to rise (due to the internal rise of decoupled gas bubbles) to when that lava dome collapsed back down onto the free surface, after the bubble burst. The average duration of these events was 5.8 seconds, with a standard deviation of 3.5 seconds. The longest event lasted for about 20 seconds though it is possible that events with durations longer than 15 seconds were closely spaced clusters of bubble bursts (i.e. clusters of events). The event with the shortest duration, in this analysis, persisted for ≤ 1 second, which was the shortest amount of observable time, due to the video's frame rate of 1 frame per second.

Events often occurred repeatedly in the same location at the lava lake's surface separated by repose periods of similar durations, after which another event would occur in the same location. A particular location would experience repeated isolated events alternating with repose periods for a few hours, before the activity at that specific location died off.

3.3.2 Cluster of Events

A total of 161 “clusters of events” were identified during the April 23 to April 24 analysis. Clusters of events are made up of numerous repeated, rapidly occurring events in the same location, which do not display any observable repose periods based on the video interval. Typically, the events composing clusters are markedly weaker in intensity and fewer in number than the events composing prolonged episodes. The weakest clusters of events generally contained 2 to 6 individual events. Clusters of events of greater intensity, and generally longer durations, were composed of events with greater frequency, making it harder to accurately distinguish and quantify individual events, based on the video’s frame rate. No clusters of events travelled along the lava lake, or moved away from their point source. The average duration of clusters of events was about 160 seconds (2.67 minutes), ranging between 1 second and 567 seconds (9.45 minutes), with a standard deviation of 90 seconds (1.5 minutes).

3.3.3 Prolonged Episodes

3.3.3.1 April 23 to April 24

21 prolonged episodes were recorded within the 24-hour period on April 24. These episodes lasted on average for about 51 minutes. The prolonged episode with the longest duration lasted for about 5.08 hours. The prolonged episode with the shortest duration lasted for 23 seconds. Despite its short duration, the 23 second prolonged episode is still considered a prolonged episode based on its spatial characteristics and intensity. Although the webcam resolution is not able to accurately discern this, the prolonged episodes with shorter durations might have been triggered by rock falls.

3.3.3.2 December 10

Additional analyses of prolonged episodes were conducted using the December 10 thermal images. A total of 29 prolonged episodes were observed during the 24-hours of

December 10. The average duration for these episodes was about 42 minutes. The maximum duration was 5.25 hours, and the minimum duration was 1 minute, which was the minimum amount of time recordable due the sampling rate of 1 frame per minute. The shortest prolonged episode was deemed a prolonged episode based on its intensity.

Six of the prolonged episodes attained their maximum spattering length within 1 minute of forming and then decreased in length until dying out. The average amount of time for a prolonged episode to attain its maximum length was 14 minutes; the longest it took for a prolonged episode to reach its maximum length was 1.2 hours. Five prolonged episodes started off at their smallest spattering length and increased in length before dying off. The average lag time from the start of an episode to when the episode was at its minimum length was 18 minutes; the maximum time was 3.12 hours. There was no trend or overarching characteristic as to when in a prolonged episode's lifespan it reached its maximum or minimum spatial length. The sources for prolonged episodes randomly varied in length throughout their existence. In general, there was no correlation between the spatial length and the lifespan of a prolonged episode, i.e., prolonged episodes with longer temporal durations did not necessarily have longer or shorter spatial lengths.

Seven prolonged episodes broke into smaller episodes, and three of these split again into additional episodes. Prolonged episodes commonly travelled along the lake margin in the general flow direction of the lava lake, although some did travel against the flow direction. Prolonged episodes travelled slower than the crustal plates moving in the general flow direction. Larger prolonged episodes were capable of locally influencing flow direction and also drawing in smaller prolonged episodes with which they would then combine.

3.3.3.3. *Comparison of Prolonged Episodes*

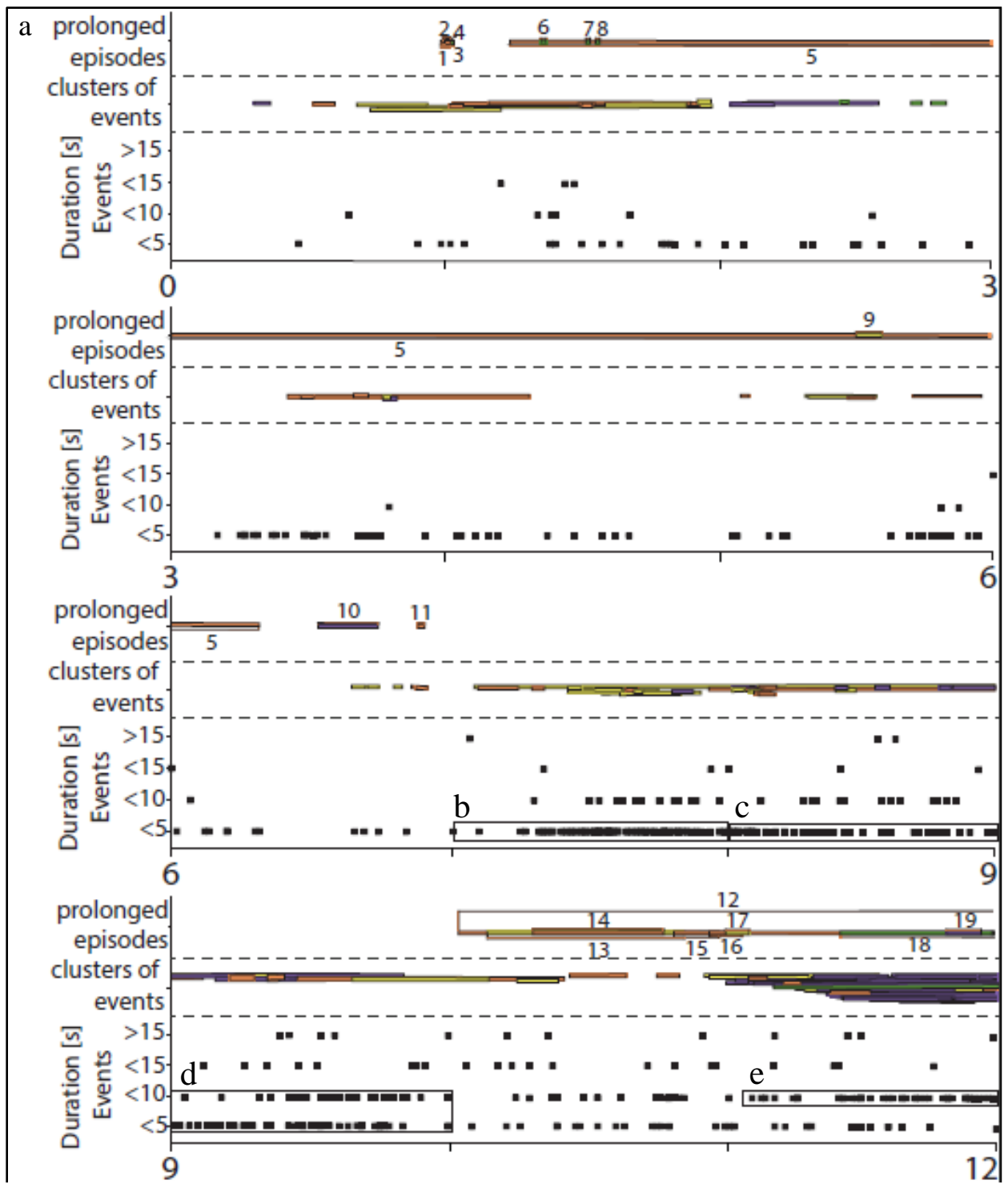
In terms of duration, both study periods had prolonged episodes with markedly similar average lifespans—51 minutes for April 23 to April 24 and 42 minutes for December 10. The longest-lasting and shortest-lasting prolonged episodes were also similar for both 24-hour periods; both were over 5 hours and under a minute respectively. At this point, without additional 24-hour analyses, I do not know if these similarities are by chance or if they represent a critical behavior pattern.

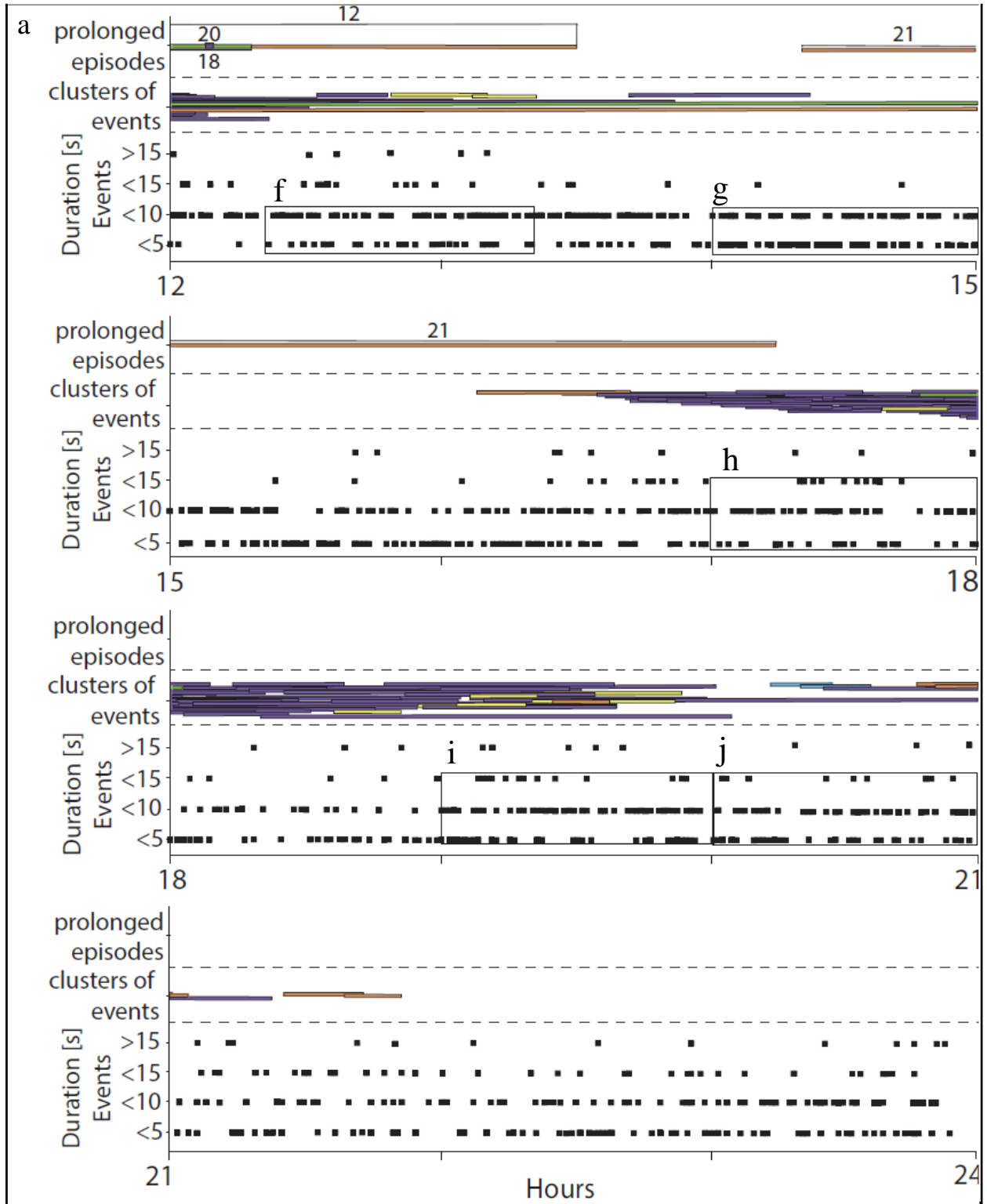
3.4 Activity Locations on the Lake

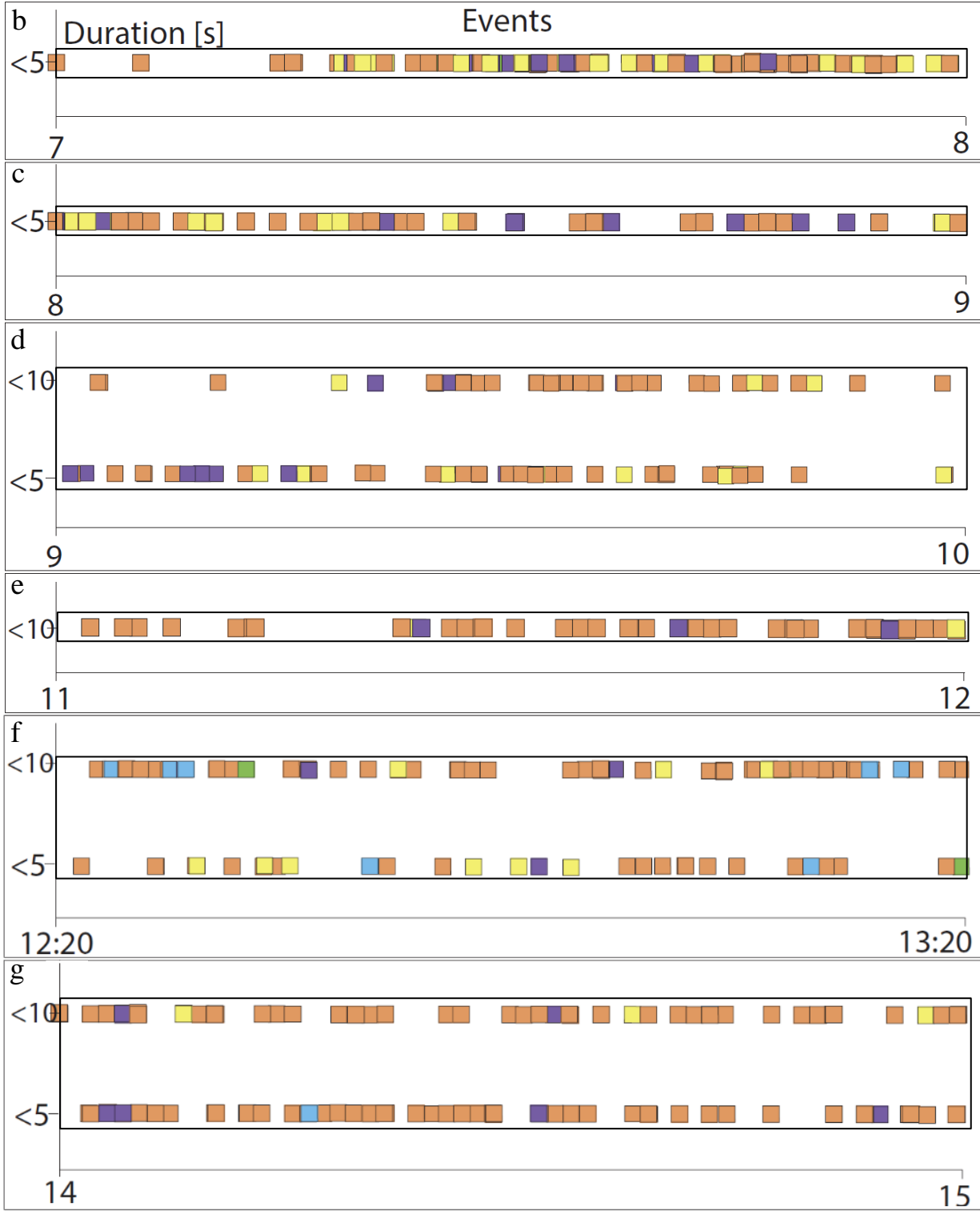
Figure 3.1 depicts the duration and positions of activity at the lava lake during the 24-hour period from 22:55 April 23 to 22:55 on April 24. In general, the lava lake flows from north-to-south, out of the field of view. I divided the lava lake into five regions based on flow direction and plate behavior observed in the 24-hour analysis. This subdivision matches well with surface motion vectors for the lava lake presented in Patrick et al., 2015. The northern region is along the northern edge of the lava lake and encompasses the zone of upwelling. The western and eastern regions of the lava lake encompass the western and eastern lake margins, respectively, as well as the immediate areas closest to the lake margins where plates tend to be drawn towards the walls while also moving with the general flow direction. Plates in the center of the lava lake are far enough away from the lake margin to not be influenced by the walls, and flow direction is almost exclusively towards the south (based on the lake's general flow direction). The southern region includes the zone of downwelling, and the southern edge of the lava lake, which is out of the field of view.

3.4.1 Isolated Events

Isolated events occurred almost continuously during the April 23 through April 24 analysis. The longest amount of time without any isolated events lasted for about 25 seconds,







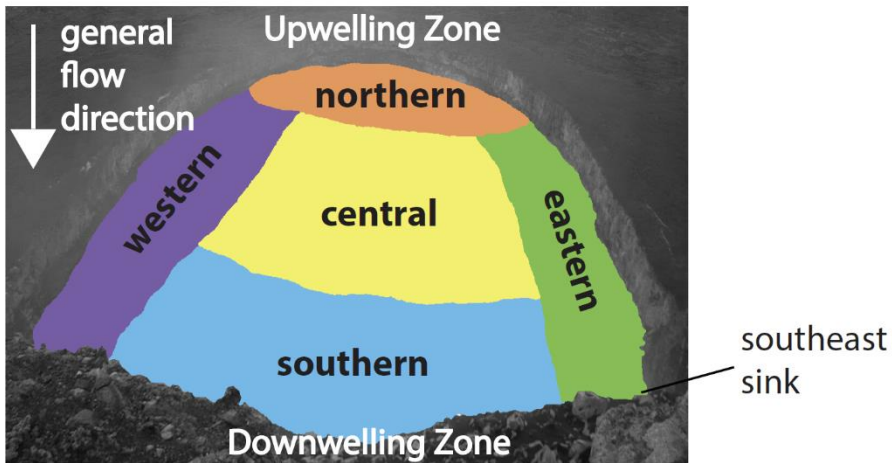
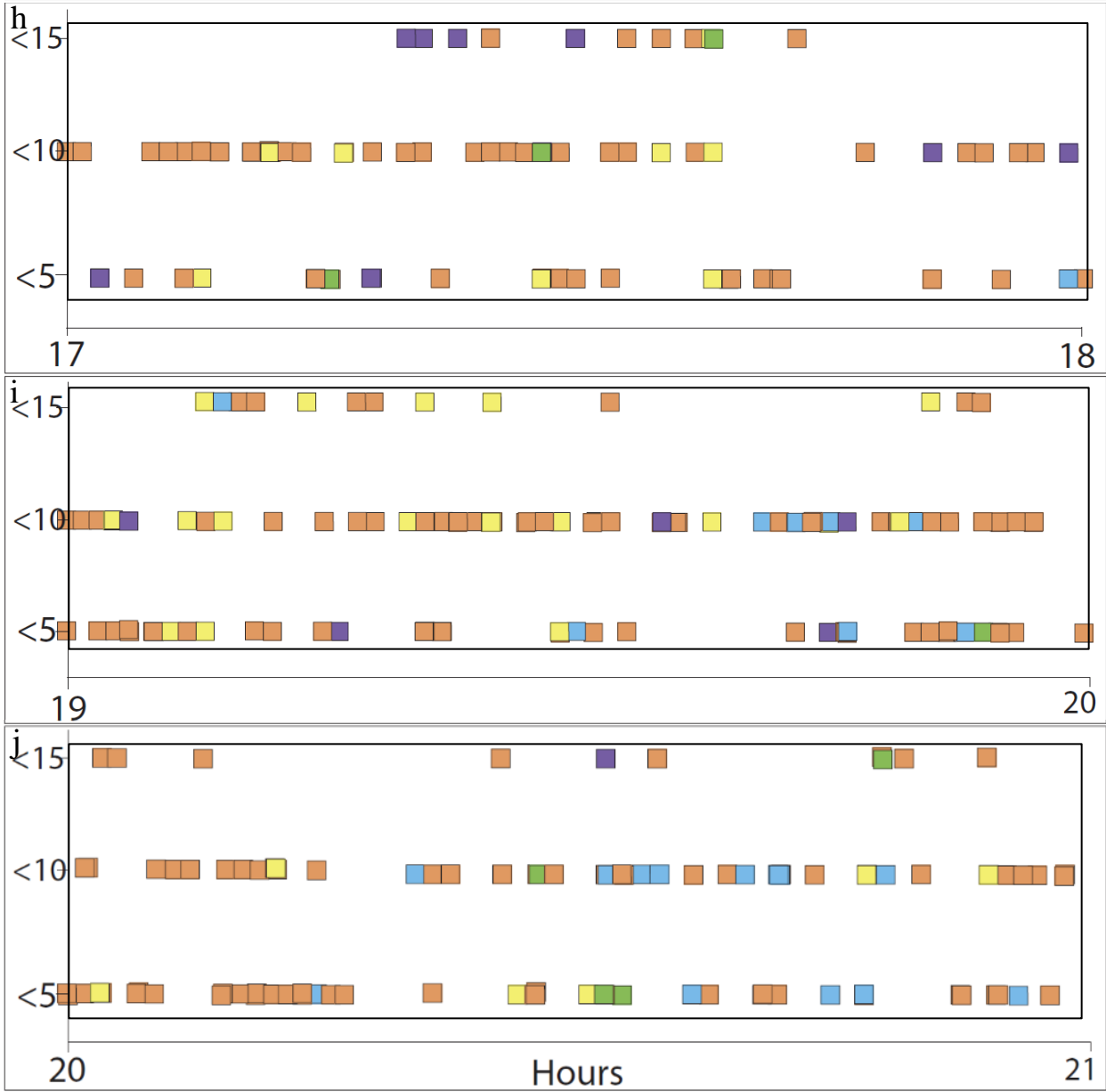


Figure 3.1 (a) Plots of the 24-hour activity at the lava lake on April 23 through April 24. The x-axis depicts 3-hour intervals of activity. Isolated events are represented as black boxes and the center of each box represents the onset of each event. Isolated events are grouped into four categories based on their durations:

< 5 = events lasting less than 5 seconds in duration

< 10 = events lasting 5 seconds or longer in duration, but less than 10 seconds in duration

< 15 = events lasting 10 seconds or longer in duration, but less than 15 seconds in duration

> 15 = events lasting 15 seconds or longer in duration

The onset and duration of clusters of events and prolonged episodes are shown as bars (scaled to represent their relative durations) and are color-coded to show where on the lava lake they occurred, based on **k**. Note there is considerable time-overlap. Prolonged episodes are numbered in order of occurrence. **(b through j)** Plot of subsets of isolated events shown at an expanded scale from **a** with time on the x-axis, duration on the y-axis, and each isolated event plotted as a box that is color-coded to show where on the lava lake the event occurred, again based on **k**. **(k)** Image showing the spatial divisions on the lava lake based on plate behavior and flow patterns. The different regions are color-coded and labeled. The general north-to-south flow direction is indicated with an arrow. The upwelling and downwelling areas of the lake are also noted.

and only happened when other forms of activity (cluster of events and prolonged episodes) were occurring elsewhere. Hours 0 through 6 saw the overall lowest frequency of isolated events. Afterwards, the number of events, particularly those lasting under 5 seconds, increased drastically. Most of the events between hours 7 and 9 occurred in the northern, western, and central regions of the lava lake. There were few events in the eastern portion of the lava lake. Many events overlapped in time. Figure 3.2 presents a histogram showing the number of events to occur per hour for the April 23 to April 24 study period.

Following the spike in events during hour 7, there was a marked increase in the number of events compared to the frequency observed in the first 6 hours. Between hours 9 and 12, an almost equal number of events occurred that were equal to 5 seconds or greater but less than 10 seconds in duration, or less than 5 seconds in duration. The number of events greater than or equal to 15 seconds in duration also increased. These events predominantly occurred in the northern portion of the lava lake, with some events occurring in the western and central regions.

Between hours 12 and 15, events started lasting even longer, with most events persisting for 5 seconds or more but less than 10 seconds, and an increase in the number of events lasting for at least 10 seconds but less than 15 seconds. Between hours 12:20 and 13:20 specifically, there was an increase in the number of events occurring in the southern portion of the lava lake, but the number of events occurring in the northern region still dominated. Some events occurred in the central portion of the lava lake, and only a few occurred in the eastern and western regions. Between hours 14 and 15, the number events in the northern region increased even more, while fewer events occurred in other portions of the lava lake.

For the remainder of the period (hours 16 to 24), event locations were random, for all durations. Events with durations from 5 seconds but less than 10 seconds remained the most

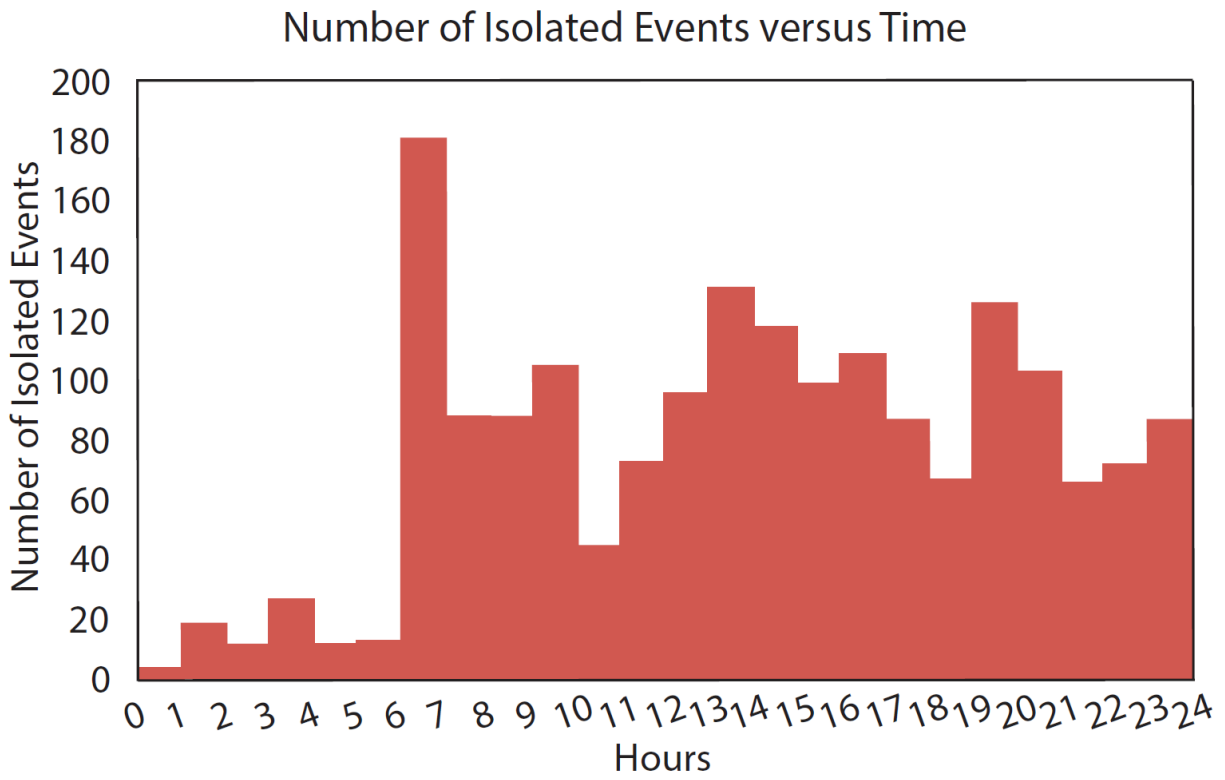


Figure 3.2 Histogram showing the number of isolated events to occur per hour during the 24-hour April 23 to April 24 study period.

frequent, but there was a significant increase in events lasting longer than 10 seconds. Between hours 17 and 18, events again occurred more frequently in the northern region, followed by events in the western region, with a few events in the eastern, central, and southern regions. From hours 19 to 20, events in the northern region were still most frequently occurring, but began to gradually be replaced by more events occurring throughout the lava lake. This trend continued for the remainder of the 24 hours. The highest frequency of events to take place in the southern region overall occurred between hours 20 and 21. The number of events occurring in the eastern region also increased between hours 20 and 21.

3.4.2 Cluster of Events

Between hours 0.5 and 2, clusters of events occurred most frequently in the central region of the lava lake, with a few occurring in the northern, western, and eastern regions. The frequency of clusters then decreased, with only a few occurring, until about hour 7. At that time, the number of clusters began to increase again, with most occurring in the central region of the lava lake, and a few in the northern and western regions. In general, the frequency of clusters continued to increase and by hour 11, occurred predominantly in the western region of the lava lake. Clusters with the longest durations occurred between hours 11 and 15, in both the eastern and northern regions. After hour 13, the clusters died off and began reoccurring at hour 16, mainly in the western region. Between hours 20 and 21, two clusters occurred in the southern region of the lava lake. By hour 20, the frequency of clusters had begun to decline, and they stopped occurring completely by about hour 22.

3.4.3 Prolonged Episodes

Prolonged episode patterns are depicted in greater detail in Figures 3.3 and 3.4 for the April 23 through April 24 study and for December 10, respectively. Over the 24-hour analyses, the position (in the lake) and the behavior of prolonged episodes exhibited a variety of trends.

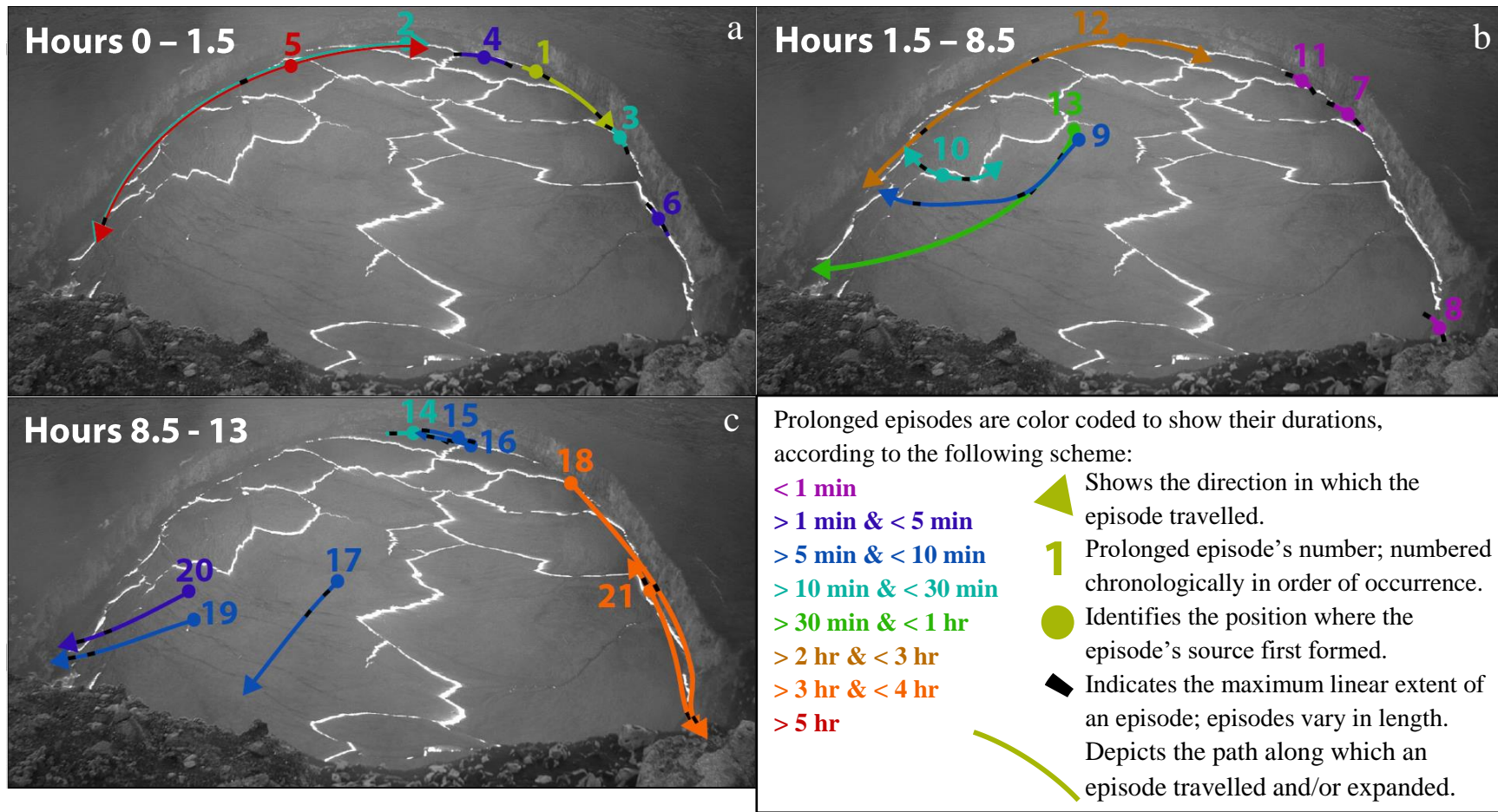


Figure 3.3 Images depicting the sources for the 21 prolonged episodes within the 24-hours of April 23 to April 24. The episodes are numbered in order of occurrence. The images show: (a) prolonged episodes 1 to 6; (b) prolonged episodes 7 to 13; (c) prolonged episodes 14 to 21. Episode 5 initially formed separately but then combined with Episode 2. Episodes 18 and 21 durations are calculated up to when they left the field of view. Likely they did not last much longer, having disappeared close to the southeast sink.

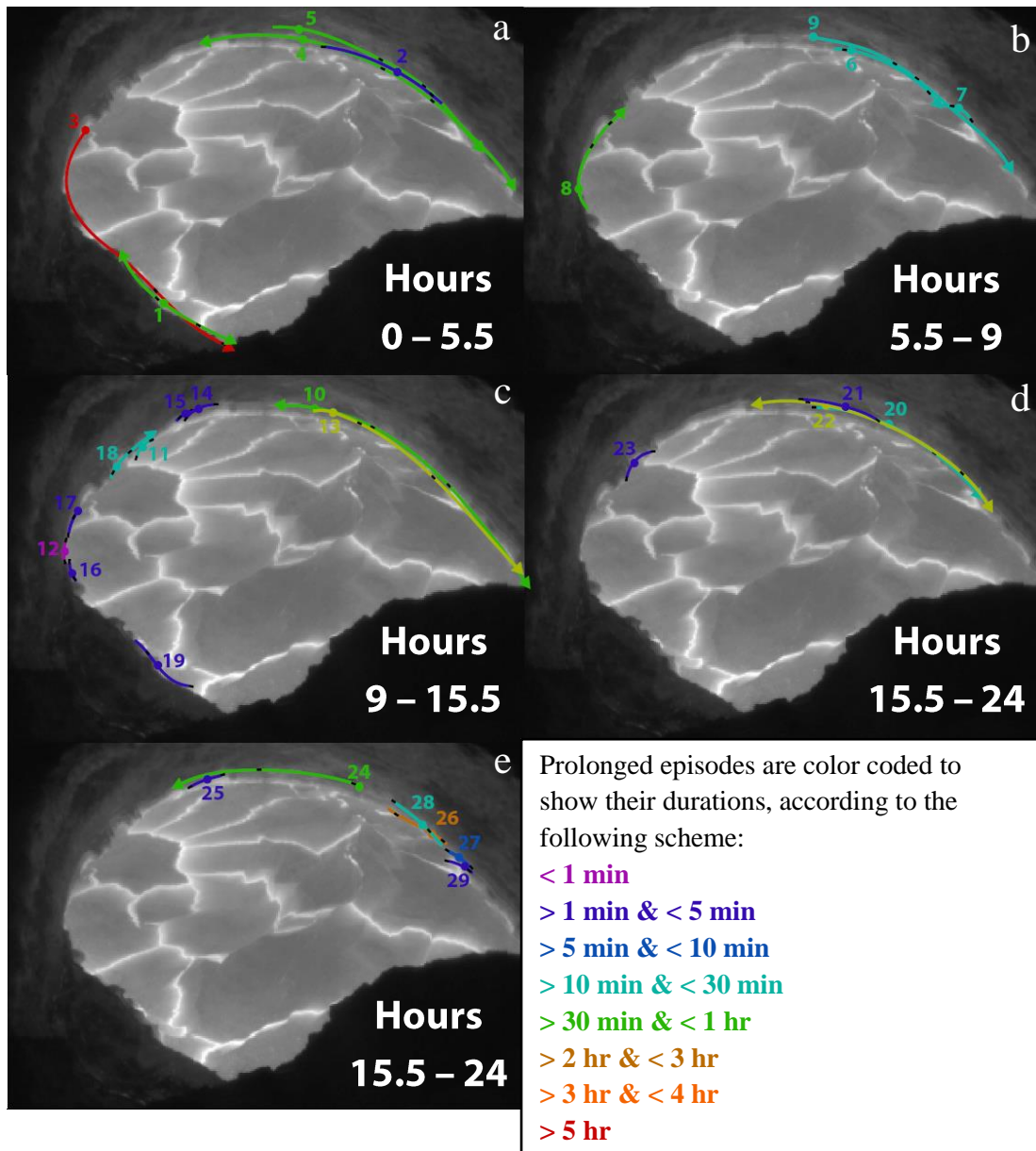


Figure 3.4 Images depicting the sources for the 29 prolonged episodes to occur within the 24-hours of December 10. The episodes are numbered in order of occurrence. The images show (a) prolonged episodes 1 to 5; (b) episodes 7 to 9; (c) episodes 10 to 19; (d) and (e) episodes 20 to 29. Episodes 1, 3, 10 and 13 durations are calculated up to when they disappeared out of the field of view. These episodes likely did not last much longer, having disappeared close to the southern downwelling region. Episodes 10 and 13 were heading towards the southeast sink when they disappeared from view. Refer to Figure 3.3 for an explanation of the symbols.

Prolonged episodes form around a shallowly-rooted source, which dictates the episode's position. Some sources travel, while others do not. Prolonged episodes that travelled followed similar paths, which are partially controlled by the general convective flow direction of the lake. Some episodes travelled both against and with the lake's general flow direction, and two prolonged episodes on December 10 travelled only against the flow direction.

Sources for most episodes formed along the lake margin; some of those sources travelled along the lake margin, while other sources remained stationary. Sources that formed away from the lake margin did not travel directly towards the south, but rather were drawn towards the nearest lake margin while moving generally south, with the predominant flow direction.

Sources for prolonged episodes varied in length throughout their lifespans. The maximum linear extent of a prolonged episode is marked by the black boundaries along their paths (Figures 3.3 and 3.4). Sources for prolonged episodes that did not travel still varied in length. Table 3.1 and Table 3.2 lists the approximate maximum length each episode reached and the approximate maximum distance over which each source travelled for April 23 through April 24 and for December 10, respectively. Travel distances are the change in position of the source's center.

3.4.3.1 April 23 to April 24

As shown in Figure 3.3a, within the first 1.5 hours of observations, episode 1 travelled with the general flow direction, and episode 3 did not travel. Episodes 4 and 6 were of relatively small durations (both between 1 and 5 minutes), and their sources did not travel with the lake. One interpretation may be that their short durations contributed to their inability to travel. Episode 2 formed before episode 5 but was large enough to locally redirect lake circulation so that episode 5 was drawn towards, and engulfed by, episode 2. The end of episode 2 is defined as the point at which episode 2 combined with episode 5. The duration of episode 5 is calculated

Table 3.1 Prolonged Episode Lengths for April 23 through April 24

Episode Number	Maximum Extent [m]	Travel Distance [m]
1	22.4	32.4
2	68.3	129.0
3	7.8	did not travel
4	15.3	did not travel
5	68.3	128.6
6	10.8	did not travel
7	13.5	did not travel
8	7.5	did not travel
9	36.1	69.3
10	15.1	27.9
11	7.2	did not travel
12	45.7	122.8
13	14.4	98.9
14	18.1	18.9
15	16.4	13.5
16	8.0	15.9
17	9.2	42.9
18	47.7	93.4
19	6.8	44.6
20	9.4	40.8
21	48.0	56.0

Table 3.2 Prolonged Episode Lengths for December 10

Episode Number	Maximum Extent [m]	Travel Distance [m]
1	24.9	65.2
2	59.0	65.0
3	43.8	145.5
4	29.4	148.5
5	24.8	145.1
6	48.1	58.0
7	11.7	16.9
8	15.5	54.3
9	12.9	118.3
10	47.0	152.7
11	11.7	did not travel
12	10.1	did not travel
13	46.1	129.5
14	15.0	did not travel
15	7.1	11.4
16	9.6	did not travel
17	7.6	13.8

18	14.3	28.0
19	27.8	36.1
20	64.1	91.5
21	38.0	did not travel
22	84.8	127.4
23	18.3	did not travel
24	49.2	90.4
25	15.9	did not travel
26	27.5	34.2
27	13.2	did not travel
28	21.6	31.4
29	11.4	13.3

from the start of episode 5 until the combination of episodes 2 and 5 was ended by a rock fall (section 3.5); this formed the longest lasting episode of the 24-hour analysis. Before merging, both episodes 2 and 5 travelled with and against the lake's general flow direction, and maintained similar travel paths. The maximum extent of episode 5 is also considered the maximum extent of episode 2 (given the combination of both episodes).

During hours 1.5 through 8.5 (Figure 3.3b), episodes 7, 8 and 11 had similar durations (all under 1 minute), and their sources formed in similar locations (along the eastern lake margin), and did not travel. Episode 12 followed similar travel and duration patterns as episodes 2 and 5. Episodes 9, 10 and 13 formed away from the lake's margin and travelled obliquely both towards the western lake margin and towards the south. Episode 13 in particular travelled towards a point that had frequently experienced clusters of events.

Throughout hours 8.5 to 13 (Figure 3.3c), episodes 14, 15, and 16 had relatively short durations and occurred from sources on the northern margin of the lava lake. Episodes 17, 19, and 20 formed away from the margin. Episode 17 travelled towards the south, but died away before going out of the field of view. Episodes 19 and 20 were similar to episode 13 in that they

too travelled towards an area that was frequently experiencing clusters of events. Episodes 18 and 21 both formed at, and travelled along, the eastern lake margin. Both episodes travelled out of the field of view; the point at which the episodes were no longer visible was considered the end of their life. Before travelling out of the field of view, these episodes appeared to be heading towards the southeast sink.

3.4.3.2 December 10

Within the first 5.5 hours (Figure 3.4a) of the December 10 study period, prolonged episodes 1 and 3 formed on the western lake margin. Episode 1 travelled back and forth along the lake margin, both with and against the general north-to-south flow direction. The durations of episodes 1 and 3 are measured up to the point at which they travelled out of the field of view. Episode 2 attained one of the greatest lengths, but remained fixed to its point source, failing to travel. Episodes 4 and 5 formed on opposite ends of the lava lake from episodes 1 and 3, and formed from sources located close to each other. These episodes also travelled along similar paths (although episode 4 travelled both with and against the lava lake's flow direction, whereas episode 5 only travelled with the flow direction), they had similar maximum extents in similar locations, and they lasted for similar durations.

Over hours 5.5 through 9 (Figure 3.4b), episodes 6, 7, and 9 had similar durations at sites along the eastern lake margin. The sources for episodes 6 and 9 travelled, but episode 7 did not. In contrast, episode 8 travelled only against the general flow direction.

During hours 9 through 15.5 (Figure 3.4c), episodes 10 and 13 formed close to each other, along the eastern lake margin, had similar maximum lengths (in similar locations along their paths), and travelled in the general flow direction. Episode 10 also travelled against the flow direction. The duration of episodes 10 and 13 is measured up to the point at which they left

the field of view. Episodes 14 and 15 formed close to each other, were of similar durations, and did not travel. Episodes 11 and 18 also formed in close proximity to each other, and had similar durations, but episode 18 travelled and episode 11 did not. Episodes 12, 16, 17, and 19 had similarly short durations, did not travel, and all formed along the western lake margin.

From hours 15.5 through 24 (Figure 3.4d, e), prolonged episodes occurred along the eastern lake margin and in the northern region. Episode 20 travelled with the flow direction, episode 22 travelled both with and against the flow direction, and episode 24 travelled against the flow direction. Episodes 21, 23, and 25 through 29 did not travel. Episodes 26 through 29 originated close to each other along the eastern lake margin.

3.4.4 Timings of Different Forms of Eruptive Behavior

As shown in Figure 3.1, the frequency and duration of isolated events continued to increase throughout the 24 hours on April 23 through April 24. Isolated events, which attained durations of 10 seconds or greater, steadily increased in frequency over the course of the 24 hours. Isolated events lasting under 10 seconds were the most frequent. Regardless of duration, isolated events increased drastically in frequency between hours 6 and 7 (Figure 3.5a). After hour 7, the average frequency of isolated events was almost an order of magnitude higher than the average frequency of isolated events prior to hour 7 (Figure 3.5a)

There were relatively few clusters of events that formed between hours 1 and 5, after which there was a spike in the frequency of clusters of events between hours 5 and 6 (Figure 3.5 a, b). The largest spike in the frequency of clusters of events occurred between hours 11 and 12, but the frequency dropped back down between hours 12 and 13 (Figure 3.1; Figure 3.5a, b). The frequency in clusters of events continued to decrease through hour 16. The frequency then

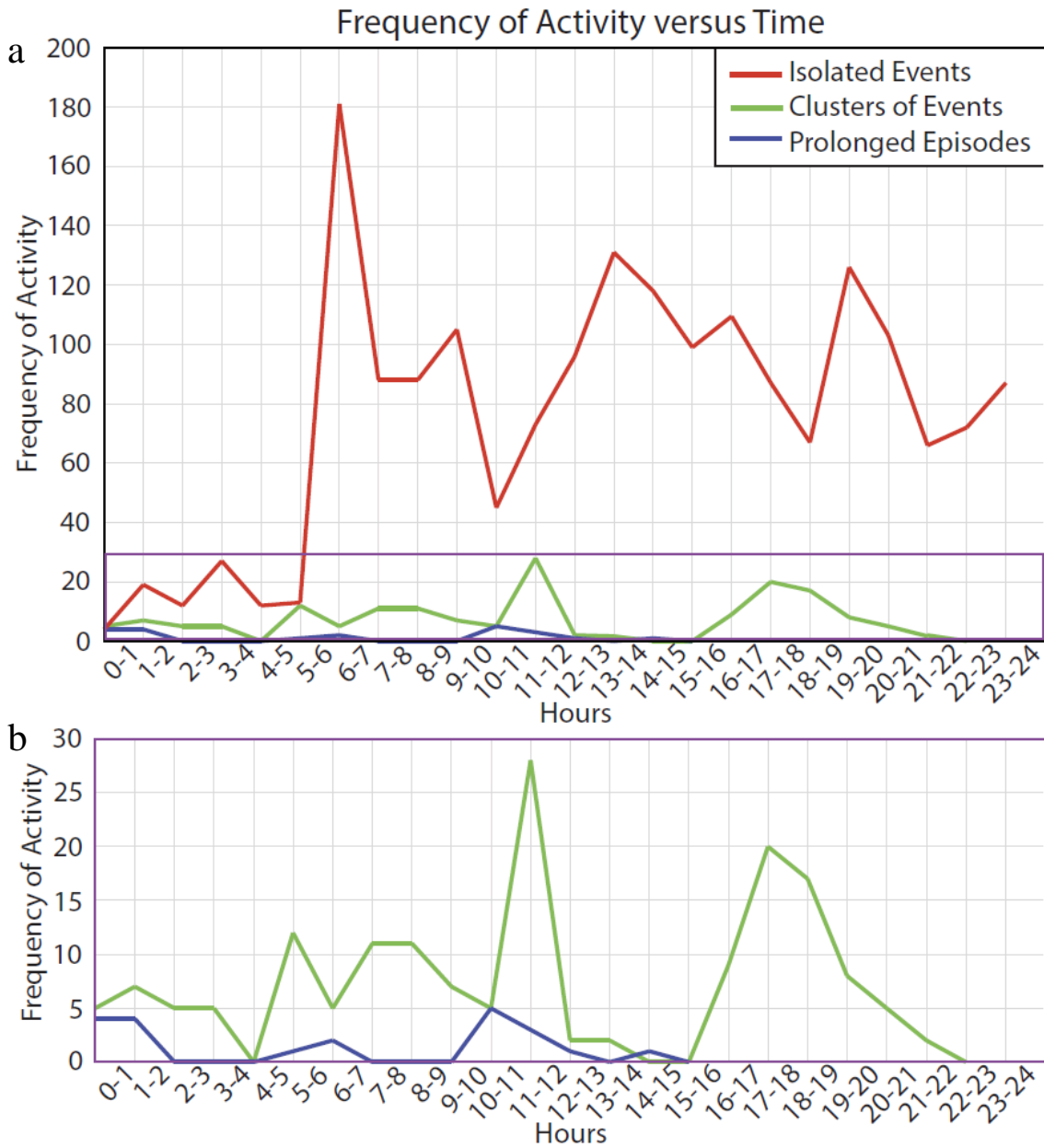


Figure 3.5 (a) Plot of frequency of isolated events, clusters of events, and prolonged episodes, versus time for the 24-hour analysis from April 23 through April 24. **(b)** Zoomed-in plot of the frequency of clusters of events and prolonged episodes versus the time.

increased again between hours 16 and 18, after which the number of clusters of events decreased until completely dying off at hour 22 (Figure 3.5 a, b).

Prolonged episodes lasted from about hour 1 to hour 17 of the analysis (Figure 3.1a) but only formed between hours 1 to 3, hours 5 to 8, and hours 10 to 16 (Figure 3.5a, b). From hour 1 to hour 7 prolonged episodes occurred almost continuously (Figure 3.1). Prolonged episodes did not form again until between hours 10 and 11 (Figure 3.5a, b). The last prolonged episode began between hours 15 and 16 (Figure 3.5a, b) and lasted until a little after hour 17 (Figure 3.1).

At the start of the analysis, all of the activity at the lava lake was relatively low in frequency. The frequency in clusters of events gradually picked up during hour 6 and the frequency in isolated events increased around hour 7. Afterwards, the frequency of both of these activities was greater compared to their frequencies prior to hours 6 and 7. No additional prolonged episodes formed after hour 16, but there was an increase in the number of clusters of events. Clusters of events stopped forming by hour 22, after which there was an increase in the frequency of isolated events (which was the only activity occurring at that time).

3.4.5 Spatial Trends of Different Forms of Eruptive Behavior

Figure 3.6 shows the position and frequency of activity at the lava lake's surface during the April 23 to April 24 analysis. Activity occurred throughout the lava lake, but most commonly along or close to the northern crater wall. Activity was also observed away from the crater walls along the center of the lake's surface, but more often in the western region of the lake than in the eastern region.

The points in Figure 3.6 are color coded to show the frequency of activity at the lava lake. The highest frequencies were observed at select locations in the northern region and in the southwestern corner of the lake. A location along the northern crater wall had the highest

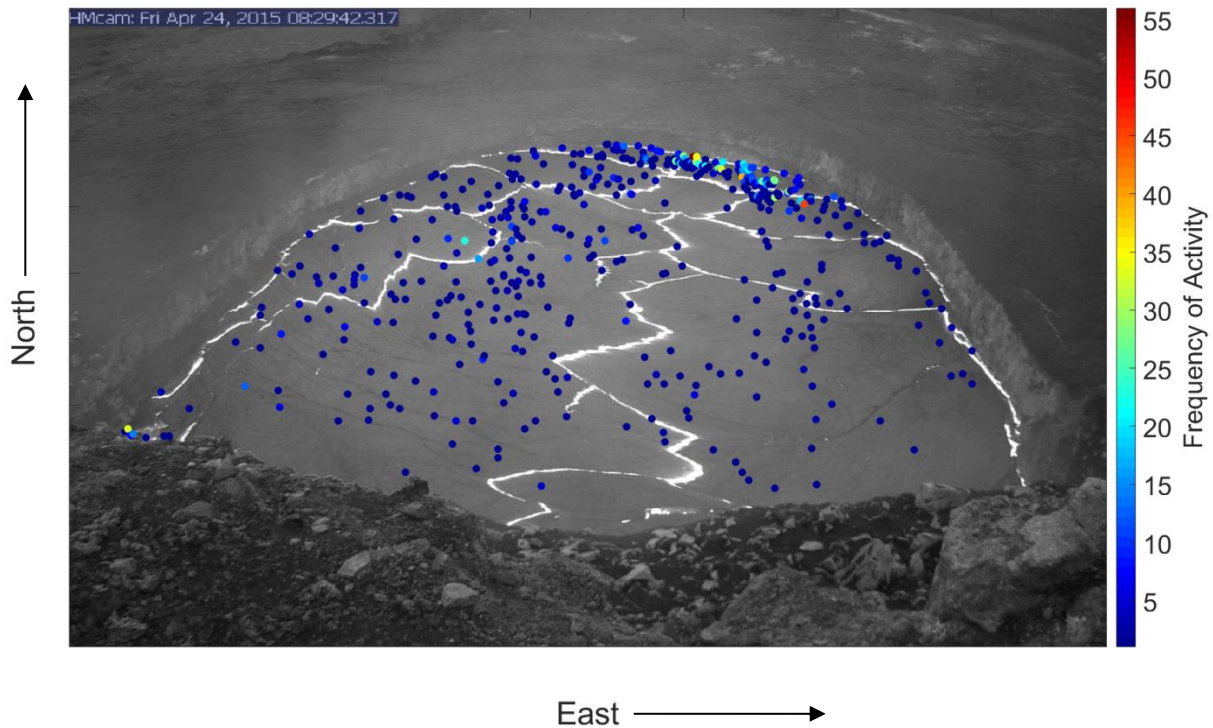


Figure 3.6 Frame from the near-IR HVO webcam. Points are overlain to show where on the lava lake’s surface the activity occurred during the 24-hour study period of April 23 to April 24. The points are colored to show the frequency of activity at each specific point on the lava lake. Based on the color bar to the right of the image, the warmer colors represent locations on the lake where the frequency of activity was high and cooler colors represent locations on the lake where the frequency of activity was lower.

frequency of occurrences; activity occurred in that particular spot 56 times. Activity overwhelmingly occurred less than 10 times at each specific location throughout the lava lake.

3.4.6 Spatial Comparison of Prolonged Episodes

There are notable similarities between the prolonged episodes from April 23 through April 24 and from December 10. Sources (from both study periods) for prolonged episodes behaved in the same fashion, in that they generally formed at the lake margin and travelled along it towards the south. Some prolonged episodes, however, travelled against flow direction. Some of the prolonged episodes from both 24-hour periods either broke apart into smaller prolonged episodes or combined with larger prolonged episodes. Larger prolonged episodes in both videos were capable of redirecting local lava lake motion towards themselves, with crustal plates foundering and being consumed within the area of spattering. Plates that are drawn towards prolonged episodes travel faster than plates traveling in the general flow direction.

3.5 Rock Fall on April 24

A large rock fall occurred on the west crater wall at approximately 05:19:56 HST on April 24, 2015, ending the combined prolonged episodes 2 and 5 (section 3.4.3.1). Spattering from events composing episodes 2 and 5 attained heights equal to or above the crater rim (about 15 meters) for much of the time. Episodes 2 and 5 had been traveling back and forth along the lake margin for 5.3 hours, but had been in the location where the rock fall occurred for just under 4 hours (before the rock fall occurred).

Immediately following the rock fall, spatter, along with a dilute plume of ash and juvenile lapilli, was thrown up and beyond the field of view of the camera. A prolonged episode source (episode 10) immediately expanded to cover about a quarter of the lava lake's surface (Figure 3.7a). Multiple waves, originating from the impact site, rippled radially across the lava lake (like

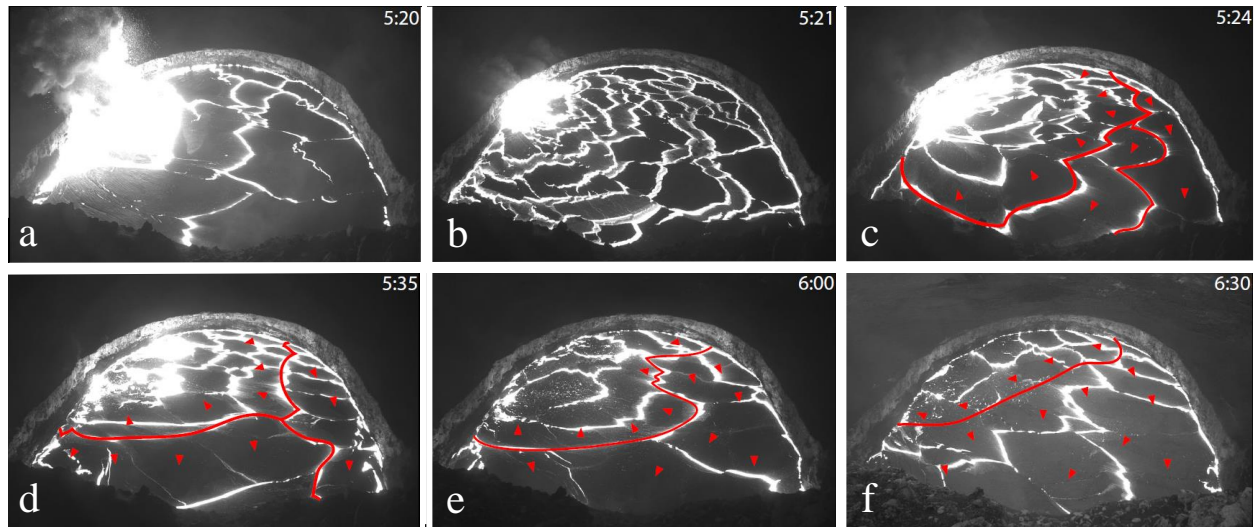


Figure 3.7 Near-IR frames depicting the immediate impact of the large rock fall, which occurred at approximately 5:19:56 HST on April 24. **(a)** Immediately after the rock fall, a plume and a large prolonged episode formed (episode 10). **(b)** About a minute after the rock fall, waves propagated through the lava lake disturbing the crust. The waves visibly rippled across the surface moving towards the east and then bounced backwards towards the west. Frames **(c)** through **(f)** show that after the waves had ended, the lava lake's flow direction was still impacted by the rock fall. Surface flow directions were redirected towards where the rock fall entered the lava lake. Red arrows indicate the flow direction of the lava lake at that time; major portions of the lava lake with varying flow directions are differentiated by red lines. With time, the lake gradually resumed its normal flow direction. By **d** the prolonged episode broke up into spatially smaller episodes. In **e** and **f** increased activity where the rock fall occurred (mostly in the form of isolated events) continued even after the prolonged episodes had died off.

rings in a pond), away from the impact site. Within a minute the waves had reached the eastern lake margin (Figure 3.7b). The plate boundaries that were aligned parallel to the ripples opened as the waves travelled away from the rock fall event (Figure 3.7b). Some plates, particularly those closer to the rock fall, broke apart from increased agitation of the surface and from the increased rate of local subduction and foundering. Most of the lava lake circulation was redirected towards the impact site, which was characterized by intense spattering (Figure 3.7c, d, e, f). Isolated events not related to the rock fall stopped occurring, including those in the northern region of the lake. The rock fall generated two prolonged episodes (episodes 10 and 11) that only lasted for 17 minutes and 1 minute, respectively (Figure 3.7 b, c, d). Once these prolonged episodes had ended, a higher frequency of isolated events began in the western portion of the lava lake (Figure 3.7 e, f).

3.6 Summary

Isolated events occurred frequently, and often repeatedly at specific locations, separated by repose periods on similar time scales to the isolated events preceding them. During the April 23 through April 24 study period, isolated events occurred throughout the lava lake, but most commonly in the northern region and least frequently in the eastern and southern regions of the lava lake. Clusters of events occurred independently of isolated events. The highest frequency of clusters on April 23 through April 24 occurred in the western region, but they were present in all other regions of the lava lake as well. Prolonged episodes occurred less frequently, but lasted for longer durations, than clusters of events. Prolonged episode sources commonly focused along, and tended to be elongate parallel to, the lake margin, and traveled with or against the lake's general flow direction. Spatially large prolonged episodes, composed of more-intense events, redirected flow directions towards themselves, sometimes drawing in and absorbing smaller

prolonged episodes. Rock falls serve as an infrequent external trigger for outgassing, and large rock falls can completely alter typical lava lake behavior.

The frequent rise of decoupled gas bubbles from beneath the free surface creates instability in the shallow foam layer of the lava lake. This instability results in three forms of activity: (a) short, repeated instances of weak outgassing for a few hours (many isolated events), (b) weak repeatedly occurring events with an average duration of a few minutes (clusters of events) or (c) more intense prolonged episodes which last, on average, for just under an hour. Overall, the 24-hour-long trends of eruptive behavior at the lava lake provide additional insight into the characteristics associated with this intermediary basaltic eruption style.

Chapter 4: Discussion and Conclusions

4.1 Discussion

4.1.1 Characterizing the 24-hour Trends of Activity at the Lava Lake

The three styles of bubble bursting and spattering eruptive activity (isolated events, clusters of events, and prolonged episodes) were distinguished based on their temporal and spatial distributions. All three of these styles occur in the lake and independently of each other in time and space. When the lake as a whole increases in outgassing, these three styles also increase in frequency, and vice versa. The three styles of activity at the lava lake result from cycles of instability in a shallow foam layer below the free surface, caused internally by the rise of the largest decoupled gas bubbles from within the lava lake system and externally (and less frequently) by rock falls.

4.1.1.1 Temporal Trends

Isolated events are the most frequent type of activity at the lava lake and result from the rise of large bubbles, often occurring repeatedly in the same location. Isolated events are separated by repose periods on a time scale similar to, or slightly longer than, the duration of the bubble bursts. On their own, isolated events are weaker than clusters of events and prolonged episodes. In all regions of the lake, isolated events often occur repeatedly in the same location. I infer that this is because each vent reforms or weakens the crust at the source making it easier for latter isolated events to occur. A rising bubble can also disturb the foam's stability, possibly resulting in repeated coalescence. I infer that perhaps a bubble may rise from depth to disturb the shallow foam layer triggering coalescence and the formation of a second bubble, and a third bubble, and so on. This could continue until stability is re-established in that area of the foam layer and coalescence ceases. Another possible explanation for the repeated nature of isolated events may be that the processes associated with the bursting bubble, including rebound, could

disrupt the melt below causing a new bubble to form. The repose periods between isolated events may result from the amount of time it takes for a bubble to coalesce and then for that bubble to make its way up to the surface.

Individual events within clusters are of higher intensity than isolated events; clusters are made up of rapidly reoccurring individual events in the same location without repose periods. I infer that they occur less frequently than isolated events, because they require more energy per unit time, and a greater state of instability to form. The increased amount of outgassing during clusters of events, compared to isolated events, serves as an obstacle towards re-establishing stability for the foam layer, because coalescing bubbles (in the foam layer) contribute to a greater state of instability.

Prolonged episodes are the highest intensity activity observed at the lava lake and occurred least frequently, during my study periods. They have the longest durations and are strong enough to even influence the larger scale flow behavior of the lake. Furthermore, the sources of prolonged episodes are capable of travelling with or against convective flow direction (or both) and can capture local flow, becoming a site of crustal foundering. The largest amount of instability within the foam layer is necessary in order to generate a prolonged episode.

For the 24-hour study period from April 23 through April 24, summing up all of the durations for all three activity styles gives the following total durations: both isolated events and clusters of events had total durations of 2.8 hours, while prolonged episodes lasted for a total of 17.9 hours. Prolonged episodes are made up of multiple overlapping bubble bursts, while clusters of events are composed of a few bubble bursts, and isolated events are merely single bubble bursts.

4.1.1.2 Spatial Trends

Isolated events occurred across the entire surface of the lava lake, but most commonly (and almost continuously) in the northern region, primarily within the zone of upwelling, but secondarily along the northern crater wall. This implies that most of the larger decoupled bubbles—those capable of generating isolated events—rise with the ascending melt. The crater wall likely represents an area of thinner, weaker, more sheared crust, making it easier for isolated events to occur there.

Clusters of events occurred randomly across the lava lake surface, but most frequently along the western crater wall. Prolonged episode sources formed mostly along the lake margin, but also in a small zone in the western region of the lava lake, away from the lake margin. Likely, the crater wall represents an area of thinner, weaker and more sheared crust, making it easier for activity to occur. Prolonged episode sources, which formed away from the crater wall, then travelled towards the crater wall and with the lake's general flow direction. I infer that the crust in the center of the lake is stronger and less sheared, making it harder for prolonged episodes to form in the center of the lake. The few prolonged episodes that did form away from the crater wall may have formed in areas where there was less shearing.

4.1.2 Event Phases

Analysis of isolated events from high-speed camera images indicates that they are made up of various phases: the bubble ascent phase, the bursting and pyroclast ejection phase, and the drain back (and rebound) phase. Below the free surface of the lava lake, decoupled gas bubbles rise buoyantly and expand, probably incorporating other smaller, slower bubbles. As a buoyantly rising gas bubble nears the free surface, the free surface will begin to dome up above that bubble. The bubble ascent velocity is inferred to be the rate at which the lake surface rises. The bubble continues to accelerate as the free surface is pushed up, until the tensile strength of the stretching

crust is exceeded, and the crust tears and falls away (i.e., the bubble bursts). I found that bubble bursting velocities correlate with bubble dimensions and event intensity.

Fragments of the tearing crust form pyroclasts that are ejected at speeds that correlate with bubble bursting velocity. Most bubbles burst symmetrically at the top of the lava domes, directing pyroclasts effectively upwards, after which the pyroclasts are dispersed both widely and on narrow arcs. Less frequently, bubbles burst to one side of the lava dome and eject pyroclasts at an angle, reflecting the location of their bursting point, i.e. bubbles that burst asymmetrically on one side ejected pyroclasts from that side and in that general direction.

Once the bubble bursts, a void is left (where the bubble had been) and melt drained inward to fill the cavity in the form of drain back. Sometimes the melt was propelled upwards; this phenomenon is referred to as rebound. The ascent velocities of rebounds can be measured, but rebounds typically do not eject any pyroclasts.

4.1.3 Pyroclast Exit Velocities and Comparison to Strombolian and Hawaiian Eruptions

Table 4.1 provides the average initial velocity of ejected pyroclasts for each event. For Strombolian explosions, ejection velocities typically range from 50 to 400 m s⁻¹ (Taddeucci et al., 2012). The initial velocities of Halema'uma'u pyroclasts are 1 to 1.5 orders of magnitude lower than Strombolian explosions (Taddeucci et al., 2012). These velocities are also likely lower than the velocities of ejecta from Hawaiian fountains, on similar scales, based on the general observations of Hawaiian fountaining behavior. Ejection velocity is one of the main parameters in determining intensity, and intensity is one parameter that is used to characterize explosive volcanism. The velocities of ejected pyroclasts relate to the flux of gas and, in some instances, melt through the shallow conduit and vent.

Table 4.1 Average Initial Pyroclast Velocities

Event	Average Initial Velocity [m s⁻¹]
A	7.8
B	7.2
C	7.4
D	11.6
E	7.4
F	8.6
G	12.7

4.1.4 Eruption Magnitude and Intensity

By comparing low and high intensity events recorded with the high-speed camera, I determined that the activity at the lava lake followed relationships previously established to describe patterns of behavior for other styles of explosive volcanism. The higher intensity events result in more fragmentation, erupt greater amounts of mass, and result in more poorly sorted clasts than the lower intensity events. Evidence for this is provided by how the total mass scales, and how the median diameter inversely scales, with the average mass eruption rate (which serves as a measure of intensity). In contrast, shape analysis of the pyroclasts showed that there was not much difference between the products of both the low and high intensity events, indicating that the viscosity of the ejected magma was similar for all events.

I also compare these events to the 2001 basaltic subplinian eruption of Etna (Scollo et al., 2007) and the May 2008 silicic Plinian eruption of Chaitén volcano (Alfano et al., 2016). When compared to these higher intensity eruptions, the weaker activity at the lava lake produces markedly coarser pyroclast assemblages. This reflects far lower thermal efficiency in terms of translating magmatic heat into mechanical energy to fragment the magma.

4.1.5 Effects and Implications of Externally Triggered Outgassing (Rock Falls)

Disturbances in the lava lake can be generated externally by rock falls, in addition to the more common cause of the rise of buoyant gas bubbles. Rock falls, when large enough, can

significantly alter the entire lava lake's flow pattern and spattering behavior for extended periods of time. As observed on April 24, a large rock fall initially caused waves to travel through the lake away from the rock fall's location, perturbing the crust over the entire lake's surface. The effects of the rock fall were observed for 1.5 hours after the event. The perturbation, which was focused where the rock fall had occurred, generated repeated isolated events, clusters of events, and prolonged episodes as the lake attempted to re-establish stability conditions. Almost an hour passed before the lake once again followed its typical north-to-south flow patterns.

A series of rock falls on December 10, provided further evidence for the occurrence of externally triggered spattering. Smaller rock falls at the start resulted in rebound as melt drained back into the impact cavity (created by the rock) in the lake surface. A larger rock fall at the end of the series generated a prolonged episode, which spattered for an additional 28 seconds.

Rock falls provide additional indications that outgassing is a shallow process resulting from disturbances of the lake's shallow foam layer. The impacts of rock falls temporally extend beyond the rock fall event itself, as the lake attempts to re-establish stability.

4.2 Conclusions

4.2.1 Overall Research Conclusions

The 2015 activity at Halema'uma'u represents another type of behavior exhibited by Kīlauea (and other basaltic volcanoes), which is informally referred to as 'spattering', but never formally defined in a quantitative fashion. It provides greater insight into the relationship between Hawaiian fountaining and Strombolian explosivity. Consequently, this activity is highly instructive in terms of: (a) the diversity of degassing/outgassing possible at basaltic volcanoes, and (b) the controls on mechanically coupled versus decoupled behavior of the gas bubbles at shallow depths.

Three styles of eruptive activity—isolated events, clusters of events, and prolonged episodes—mostly result from mechanically decoupled large gas bubbles rising buoyantly through the free surface, but also can be triggered by rock falls into the lava lake. During my study, the Halema‘uma‘u activity was often continuous over timescales similar to Hawaiian fountaining but was markedly less steady than high fountains, and clearly was ‘fed’ by the arrival of individual, approximately meter-sized, bubbles. In this fashion, a significant portion of the gas phase was released as discrete bubble bursts, but with frequencies two or three orders of magnitude higher than typical bubble bursts at Stromboli. During episodes, the close spacing of the bubble bursts permitted sustained, but not steady, jetting of gas, and ejection of bombs and lapilli. Initial velocities of the ejecta tended to be lower by 1 to 1.5 orders of magnitude than both Strombolian explosions and Hawaiian fountains (Taddeucci et al., 2012). The form and scale of the activity compares predictably with the size of the decoupled gas bubbles. Bubble ascent velocities scale with bubble dimensions, and larger bubbles produce higher initial pyroclast velocities and higher mass eruption rates.

Based on Figure 4.1, individual events are weaker and are shorter in duration than Strombolian explosions. However, when events at the lava lake combine collectively they occur more frequently than Strombolian explosions, and form prolonged episodes which do plot in between Strombolian explosions and Hawaiian fountains. Prolonged episodes are more prolonged than Strombolian explosions and are less steady than Hawaiian fountains. Globally, the intensity of this activity fits on the lower end of basaltic explosive behavior, but in style it sits in a field between typical high fountaining events and isolated Strombolian explosions (Figure 4.1).

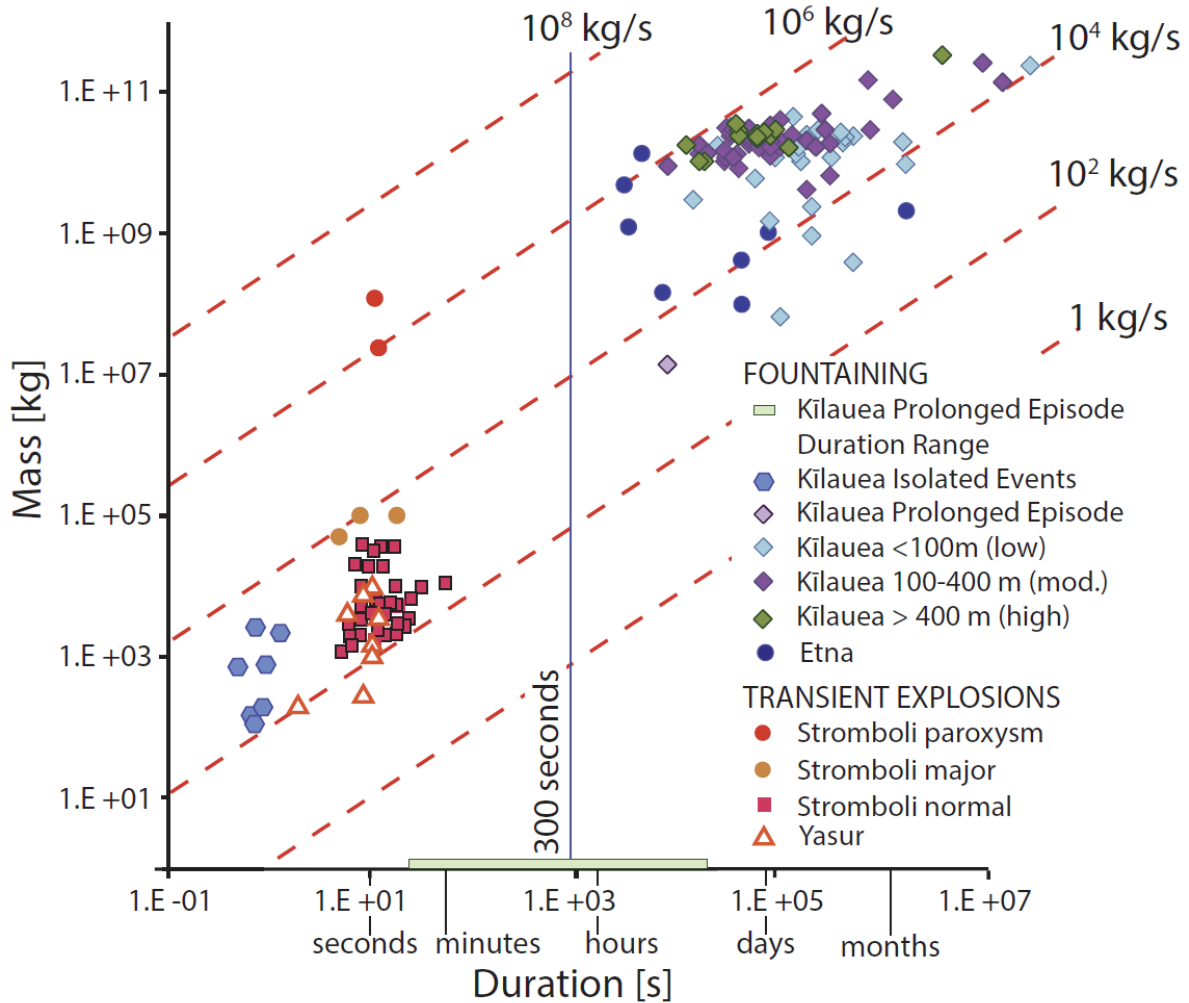


Figure 4.1 Plot from Houghton et al., 2015, of duration and mass of basaltic activity at select volcanoes with the results from this study overlain. As described in Figure 1.1b, this plot more aptly differentiates basaltic explosive eruption styles by duration as opposed to product dispersal and fragmentation. The red dashed lines represent equal mass discharge rate. The purple diamond is the prolonged episode captured in Video II from which I quantified four events. The green bar is the range of durations observed from all the prolonged episodes identified in both of the 24-hour study periods. The duration range shows that indeed prolonged episodes are an intermediary basaltic eruption style that falls between the classical end members. The blue hexagons are the seven events I quantified in Chapter 2.

This 2015 outgassing at the lava lake must be considered an intermediary basaltic eruption style. A set of numerical parameters to describe this activity has been established. The use of high-speed cameras has enabled this eruption style to be properly defined and quantified. This is the first time a detailed classification has been conducted on a basaltic eruption style that was not a classical basaltic end member.

4.2.2 Current Research Limitations

4.2.2.1 Velocimetry Study

4.2.2.1.1 Manual Analysis

Every velocity measurement (bubble ascent rate, initial pyroclast velocities, rebound ascent rate, etc.) was conducted by manually selecting reference points in each high-speed video frame. Manual selection is beneficial for quantifying and accurately characterizing activity in a fashion which, to date, has not been looked at in detail. For instance, one of the many determinations I made during this analysis was deciding when a bubble started to rise through the free surface, based on the onset of vertical surface motion. In doing so repeatedly for many bubbles, I formally established what constitutes the start of an event. A computer would be incapable of automatically determining the onset of an event without a scientist first manually establishing the criteria for the onset.

High-speed videos generate large amounts of data, making it impossible to manually process all of it, because manual analysis is time consuming. As volcanologists improve our definition of this eruption style, we can create programs to analyze more data related to this style. This would enable additional data to be classified, thus increasing our understanding of the activity at the lava lake. Given that each of my seven events had unique characteristics, I do not know how reproducible automated analysis would be.

4.2.2.1.2 Hawaiian Fountaining

I compared the 2015 intermediary basaltic eruption style to the classical basaltic eruption styles. Several papers have been published that focus on high-speed video analyses of Strombolian explosions including: Taddeucci et al., 2012; Gaudin et al., 2014, Gaudin et al, 2017; Taddeucci et al, 2015. These papers enabled us to make a thorough comparison between our intermediary basaltic eruption style and Strombolian explosions.

However, high-speed video analyses have not been performed on high Hawaiian fountains or on low-fountaining fissure eruptions due to the infrequency of events, and the paucity of research groups with high-speed cameras. I compared my analysis to the general knowledge base of Hawaiian fountaining, but, although I feel my study was thorough, a more complete analysis (similar to the comparisons made with Strombolian explosions) would clearly have been advantageous.

4.2.2.2 24-Hour Study

4.2.2.2.1 Manual Analysis

The 24-hour analyses were mostly conducted by watching the two 24-hour videos, noting when and where events occurred and calculating their durations. This was an extremely time consuming task. If an automated program was developed to pick out when, where, and for how long, events or spattering episodes occurred during each video, the analysis could have been completed much quicker and perhaps allowed enough time for a longer analysis (such as a week) to be conducted, without sacrificing the details of the observations. Similar to the challenges discussed regarding automatic analyses in Chapter 2, this was the first time these three styles of spattering activity and their related parameters, including duration, frequency, and spatial trends, were analyzed at any lava lake with this level of detail. I had to manually establish criteria for the

behavior, something a computer would be unable to do without a manual analysis first being performed.

4.2.2.2.2 Field of View

The more detailed 24-hour analysis (using the near-IR camera) was conducted for April 23 through April 24, when Events A to E occurred. These events were thus placed within a 24-hour context. Events F and G occurred in the southeast sink on December 8, out of site of the continuously monitoring cameras. The field of view of both the near IR and the thermal IR camera did not include the southeast sink, or the edges of the southern region. Having a 24-hour video with a view of the southeast sink would have placed Events F and G within the broader context of activity.

A 24-hour video with a field of view of the entire lava lake could have added to the 24-hour activity trends, though such a viewing geometry was not possible. Although my analysis was thorough there is no way to know how many isolated events or clusters of events occurred outside of the field of view. It is important to note, however, that the southern region contained the lowest number of events over the 24-hour analysis. Given that the majority of observed events occurred outside the southern region, being unable to record the events in portions of the southern region likely did not impact the overall relevance of the data set. Regardless, a view including the southern region would have been important for quantifying activity in the southern region and the southeast sink.

4.2.2.2.3 Higher Resolution 24-Hour Videos

Additional information could have been gained if the frame rate/resolution of the 24-hour videos was higher. For the most part, the resolution was inadequate to determine how many events make up a cluster of events or prolonged episodes. This detail would have further

enhanced the study and created a more direct comparison to previous studies conducted at Stromboli, such as the study by Gaudin et al. 2017, who discuss, among other topics, how many “ejection pulses” make up various styles of Strombolian explosions.

4.2.3 High-Speed Cameras and Volcanology

Basaltic volcanic activity occurs too quickly to make quantitative measurements or even detailed qualitative descriptions without the field use of high-speed cameras. Small, low-intensity basaltic eruptions may not produce deposits accessible for study, further emphasizing the usefulness of high-speed cameras. High-speed cameras have revolutionized the study of basaltic volcanism by enabling improved quantifications and more accurate descriptions of classical basaltic end member eruption styles, i.e. Hawaiian and Strombolian eruption styles. From such data, duration, rather than dispersal, has been identified as a more accurate means of classifying these eruptive styles (Houghton et al., 2015). By using high-speed cameras, volcanologists can also quantify previously undecipherable activity (including activity on the basaltic eruption spectrum between the two defined end members).

4.2.4 Natural Hazard Implications

Improving our understanding of basaltic volcanism is extremely important from a hazard and risk perspective. Volcanoes are becoming increasingly common tourist attractions—over 100 million people visit volcanoes annually (Pratt, 2012). According to the National Park Service, 1.8 million people visited Hawaii Volcanoes National Park in 2015, drawn by hopes of seeing an active lava lake from the Jaggar Museum Overlook. At Stromboli volcano, in Italy, guides offer tours to the summit daily. Stromboli volcano erupts regularly, hosting numerous explosions every day, with larger paroxysms occurring on a roughly decadal basis (Rosi et al., 2013). Tourism and curiosity in volcanology should be encouraged as this informs and educates the public, and people who have a greater awareness regarding natural hazards, such as those

posed by volcanoes, are more likely to listen to authorities and to respond properly in the event of an emergency. The increased public interest in volcanoes emphasizes the importance of increased scientific understanding, in order to ensure the public safety of visitors to volcanoes, while maintaining the safety of people residing close to volcanoes.

Scientists need to understand the variety of potential eruption styles and associated hazards (at a particular volcano) if they are to effectively communicate with emergency responders and public officials. In an emergency situation, people rely on scientists to determine what the volcano is doing and to relay this information to public officials. If scientists are in disagreement over the nature of the hazard, then they will lose credibility with politicians and with the public. An accepted classification system, amongst scientists, is a key feature for improved communication between scientists and the public, particularly during an emergency situation.

4.2.5 Future Work

Future high-speed video analyses should also be conducted on other basaltic eruption styles, such as low-fountaining fissure eruptions and high Hawaiian fountains. Improved classification of other eruption styles will shed more light on the range of eruptive activity that occurs within the spectrum of basaltic eruptions. In particular, high-speed video analyses of high Hawaiian fountains will provide another benchmark (in addition to Strombolian explosions) for which to compare intermediary basaltic eruption styles.

The 24-hour video analysis I conducted could be expanded and done on a daily basis with the help of HVO volunteers or on a continuous basis programmatically, as part of HVO's monitoring program. Automatic or semi-automatic methods for all of the analyses conducted in this study can be developed to speed up investigations (without sacrificing detail). This would

enable additional video footage (both high-speed and real time) to be analyzed and would increase the amount of activity we can classify and the amount of diversity we can identify within this activity. In doing so, weekly, monthly, and even yearly trends of spattering and bursting activity at the lava lake could be established.

The findings of this study should be summarized and presented to Hawaii Volcanoes National Park Rangers. Rangers can use this information to inform visitors at the viewing area outside of the Jagger Museum. From the viewing area, visitors can often see a glow (particularly at night) from the lava lake within the caldera, and when the lava lake is high enough, viewers can directly observe the spattering activity that was the focus of this study. If rangers could describe in a few sentences what this activity is, or provide a fact or two about it, this would increase the public's knowledge of eruptive activity at the lava lake, and potentially enhancing their experience.

References

- Alfano, F., Bonadonna, C., and Gurioli, L., 2012. Insights into eruption dynamics from textural analysis: the case of the May, 2008, Chaitén eruption. *Bulletin of Volcanology*, v. 74. 9, p. 2095 – 2108. doi:10.1007/s00445-012-0648-3
- Cas, R.A.F., and Wright, J.V., 1987. *Volcanic Successions, Modern and Ancient: A Geological Approach to Processes, Products and Successions*. p. 528.
- Clauge, D.A., and Dalrymple, G.B., 1987. The Hawaiian-Emperor volcanic chain; part 1. Geologic evolution. *in*: Decker, R.W., Wright, T.L., Stauffer, P.H., (eds.), *Volcanism in Hawaii*: U.S. Geological Survey Professional Paper 1350 (1), p.5 – 54.
- Eaton, J.P., and Mrata, K.J., 1960. How volcanoes grow: *Science*, v. 132.3432, p. 925 – 938, doi: 10.1126/science.132.3432.925.
- Ellis, W., 1825. *A Journal of a Tour Around Hawaii, the Largest of the Sandwich Islands*. Crocker and Brewster, Boston, p. 264.
- Gaudin, D., Taddeucci, J., Scarlato, P., Moroni, M., Freda, C., Gaeta, M., Palladino, D.M., 2014. Pyroclast tracking velocimetry illuminates bomb ejection and explosion dynamics at Stromboli (Italy) and Yasur (Vanuatu) volcanoes. *J. Geophys. Res.* v. 119, p. 5384 - 5397. <http://dx.doi.org/10.1002/2014JB011096>.
- Gaudin, D., Taddeucci, J., Scarlato, P., del Bello, E., Ricci, T., Orr, T., Houghton, B., Harris, A., Bucci, A., 2017. Integrating puffing and explosions in a general scheme for Strombolian-style activity. *J. Geophys. Res. Solid Earth*. doi:10.1002/2016JB013707
- Hon, K., Kauahikaua, J., Denlinger, R., Mackay, K., 1994. Emplacement and inflation of

- pahoehoe sheet flows: observations and measurements of active lava flows on Kilauea Volcano, Hawaii, *Geol. Soc. Am. Bull.* V. 106, p.351-370.
- Houghton, B.F., Taddeucci, J., Andronico, D., Gonnermann, H.M., Pistolesi, M., Patrick, M.R., Orr, T.R., Swanson, D.A., Edmonds, M., Gaudin, D., Carey, R.J., and Scarlato, P., 2015. Stronger or Longer: Discriminating Between Hawaiian and Strombolian Eruption Styles. *Geology*, v. 44.2, p. 163 – 166, doi:10.1130/G37423.1
- Houghton, B.F.; Carey, R.J. Pyroclastic fall deposits. 2015. In: Sigurdsson, H.; Houghton, B.F.; McNutt, S.; Rhymer, H.; Stix, J. (eds) *Encyclopaedia of Volcanoes*, 599-616 pp. Academic Press, San Diego.
- Jagger, T.A., and Finch, R.H., 1924. The explosive eruption of Kilauea in Hawaii, 1925. *Am. J. Sci.*, v. 5.8, p.353 - 374 (ser).
- Keller, G.V., Grose, L.T., Murray, J.C., and Skokan, C.K., 1979. Results of an experimental drill hole at the summit of Kilauea Volcano, Hawaii. *Journal of Volcanology and Geothermal Research* v. 5(3-4), p. 345 – 385.
- Kinoshita, W.T., Koyanagi, R.Y., Wright, T.L., Fiske, R.S., 1969. Kilauea Volcano: the 1967 – 68 summit eruption. *Science* v.24, p. 459 – 468.
- Macdonald, G.A., 1972. *Volcanoes*, Engelwood Cliffs, New Jersey, Prentice-Hall, Inc., 510 p.
- Macdonald, G.A., Abbott, A.T., Peterson, F.L., 1983. *Volcanoes in the sea: the geology of Hawaii*. University of Hawaii Press.
- Macdonald, G.A., Abbott, A.T., Peterson, F.L., 1986. *Volcanoes in the sea: the geology of Hawaii*. University of Hawaii Press, (second edition), p.80-81.

Mercalli, G., 1881. Natura nelle eruzioni dello Stromboli ed in generale dell'attività sismico

Vulcanica delle Isole Eolie: Atti Società: Italiana Scienze Naturali, v. 24, p. 105 – 134.

Moore J.G., and Clague, D.A., 1992. Volcano growth and evolution of the island of Hawaii:

Geological Society of American Bulletin, v. 104.11, p. 1471 – 1484, doi:10.1130/0016-7|
606(1992)10.

Morgan, W.J., 1972. Deep mantle convection plumes and plate motions: American Association
of Petroleum Geologists Bulletin, v. 56.2, p.203 – 213.

Orr T., Houghton B., Taddeucci J., Del Bello E., Scarlato P., Patrick M., 2014. The bubble's
wake—Localized rebound of Kīlauea's summit lava lake following minor bubble bursts:
Abstract #V41D-05 presented at 2014 Fall Meeting, AGU, San Francisco, Calif., 15–19
Dec.

Patrick, M.R., Orr, T., Sutton, A.J., Elias, T., Swanson, D., 2013. The First Five Years of
Kīlauea's Summit Eruption in Halema'uma'u, 2008 – 2013e. U.S. Geological Survey
Fact Sheet, pp. 2013 – 3116.

Patrick, M.R., Orr, T., Sutton, A.J., Lev, E., Thelen, W., Fee, D., 2015. Shallowly driven
fluctuations in lava lake outgassing (gas pistonning), Kīlauea Volcano. Earth Planet. Sci.
Lett. <http://dx.doi.org/10.1016/j.epsl.2015.10.052>.

Patrick, M.R., Orr, T., Swanson, D.A., Lev, E., 2016. Shallow and deep controls on lava lake
surface motion at Kīlauea Volcano, J. Volcanol. Geotherm. Res.

<http://dx.doi.org/10.1016/j.jvolgeores.2016.11.010>.

- Perret, F.A., 1913a. The lava fountains of Kilauea. *Am. J. Sci.*, v.4.35, p. 139 – 148 (ser).
- Perret, F.A., 1913b. The circulatory system in the Halemaumau lake during the summer of 1911. *Am. J. Sci.*, v.4.35, P. 273 – 282 (ser).
- Poland, M.P., Miklius, A., and Montgomery-Brown, E.K., 2014. Magma Supply, Storage, and Transport at Shield-Stage Hawaiian Volcanoes, *in*: Poland, M.P et al., eds., Characteristics of Hawaiian Volcanoes, U.S. Geological Survey Professional Paper 1801, p. 179 – 234.
- Pratt, S. E. "Danger in paradise: The hidden hazards of volcano geotourism." *Earth* 19 Mar. 2012
- Rosi, M., Pistolesi, M., Bertagnini, A., Landi, P., Pompilio, M., and Di Roberto, A., 2013. Stromboli volcano, Aeolian Islands (Italy), in Lucchi, F., et al., eds., *The Aeolian Islands Volcanoes: Present eruptive activity and hazards: Geological Society of London Memoir* 37, p. 473–490, doi:10.1144/M37.14.
- Scollo, S., Del Carol, P., and Coltelli, M., 2007. Tephra fallout of 2001 Etna flank eruption: Analysis of the deposit and plume dispersion. *Journal of Volcanology and Geothermal Research*. v. 160, p. 147 – 164. <http://dx.doi.org/10.1016/j.jvolgeores.2006.09.007>
- "Stats Report Viewer." National Parks Service. U.S. Department of the Interior, Web. 11 Mar. 2017.
- <[https://irma.nps.gov/Stats/SSRSReports/Park%20Specific%20Reports/Annual%20Park%20Recreation%20Visitation%20\(1904%20%20Last%20Calendar%20Year\)?Park=HAVO](https://irma.nps.gov/Stats/SSRSReports/Park%20Specific%20Reports/Annual%20Park%20Recreation%20Visitation%20(1904%20%20Last%20Calendar%20Year)?Park=HAVO)>.

- Swanson, D.A., Rose, T.R., Mucek, A.E., Garcia, M.O., Fiske, R.S., Mastin, L.G., 2014. Cycles of explosive and effusive eruptions at Kīlauea Volcano, Hawai‘i. *Geology*. v. 42.7, p. 631 - 634.
- Swanson, D.A., Orr, T.R., Patrick, M.R., 2016. Changes in mass flux of tephra from the lava lake in Overlook crater, Kīlauea Volcano, Hawai‘i. Abstract #V43A-3122 presented at Fall Meeting, presented at 2016 Fall Meeting, AGU, San Francisco, Calif., 12–16 Dec.
- Taddeucci, J., Scarlato, P., Capponi, A., Del Bello, E., Cimarelli, C., Palladino, D.M., Kueppers, U., 2012. High-speed imaging of Strombolian explosions: the ejection velocity of pyroclasts. *Geophys. Res. Lett.* 39. L02301. <http://dx.doi.org/10.1029/2011GL050404>.
- Taddeucci, J., Edmonds, M., Houghton, B.F., James, M.R., and Vergnolle, S., 2015. Hawaiian and Strombolian eruptions, *in* Sigurdsson, H, et al., eds., *The Encyclopedia of Volcanoes* (second edition): London, Academic Press, p. 485 – 505.
- Tilling, R.I., and Dvorak, J.J., 1993. Anatomy of a basaltic volcano: *Nature*, v. 363, no. 6425, p. 125 – 133, doi:10.1038/363125a0.
- Walker, G.P.L., 1973. Explosive volcanic eruptions – A new classification scheme: *Geologische Rundschau*, v. 62, p. 431 – 446, doi:10.1007/BF01840108.
- Wilson, J.T., 1963. A possible origin of the Hawaiian Islands. *Canadian J. Phys.*, v. 41. p.863 - 870, doi: 10.1139/p63-094.
- Wilson, D., Elias, T., Orr, T., Patrick, M., Sutton, A.J., Swanson, D., 2008. Small explosion from new vent at Kīlauea’s summit. *Eos* v. 89, p. 203.